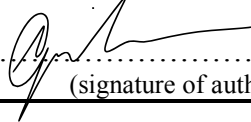




Universitetet  
i Stavanger

FACULTY OF SCIENCE AND TECHNOLOGY

## MASTER'S THESIS

Study programme/specialisation:  Offshore Technology Marine and Subsea	Spring / Autumn semester, 20.17.  Open/ <del>Confidential</del>
Author:  Asdren Gjuka	 ..... (signature of author)
Programme coordinator:  Supervisor(s): Professor Muk Chen Ong Dr. Kai Wang Dr. Svein Ersdal	
Title of master's thesis:  Dynamic Analysis of Feed Pipes for Fish Farming in Open Sea	
Credits: 30	
Keywords: - Aquaculture - Feed Pipes - OrcaFlex - GeniE, Wadam - Dynamic Analysis - Numerical modelling - Time domain - Hydrodynamics	Number of pages: .....90.....  + supplemental material/other: ...8.....  Stavanger, .....15.06.2017..... date/year





---

Universitetet  
i Stavanger

Dynamic Analysis of Feeding Pipes for Fish  
Farming in Open Sea

Asdren Gjuka

June 2017

MASTER THESIS

Dept. of Mechanical and Structural Engineering and Materials Science

University of Stavanger

Supervisor 1: Professor Muk Chen Ong

Co-supervisor 2: Dr. Kai Wang

Co-supervisor 3: Dr. Svein Ersdal



# Acknowledgment

This master thesis was written during the spring of 2017 and submitted to the University of Stavanger for partial fulfillment of the requirements for the degree of Master of Science in Marine-and Subsea Technology.

I would like to show my deepest gratitude to my supervisor Professor Muk Chen Ong. I am grateful for his guidance, patience and motivating words throughout this period. The passion he expressed for the field of Marine Technology has been an inspiration to me.

In addition, I would like to acknowledge Dr. Kai Wang from Aker Solutions for his valuable comments on this thesis and for being available through meetings. The expertise inhabited by him has proven to be a great resource to me.

My appreciation goes to Dr. Svein Ersdal from Aker Solutions for showing interest and spending time on the project. Thank you for sharing the knowledge you possess and for answering questions with a professional tone.

Finally, I would like to thank my beautiful family for the unconditional support and continuous encouragement throughout my years of study. My achievements would not have been possible without them.

Asdren Gjuka

*Stavanger, 15<sup>th</sup> June 2017*



# Abstract

The demand for seafood is continuously growing throughout the world, while the number of sheltered locations for fish farming is decreasing. Consequently, the industry is pushed to find new and innovative solutions to this problem. One solution is to move the fish farms in non-sheltered locations, which requires extensive research on all structural parts of a fish farm, including components of the feeding system.

The main goal of this thesis is to predict the hydrodynamic loads on feed pipes used by fish farmers in the industry, which is an important aspect of design to assure successful operation. The aquaculture industry has expressed the need for increasing the knowledge on feed pipes for fish farming. The bending of the pipes is of particular concern, especially when introducing non-sheltered locations.

The hydrodynamic loads of the feed barge were obtained by generating a finite element model in GeniE and performing hydrodynamic analysis in frequency domain with the potential solver Wadam. The displacement RAOs of the feed barge were imported into OrcaFlex after conducting a sensitivity-and convergence study to verify the results.

Dynamic simulations of the feed pipes were carried out in time domain using OrcaFlex, where the design basis was established using typical environmental and design data for Norwegian salmon farming. Analyses were performed under different sea, investigating different responses of the feed pipe. Due to the limited work available on the force coefficients for floating pipes on the sea surface, a sensitivity study regarding the force coefficients was carried out. It was concluded to implement a variable data set for the drag-and added mass coefficient of the feed pipes.

The results obtained for the selected cases resulted in high loads for all feed pipe lengths. The main problem that was found for the feed pipes was the large bending moment at the connection points, i.e. at the fish cage and the feed barge. For this reason, bend stiffeners at the connection points were installed. A reduction of 846% for the bending moment was observed with the bending stiffener attached to the pipe.

To conclude, the dynamic analysis exhibits too large hydrodynamic loads for offshore use. The use of bending stiffeners seems inevitable for the harsh environment in the open sea. More research on the feed pipes must be carried out to secure safe operation offshore.

# Contents

Acknowledgment . . . . .	i
Abstract . . . . .	ii
Nomenclature . . . . .	x
<b>1 Introduction</b>	<b>1</b>
1.1 Objective . . . . .	2
1.2 Outline of the Thesis . . . . .	3
<b>2 Fish Farming</b>	<b>4</b>
2.1 Fish Cages . . . . .	5
2.1.1 Relevant Scientific Research on Fish Cages . . . . .	6
2.2 Feeding System . . . . .	7
2.3 Feed Pipes . . . . .	10
2.4 Feed Barge . . . . .	12
2.5 Bend Stiffeners . . . . .	13
<b>3 Background Theory</b>	<b>15</b>
3.1 Environmental Conditions . . . . .	15
3.2 Wave Theory . . . . .	17
3.2.1 Linear Wave Theory . . . . .	17
3.2.2 Irregular Sea and the Wave Spectra . . . . .	20
3.3 Hydrostatics for a Floating Cylinder . . . . .	22
3.3.1 Water Plane Stiffness and Buoyancy . . . . .	23
3.4 Wave Loading for a Floating Horizontal Cylinder . . . . .	23
3.4.1 Hydrodynamic Forces . . . . .	24
3.4.2 Wave Forces on an Inclined Slender Cylinder . . . . .	25
3.4.3 Hydrodynamic Forces on Oscillating Objects . . . . .	26
3.4.4 Hydrodynamic Coefficients . . . . .	26



3.4.5	Drag Coefficient . . . . .	27
3.4.6	Added Mass Coefficient . . . . .	28
3.4.7	Effect of Free Surface . . . . .	29
3.5	The Response Amplitude Operator . . . . .	30
3.6	Frequency Domain . . . . .	33
3.7	Time Domain . . . . .	34
<b>4</b>	<b>Hydrodynamic</b>	
	<b>Modelling of Feed Barge</b>	<b>35</b>
4.1	Panel Model of Feed Barge . . . . .	36
4.1.1	Mesh Properties . . . . .	39
4.2	Frequency Domain Analysis of Hull . . . . .	40
4.2.1	Direction and Frequency Set . . . . .	41
4.3	Frequency Domain Results . . . . .	42
4.3.1	Sensitivity Study . . . . .	42
4.3.2	Optimal Frequency Set . . . . .	43
4.3.3	Convergence Study . . . . .	45
4.3.4	Summary . . . . .	47
<b>5</b>	<b>OrcaFlex -</b>	
	<b>Time-domain Analysis</b>	<b>49</b>
5.1	General Data . . . . .	49
5.1.1	OrcaFlex Coordinate System . . . . .	49
5.1.2	Statics . . . . .	50
5.1.3	Dynamics . . . . .	50
5.1.4	Line Model . . . . .	51
5.1.5	Integration and Time Steps . . . . .	54
5.2	Set-Up in OrcaFlex . . . . .	55
5.2.1	Environmental condition . . . . .	55
5.2.2	Modelling of Fish Cage . . . . .	57
5.2.3	Modelling of Feed Pipe . . . . .	58
5.2.4	Modelling of Feed Barge . . . . .	61
5.2.5	Modelling of Bend Stiffener . . . . .	61

<b>6</b>	<b>Dynamic Analysis -</b>	
	<b>Results &amp; Discussion</b>	<b>63</b>
6.1	Deformation of Net Under Current Flow . . . . .	63
6.2	Feed Pipe Analysis . . . . .	65
6.2.1	Sensitivity Study of Force Coefficients . . . . .	65
6.2.2	Conclusion from Sensitivity Study . . . . .	69
6.3	Pipe Configuration Study . . . . .	70
6.3.1	Case 1: 50m Pipe . . . . .	71
6.3.2	Case 2: Varying Lengths . . . . .	75
6.3.3	Case 3: Varying Line End Orientation at End B . . . . .	77
6.4	Pipe Responses With Bend Stiffener . . . . .	79
6.4.1	Validation of Design . . . . .	80
6.4.2	Case 4: Pipe Responses with BSR . . . . .	81
<b>7</b>	<b>Conclusion</b>	<b>84</b>
<b>8</b>	<b>Further Work</b>	<b>86</b>
	<b>Bibliography</b>	<b>87</b>
<b>A</b>	<b>Wadam Input</b>	<b>91</b>
<b>B</b>	<b>OrcaFlex Input</b>	<b>93</b>
B.1	General data . . . . .	93
B.2	Force Coefficients . . . . .	97

# List of Figures

- 2.1 Fish farm with feed barge, fish cages and feed pipes . . . . . 5
- 2.2 Typical fish cage . . . . . 6
- 2.3 Local feeding system . . . . . 8
- 2.4 Central feeding system . . . . . 9
- 2.5 Concept drawing . . . . . 10
- 2.6 Proposed feed pipe arrangement by Aker Solutions . . . . . 12
- 2.7 AC650 Panorama feed barge . . . . . 13
- 2.8 Conical bend stiffener . . . . . 14
  
- 3.1 Current velocity with respect to depth . . . . . 16
- 3.2 Sketch of progressive wave . . . . . 18
- 3.3 Water particle path . . . . . 20
- 3.4 Effect of the peak shape parameter for JONSWAP-spectrum . . . . . 22
- 3.5 Inclined cylinder . . . . . 25
- 3.6 Drag coefficient . . . . . 28
- 3.7 Variation of added mass with submergence . . . . . 29
- 3.8 Dry vs. fully submerged pipe . . . . . 30
- 3.9 Description of RAO . . . . . 32
- 3.10 Principle of transfer of waves into response . . . . . 33
  
- 4.1 Hydrodynamic modelling process . . . . . 35
- 4.2 GeniE modelling process . . . . . 36
- 4.3 Barge dimensions . . . . . 37
- 4.4 Illustration of hydrodynamic properties in GeniE . . . . . 38
- 4.5 Visualisation of mesh identity m2, i.e. 0.5 m element length . . . . . 40
- 4.6 Wadam - Required input data to run analysis . . . . . 40
- 4.7 Direction set - increment value of 15° between 0° and 90° . . . . . 41
- 4.8 Heave motion with coarse frequency . . . . . 42
- 4.9 Pitch motion with coarse frequency . . . . . 43

4.10	Roll motion with coarse frequency . . . . .	43
4.11	Heave motion with refined frequency . . . . .	44
4.12	Pitch motion with refined frequency . . . . .	44
4.13	Roll motion with refined frequency . . . . .	44
4.14	Comparison of frequency sets . . . . .	45
4.15	Convergence study in heave . . . . .	46
4.16	Convergence study in pitch . . . . .	47
4.17	Convergence study in roll . . . . .	47
5.1	OrcaFlex coordinate system . . . . .	50
5.2	Segmentation of Lines in OrcaFlex . . . . .	51
5.3	Declination angle . . . . .	52
5.4	Detailed mathematical model of Lines . . . . .	53
5.5	JONSWAP spectrum for EC1, EC2 and EC3 . . . . .	56
5.6	Side view and top view of the fish cage . . . . .	57
5.7	Feed pipe cross-section . . . . .	60
5.8	BSR profile graph . . . . .	62
6.1	Fish cage under various current velocities . . . . .	64
6.2	Sketch of model . . . . .	66
6.3	Comparison between the drag coefficient and the responses on the feed pipe	67
6.4	Illustration of Reynolds number and relative velocity of the pipe . . . . .	68
6.5	Comparison between the added mass coefficient and the responses on the feed pipe . . . . .	69
6.6	Coupled system in OrcaFlex . . . . .	70
6.7	Heave motion of barge . . . . .	71
6.8	Pitch motion of barge . . . . .	72
6.9	Roll motion of barge . . . . .	72
6.10	Range graph 50m . . . . .	73
6.11	50m long pipe results for different sea states . . . . .	75
6.12	Comparison of pipe length . . . . .	77
6.13	Comparison of different pipe length and declination angle . . . . .	79
6.14	Curvature vs. bending moment of feed pipe and bend stiffener . . . . .	81

6.15 The slamming force on feed pipe with BSR attached . . . . .	82
6.16 Comparison of responses with and without BSR . . . . .	83

# List of Tables

- 3.1 NS 9415 Wave classes . . . . . 16
- 3.2 NS 9415 Current classes . . . . . 17
  
- 4.1 Feed barge properties . . . . . 38
- 4.2 Mesh properties . . . . . 39
- 4.3 Comparison of frequency sets . . . . . 45
  
- 5.1 Environmental conditions used in dynamic simulation . . . . . 56
- 5.2 Fish cage characteristics . . . . . 58
- 5.3 Feed pipe dimensions . . . . . 58
- 5.4 Mechanical properties of HDPE . . . . . 59
- 5.5 Feed barge characteristics . . . . . 61
- 5.6 Protected region of feed pipe - Large BSR . . . . . 62
  
- 6.1 Pipe responses with different drag coefficients . . . . . 67
- 6.2 Pipe responses with different added mass coefficients . . . . . 68
- 6.3 Pipe responses with variable added mass . . . . . 69
- 6.4 Summary of results - 50 *m* pipe length . . . . . 74
- 6.5 Summary of results for sea state EC3 with wave direction of 90°- Varying  
lengths . . . . . 76
  
- B.1 Lines types . . . . . 96

# Nomenclature

## Acronyms

3D	Three-dimensional
BSR	Bend stiffener
DOF	Degree of freedom
FEM	Finite element method
HDPE	High-density polyethylene
JONSWAP	Joint North Sea Wave Project
KC	Keulegan-Carpenter
MBR	Minimum bend radius
RAO	Response amplitude operator
SDR	Standard dimension rate
SWL	Still water line

## Greek Symbols

$\nabla$	Volume of submerged part of object
$\omega$	Angular frequency
$\rho$	Density
$\sigma$	Stress
$\varphi$	Potential function
$\xi$	Wave amplitude

## Latin Symbols

$A_w$	Water plane area
$A$	Cross sectional area
$a$	Radius
$D_i$	Inner diameter of pipe
$D_o$	Outer diameter of pipe
$e$	Wall thickness
$H_s$	Significant wave height
$H_{max}$	Maximum wave height

$k_w$	Water plane stiffness
$k$	Wave number
$T_p$	Wave period
$u$	Wave velocity
$w_w$	Water pane width



# 1 | Introduction

Aquaculture has experienced tremendous growth during the past decades, due to the the increase in global demand for seafood. While the wild fisheries capture has been quite stable for the last 20 years, the aquaculture production has increased from around 20 to nearly 70 mill. metric tonnes (Bakketeig et al., 2016). Norway, which is the second major exporter of farmed fish after China, face great challenges related to technical and operational aspects of fish farming. The current fish farms in Norway are located in the fjords and in shallow waters along the coast. This is not sustainable with respect to both the environment and the fish welfare, so new solutions are inevitable. The biggest challenges of fish farming today are space limitation, sea lice, spreading of sickness and environmental pollution. As a result, the Directorates of Fisheries in Norway has announced development licenses that can be awarded to companies with new concepts which can cope with the challenges.

One of the promising solutions is to move the fish farms out in exposed locations. This could potentially eliminate and reduce the challenges discussed above. Due to the large change-out of water, the environment for the fishes will be better. Also, the larger area in the exposed locations could reduce the local environmental impact, caused by the produced waste by the fishes. The sea lice problem could also be eliminated by moving to deeper waters, which is a major driver to reallocate the fish farms to open waters.

By moving the fish farms towards more exposed locations, there will naturally be greater hydrodynamic loads acting on the fish farm. The environmental loads, such as waves, currents and winds are much higher in non-sheltered locations than of sheltered locations, so care should be taken. This introduces new types of challenges with respect to operations, structural integrity and equipment. The feed pipes used for fish farming is of interest, due to the high operational cost of the feeding system. Because of the general lack of knowledge in feed pipes for offshore use, the industry eagerly wants to increase the research on this topic.

## 1.1 Objective

The objective of this thesis is to conduct dynamic analyses and study the responses on feed pipes used by the aquaculture industry for feeding of fishes. Time domain simulations in exposed sea should be done, studying the responses like effective tension and bending moment are of particular interest. A study on different configurations should be done.

The selection of the correct force coefficients for the floating feed pipe is an essential part of the thesis since previous work on the subject is very limited. It has been placed great emphasis on the drag and added mass coefficient throughout the thesis. A study on how the force coefficient affects the loads on the pipe should be conducted.

To obtain an accurate description of the fish farm system, both the fish cage and the feed barge should be modelled. The feed barge should be modelled in the frequency domain to obtain the displacement RAOs.

As a consequence of high environmental loads on the feed pipe, measures to control the bending of the pipe should be implemented. Therefore, bend stiffeners at termination points should be designed and installed.

## 1.2 Outline of the Thesis

**Chapter 1** is an introduction to the thesis work, with motivation and objectives of the work which should be done.

**Chapter 2** gives a description of the main components in a fish farm system. The chapter serves as an literature review, highlighting the main challenges expressed by the industry today.

**Chapter 3** presents the theory necessary to estimate the hydrodynamic loads on the feeding pipes. Environmental conditions by NS9415 is briefly discussed. The potential function is explained together with wave loads described by the Morison equation.

**Chapter 4** presents the hydrodynamic modelling of the feed barge in frequency domain. A general description of the software utilised, as well as results from the hydrodynamic results, is presented and discussed.

**Chapter 5** introduces OrcaFlex as the time domain analysis software used in the thesis. Relevant background theory about OrcaFlex is presented, followed by the modelling set-up of the fish farm system.

**Chapter 6** presents the result and discussion from the dynamic simulations conducted in OrcaFlex. A short study on the fish cage is showed, followed by a feed pipe configuration study. The effect of the given sea states is discussed, as well as the effect of different pipe lengths and declination angle. The chapter ends with a study on the feed pipe with bending stiffener attached to the feed pipe.

**Chapter 7** presents the conclusion of the report, where the main findings is presented.

**Chapter 8** discusses the future work needed to improve the numerical model.

## 2 | Fish Farming

Aquaculture has been around for thousands of years, but it is not until the past two decades the aquaculture production has surpassed the wild capture of aquatic organisms. The aquaculture industry has expanded tremendously the past decade due to the increase in worldwide global demand for aquatic products, which in turn has accelerated the technological development with innovative solutions. As mentioned previously, the growing market demand for sea products and competition for land and water space, are motivating factors for the development of farming structures in open waters (Cardia and Lovatelli, 2015).

A fish farm has many advanced technical components, and may be roughly summarised as following components (Lekang, 2013):

- Production unit
- Feeding equipment
- Working boat
- Base station

Figure 2.1 illustrates the major technical components that make up a fish farm.

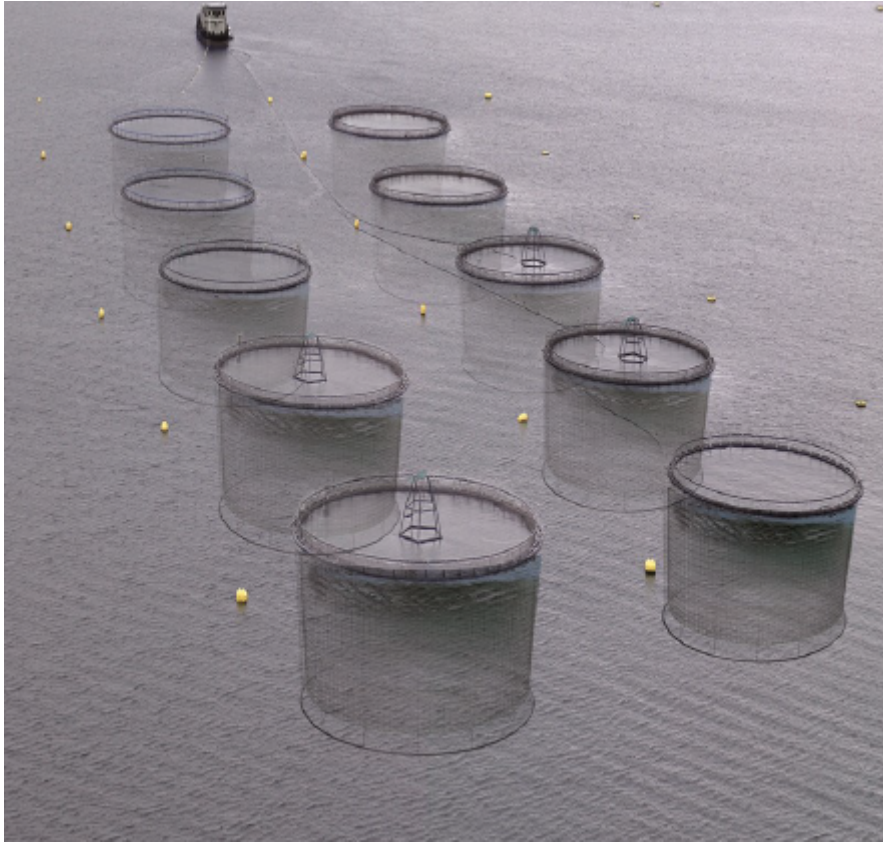


**Figure 2.1:** Typical fish farm with feed barge, fish cages and feed pipes (AKVA Group ASA, 2015b)

## 2.1 Fish Cages

Fish cages used in the aquaculture industry vary a lot both in shape and size. There exist many geometries of cages, where the cylindrical cage is the most frequently used.

The most popular fish farm design used today is the cage farming design, with high-density polyethylene (HDPE) floating cages as the main material selection. HDPE is a highly versatile material, with simple handling and low overall cost. A typical fish cage structure is made up of HDPE pipes producing collars of different shapes and sizes. The fish net pen is attached to the floating collar, forming a fish cage. The fish net pen maintains the shape and volume by fixing a series of weights at the bottom of the fish net pen, called a sinker system. Such systems are called gravity cages, which are widely used in the industry (Cardia and Lovatelli, 2015). The main parts of a fish cage are (Lekang, 2013):

- A cage collar to provide buoyancy and spread the net
- A net bag with weights in the bottom
- A mooring system
- A jumping net to prevent fish escape

Figure 2.2 below illustrates a simple cylindrical fish cage with HDPE as the main material selection.

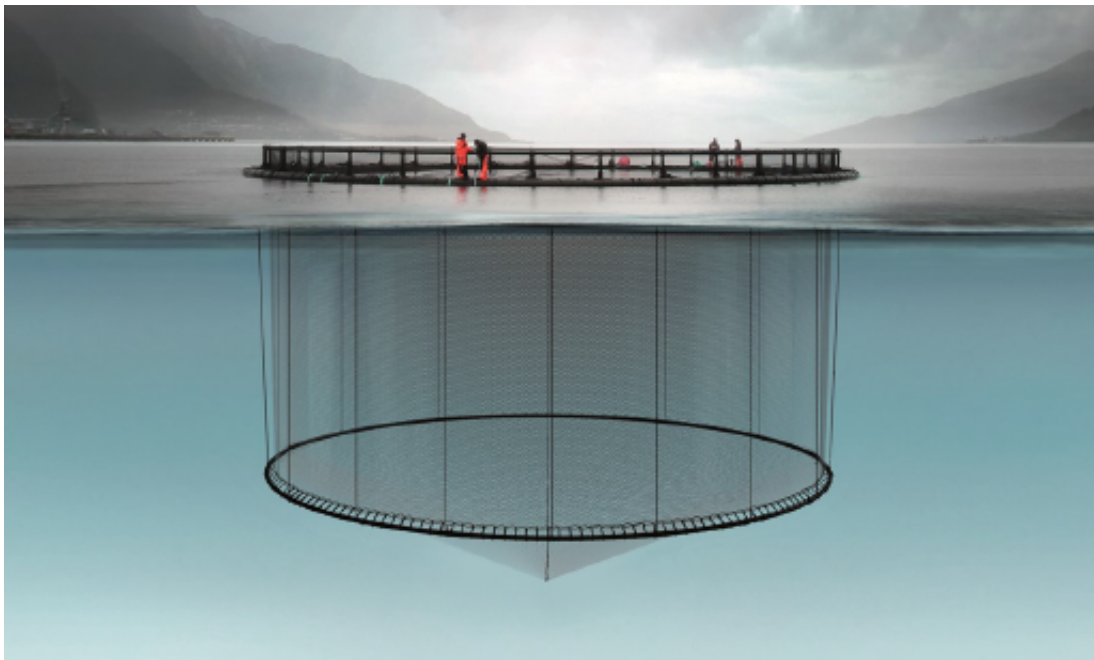


**Figure 2.2:** Typical fish cage (AKVA Group ASA, 2015b)

Fish cage systems are influenced by various oceanic conditions, where the safety of the system can be compromised by the movement and deformation of the system. The next section discusses some of the research done on this topic.

### **2.1.1 Relevant Scientific Research on Fish Cages**

In recent years, a lot of research has been done on fish cages used for aquaculture. Since the industry is looking to move the fish farms in exposed locations, extensive research such as hydrodynamic analysis and structural analysis has been done. One of the major challenges

is the reliability of the framework and the nets on fish cages in exposed locations, where waves and current are more extreme.

The dynamic response of a fish cage is a popular topic among researchers in the community. The focus is on the motion behaviour, i.e. the displacement and deformation caused by waves and current. The drag force is also a major issue concerning the solidity of the net and the attack angle.

Thomassen (2008) analysed a floating fish farm in waves by nonlinear FEM. The simulation was done in time-domain of a nonlinear structure in irregular waves. The main finding was that a linear analysis yields a more conservative result than a nonlinear analysis. A fatigue analysis was also done, showing that it is realistic to design a steel floater for a 20-year fatigue life.

Lee et al. (2015) did a dynamic behaviour and deformation analysis of a fish cage system using mass-spring model. The cage consisted of netting, mooring ropes, floats, sinker and floating collar. All the elements were modelled by use of the mass-spring model. The structures were divided into finite elements and mass points were placed at the mid-point of each element. The model can be applied to analyse the performance of fish cages against currents and waves.

Lader and Enerhaug (2005) conducted an experimental investigation of forces and geometry of a net cage in uniform flow using a vertical-type circular water channel driven by four impellers. The model was composed of a ring, a net and several of weights attached to the bottom of the net. The main findings from the experiment, show that the forces on and the deformation of a flexible net structure are mutually independent on each other. Also, the global forces on a flexible net structure give large errors using simple drag formulas derived from stiff net experiments.

## 2.2 Feeding System

To assure successful operation of a fish farm, a reliable system for feeding the fish is vital. A system that takes the feed from the storage unit, transport it to the fish production and at the end distributes it to the fish, is called a feeding system (Lekang, 2013). By

optimising the feed system, production efficiency is increased, enhancing both the quality of the product and increasing profit. In an efficient fish farm, feed accounts for roughly 50-75 percent of the overall operating cost, making the feed system one of the main operational issues (Cardia and Lovatelli, 2015). The environmental impact is also reduced if the feed system is handled in the correct way. This is particularly important for exposed sites, where safety and reliable operation is crucial.

Feeding can be done by hand or by automatic feeding systems, where the latter is preferred for large fish farms. In essence, all feeding systems are either automatic or semi-automatic. The feeding can be divided into two categories; local or central system (Sunde et al., 2003). The local feeding system works by having a food storage on each fish pen whereas the latter works by transporting the food from a central feeding barge through transportation pipes. The local system, as seen in Figure 2.3, consist of having the feed silo and the spreader/canon attached to the fish cage floater. Several other solutions exist such as placing the feed storage on a working station or a service vessel.



**Figure 2.3:** Local feeding system (Betten Maskinstasjon, 2016)

The centralised feeding system serves many cages at once from a single location where the feed is stored, often on a purposely built barge. The system is highly advanced and



consists of many components, such as:

- Feed silos
- Energy unit for power delivery
- Air blowers and air generators
- Distribution systems
- Feed delivery pipes
- Feeder control system
- Rotor spreaders and feed canons

The amount of feed used in the centralised feeding system is often decided by advanced software and detectors based on technology such as sonar, lift-up and cameras (Sunde et al., 2003). Figure 2.4 below shows a central feeding system by AKVA Group ASA. From the central feed silos, the feed is transported to the fish cages through a feed pipe. The centralised feed system suits larger fish farms with many cages located at the same place.



**Figure 2.4:** Central feeding system, Akvasmart (AKVA Group ASA, 2015b)

## 2.3 Feed Pipes

The transportation method for the feed between the centralised feeding system and the fish cages is done by using feed pipes. The material selection for feed pipes is mainly HDPE, which is well-suited for use in ocean environment. Main advantages of HDPE pipes are no galvanic corrosion or decay and virtually no risk of marine growth accumulating on the pipes (Pipelife Norge AS, 2002). The density of HDPE is about 94% of salt water, which makes the feed pipes float on the water surface. This allows for easy installation and maintenance of the pipes. The pipes are also flexible, which makes it suitable for the rough weather conditions in open sea, allowing the pipe to follow the wave condition. Even though HDPE pipes are well-suited offshore, the lifetime of feeding pipes today are considered short in relation to the fish cages, so even shorter lifetime is expected in exposed locations.

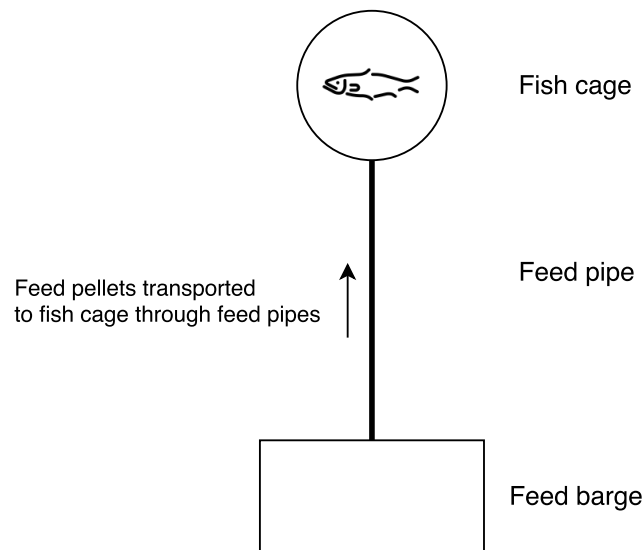


**Figure 2.5:** Concept drawing showing the purpose of feed pipes

The feed is driven by compressed air from the feed silos to the fish cages through the pipes floating on the water surface. With a maximum feed capacity of 5000-11520 kg/hr, depending on the type of equipment and the length of the pipe, one can understand the importance of having a feed system that operates smoothly. The high pressure necessary to transport the feed can make the air inside the pipes warm. This can melt the fat from the feed pellets, contributing to clogging of the pipes. Also, the crushing of feed pellets is

a concern due to the high air speed and the routing of the pipe (Sunde et al., 2003). New developments to minimise the crushing has been made, such as driving the feed with sea water instead of air has shown success with respect to lowering the crushing of the feed pellets. Feed pipe cleaners have also been introduced to the market, potentially saving fish farmers for thousands of NOK. Also, new feed pipes with transparent material reduce the heating from the sun and make it easier to prevent and locate accumulation of feed dust.

According to Lillevik (2014), another challenge related to feed pipes is the interaction between feed pellets and the HDPE pipe, which accumulates static electricity and may endanger the life and health of working personnel. When doing maintenance work, such as cutting the pipe, powerful electrical shock may be fatal for the user. Handling of the feed pipe can therefore be a risky operation for both people and equipment. The development of antistatic HDPE pipes has thus increased by request from the industry, which eliminates the risk of electric shock and securing the health of working personnel. More information about the accumulation of electricity in feed pipes can be found in the SINTEF report (Lillevik, 2014).

Regardless of what kind of system is used, correct design and use of the feed pipes is important to avoid breakage and downtime in production. A significant amount of focus and work is done on reducing the amount of feed crushed during transport from the feed silo to the fish cages. The most important factors to avoid this is (Sunde et al., 2003):

- Compressed air pressure
- Temperature and speed of the compressed air
- Design of feed silo
- Design and material selection of feed pipes
- Bending of feed pipes

The mentioned factors should be even more taken care of when moving the fish farms to exposed location. The configuration of the feeding pipes is also a concern for the fatigue performance of the pipes. Aker Solutions has proposed a configuration of the pipes shown in Figure 2.6 below.

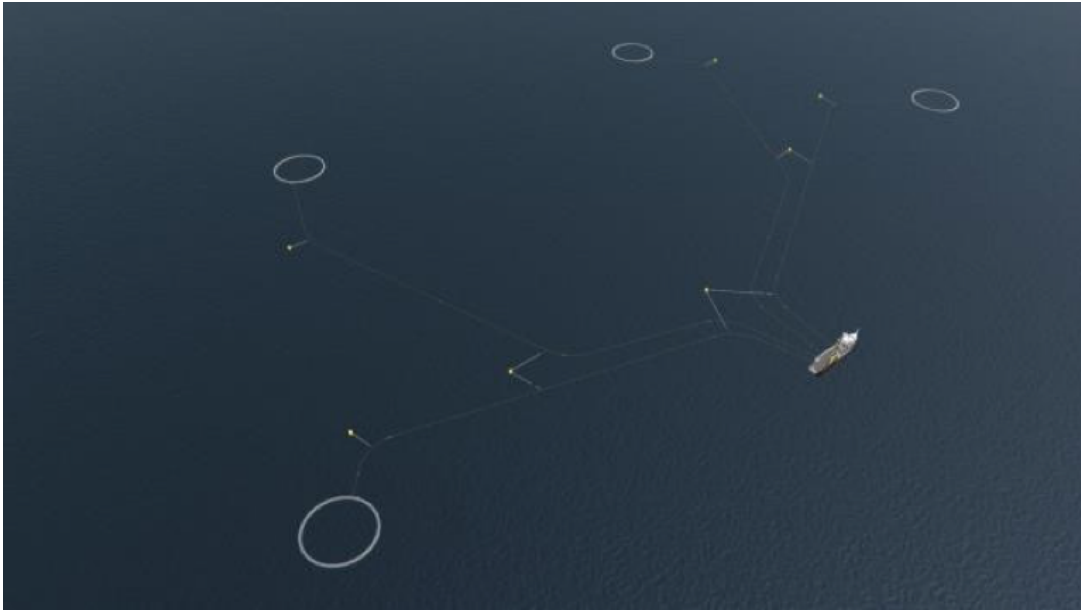


**Figure 2.6:** Proposed feed pipe arrangement by Aker Solutions

## 2.4 Feed Barge

For distances larger than 500 *m* between land and the fish cages, the storage unit for the feed is often on a feed barge. As the fish farms are located further out on the sea, the feed barge is often considered as the heart of the fish farm. The feed barges are constructed of either steel or concrete and is a floating storage unit which serves as a workstation for personnel. Feed barges can be designed for a wide range of sites and climates, from operational use within the fjords to offshore areas. Modern feed barges include feed systems, generators, control rooms, living quarters and equipment. A sophisticated feed barge is thus necessary to maintain production at a desirable level and make operations run smoother. The storage capacity of a single feed barge varies from about 100 up to 850 metric tonnes of feed depending on the size of the barge and the size of the fish farm. Feed pipes are connected to the feed barge with a rigid connection and can have as much as twelve parallel feed pipes running at once. It is desirable to decrease the distance between the feed barge and the fish cages due to the challenges discussed in Section 2.3. Since the fish farms in recent years are placed further out on the sea, the feed barges are designed so that it can handle rougher sea. The demand for the increase in knowledge regarding stability and loads of feed barges has increased in recent years, so research on the topic

is inevitable.

Feed barges in Norway must follow rules and regulations set by the following certification societies:

- Standard Norge
- NYTEK
- DNV
- NMD

Figure 2.7 illustrates one of the largest feed barges by AKVA Group ASA. The feed silos are shown inside the barge and the feeding system (yellow) is attached on the hull of the barge.

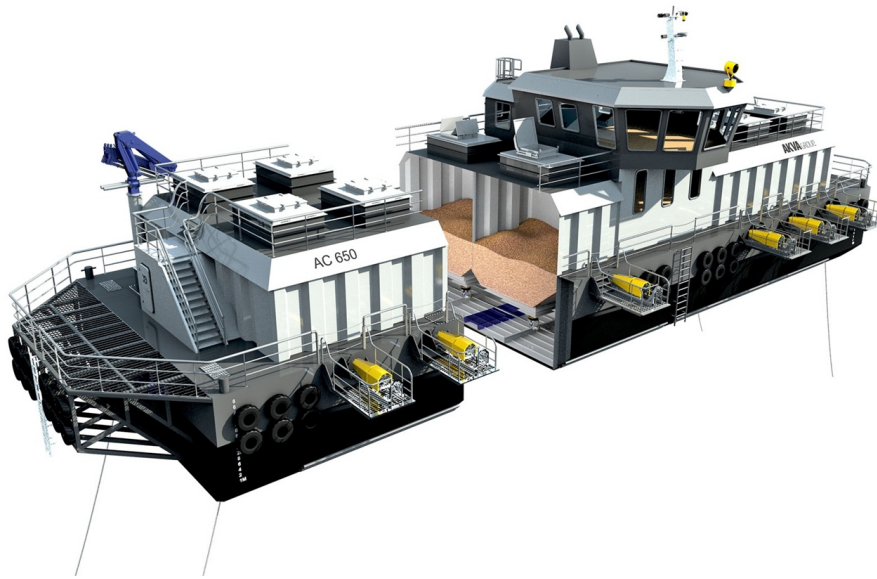


**Figure 2.7:** AC650 Panorama feed barge (AKVA Group ASA, 2015a)

## 2.5 Bend Stiffeners

The dynamic loading during operation and the loads during installation of feed pipes can cause over-bending, where failure through e.g. collapse, rupture or kinking may occur (Trelleborg, 2016). A bend stiffener (BSR) is a bend restrictor device that provides stiffness to the protected line in order to distribute the bending more widely. It is used

extensively in the petroleum industry to secure the structural integrity of risers. The BSRs main purpose is to maintain the manufacturers recommended bend radius (MBR), by distributing the load and reducing the point loading at the termination of the pipe. The BSR has typically a conical shape, which can be seen in Figure 6.16. This conical shape gradually increases the overall stiffness on the protected line, making the protected line more resistant to bending (Trelleborg, 2016).

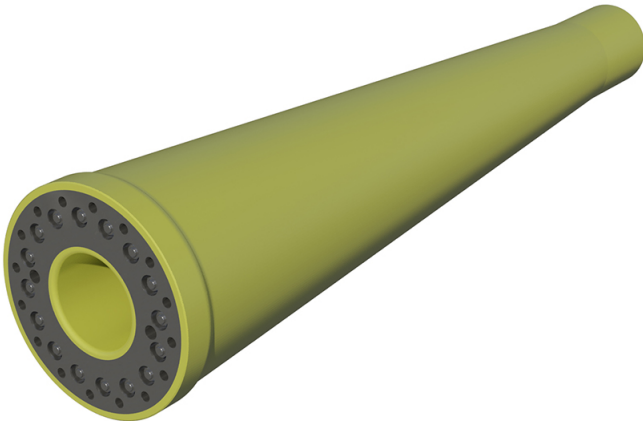


**Figure 2.8:** Conical bend stiffener (Trelleborg, 2016)

## 3 | Background Theory

In this chapter necessary theory for understanding the hydrodynamic loads on the feeding pipe will be introduced and discussed. Basic theory such as linear potential theory is presented, whereas the wave loads on the feed pipe are explained by the Morison equation. Since research and experiments on floating pipes are limited, especially on feed pipes for fish farming, one of the main challenge is to determine the hydrodynamic coefficients for a floating pipe on the sea surface.

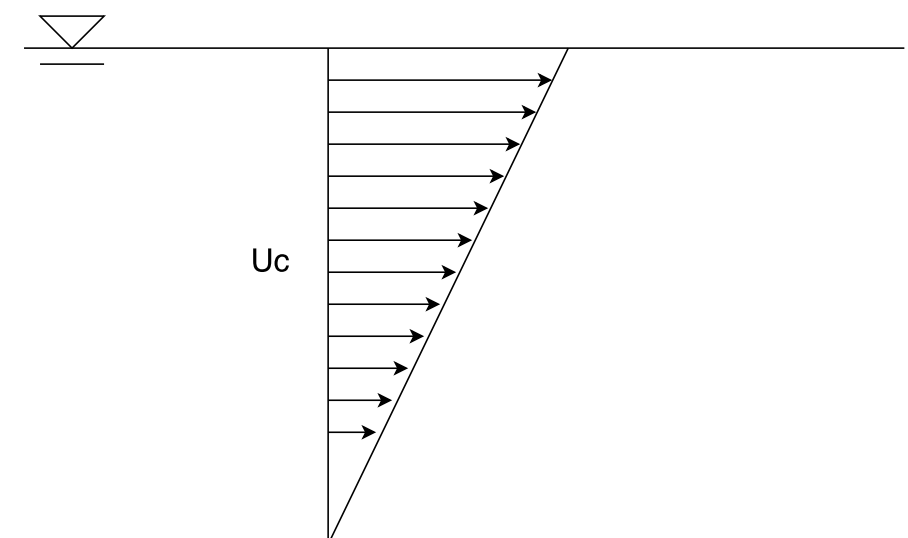
### 3.1 Environmental Conditions

In this section, the environmental conditions for waves and current are discussed. The standard used for fish farming in Norway today is defined by Norsk Standard NS 9415 (Standard Norge, 2003). The wave classes in NS 9415 specifies typical wave conditions in Norway and its intention is to reduce the risk of fish escape as a result of structural failure of the fish farm. According to NS 9415 (Standard Norge, 2003), the wave classes can be specified in the given intervals as shown in Table 3.1. The wave classes of interest for this thesis are the classes which give high and extreme exposure. This is due to the fact that fish farms are moving more and more into exposed locations. Wave class D and E is therefore considered in the dynamic analysis, with a water depth of  $40m$ . The waves have a 50-year return period, i.e. 2% chance of annual exceedance and are wind-generated which means that swells are neglected.

**Table 3.1:** NS 9415 Wave classes

Wave classes	$H_s$ [m]	$H_{max}$ [m]	$T_p$ [s]	Designation
A	0.0 - 0.05	0.0 - 0.95	0.0 - 2.0	Light exposure
B	0.5 - 1.0	0.95 - 1.9	1.6 - 3.2	Moderate exposure
C	1.0 - 2.0	1.9 - 3.8	2.5 - 5.1	Large exposure
D	2.0 - 3.0	3.8 - 5.7	4.0 - 6.7	High exposure
E	>3.0	>5.7	5.3 - 18.0	Extreme exposure

Current can be described by several different categories, where wind generated currents are the most usual one. This is caused by wind stress throughout a storm. A rule of thumb is that the wind generated current is 2% of the wind velocity, where a long fetch length can increase the current velocity (Standard Norge, 2003). The wind current is strongest at the surface and decreases with depth, as shown in Figure 6.1.

**Figure 3.1:** Current velocity with respect to depth

Current is of particular interest for the operational aspect of a fish cage, because of the deformation of the net pen caused by current current. This is a major issue in industry, so a lot of time and money is spent on this particular concern. Table 3.2 below shows the current classes in defined by NS 9415 (Standard Norge, 2003).



**Table 3.2:** NS 9415 Current classes

Current classes	Uc [m/s]	Designation
a	0.0 - 0.3	Light exposure
b	0.3 - 0.5	Moderate exposure
c	0.5 - 1.0	Large exposure
d	1.0 - 1.5	High exposure
e	>1.5	Extreme exposure

## 3.2 Wave Theory

### 3.2.1 Linear Wave Theory

Linear wave theory gives a linearised description of gravity waves on the surface of a fluid. The theory is one of the simplest forms of describing ocean waves and is considered the core of marine technology. Some assumptions of the fluid are necessary to state before introducing the potential function (Massie and Journée, 2001):

- Constant mass flow
- Incompressible fluid – no change in density
- No friction in fluid – ideal fluid
- Irrotational fluid – no rotation of mass with respect to the centre of gravity

Waves can be regular or irregular, unidirectional or omnidirectional, linear or nonlinear (Sarpkaya, 2010). Figure 3.2 below illustrate a progressive linear wave by a uniform sinusoidal shape.

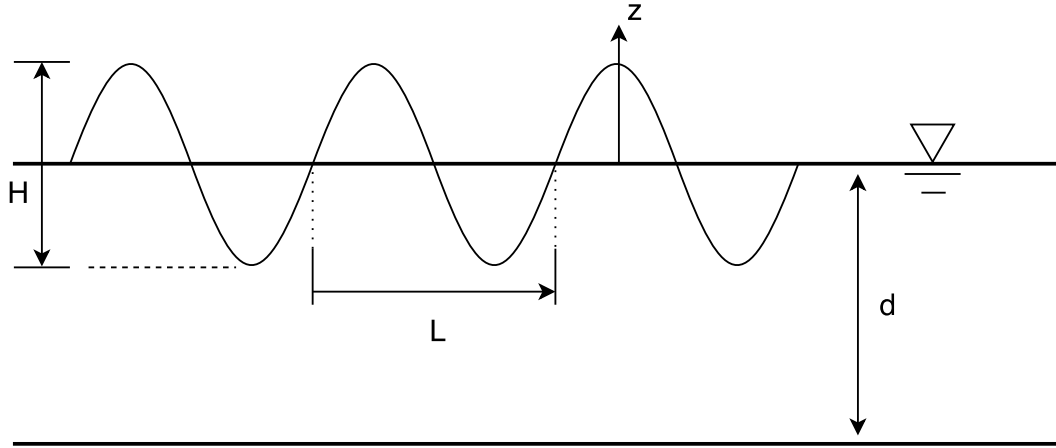


**Figure 3.2:** Sketch of progressive wave

The potential function for linearized conditions is derived from the Laplace equation by using the dynamic boundary conditions given by the equation below (Gudmestad, 2015)

$$\varphi(x, z, t) = \frac{\xi_0 g \cosh k(z + d)}{\omega \cosh(kd)} \cos(\omega t - kx) \quad (3.1)$$

where  $\xi_0$  is the amplitude of the wave,  $g$  is the acceleration of gravity,  $\omega$  is the angular frequency,  $k$  is the wave number,  $d$  is the water depth,  $z$  is the reference depth,  $t$  is time and  $x$  is position. From the potential function, velocities and accelerations of water particles horizontally and vertically under the wave can be determined by taking the derivative of the potential function, as shown below

$$u = \frac{\partial \varphi}{\partial x}, \quad \dot{u} = \frac{\partial u}{\partial t}, \quad w = \frac{\partial \varphi}{\partial z}, \quad \dot{w} = \frac{\partial w}{\partial t}$$

where  $u$  and  $\dot{u}$  represent the velocity and the acceleration in the horizontal plane, whereas  $w$  and  $\dot{w}$  represent the velocity and acceleration in the vertical plane.

The potential function can be simplified by using the deep water classification. The term "deep water" is used in the offshore industry for water depth of 500 meters or more. However, it might be interesting to relate water depth to wave length and do a classification with respect to this relation, expressed by the equation below (Gudmestad, 2015)

$$\frac{d}{L} > 0.5 \quad (3.2)$$

By using the deep water classification, the potential function can be expressed as

$$\varphi_{deep}(x, z, t) = \frac{\xi_0 g}{\omega} e^{kz} \cos(\omega t - kx) \quad (3.3)$$

where the velocities in deep water is

$$u_{deep} = \frac{\xi_0 g}{\omega} e^{kz} \sin(\omega t - kx) \quad (3.4)$$

$$w_{deep} = \frac{\xi_0 g}{\omega} e^{kz} \cos(\omega t - kx) \quad (3.5)$$

as well as the acceleration in deep water

$$\dot{u}_{deep} = \xi_0 k g e^{kz} \cos(\omega t - kx) \quad (3.6)$$

$$\dot{w}_{deep} = -\xi_0 k g e^{kz} \sin(\omega t - kx) \quad (3.7)$$

Another important parameter for wave kinematics is the wave number  $k$ , which can be expressed, for deep water, by the following equation

$$k = \frac{2\pi}{L} \quad (3.8)$$

and the wavelength  $L$  can be expressed by the dispersion relation for deep water

$$\omega^2 = gk \quad (3.9)$$

$$\left(\frac{2\pi}{T}\right)^2 = g \frac{2\pi}{L} \quad (3.10)$$

$$L = \frac{g}{2\pi} T^2 \quad (3.11)$$

Figure 3.3 below illustrates the particle paths and the direction of the velocity with depth, where it is shown that the velocity decreases with depth (Sarpkaya, 2010).

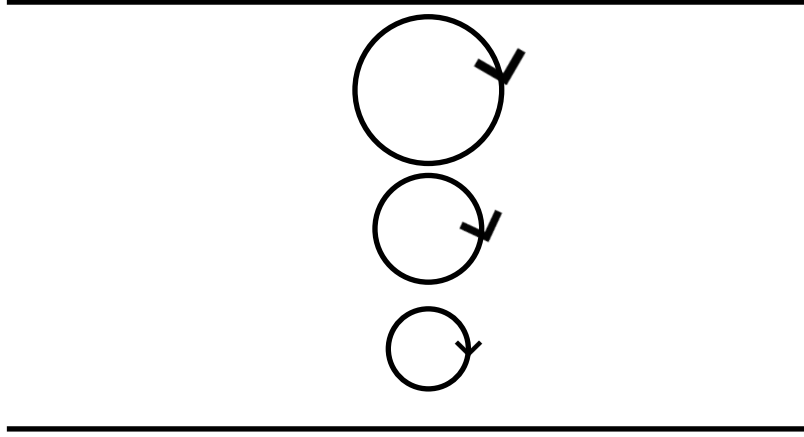


**Figure 3.3:** Water particle path

### 3.2.2 Irregular Sea and the Wave Spectra

Waves can be described as both regular and irregular waves. Regular waves propagate with permanent form, whereas irregular waves can be called random waves and is a stochastic process in nature. In practice, linear wave theory is used to simulate irregular sea. The wave elevation of a long-crested irregular sea propagating along the positive  $x$ -axis described by a sea spectrum  $S(\omega)$ , can be written as the sum of a large number of wave components, i.e. (Faltinsen, 1990)

$$\xi = \sum_{j=1}^N A_j \sin(\omega_j t - k_j x + \epsilon_j) \quad (3.12)$$

where  $A_j$ ,  $\omega_j$ ,  $k_j$  and  $\epsilon_j$  is respectively the wave amplitude, circular frequency, wave number and random phase angle of wave component  $j$ . The random phase angles are distributed uniformly between 0 and  $2\pi$  and constant with time. The amplitude  $A_j$  can be expressed from the sea spectrum  $S(\omega)$  using the following expression

$$\frac{1}{2} A_j^2 = S(\omega_j) \Delta\omega \quad (3.13)$$

where  $\Delta\omega$  represents a constant difference between successive frequencies. The wave spectrum can be estimated from wave measurements and is usually expressed as a short-term description of the sea, i.e. less than 10-hours (Faltinsen, 1990). The measurements are based on constant significant wave height  $H_s$  and wave peak period  $T_p$  for short-term

sea states because the parameters are not likely to change within the time interval. The significant wave height  $H_s$  is defined as the mean of the one-third highest waves and the wave period  $T_p$  is the peak period for which the maximum energy density appears.

Wave spectrum is used to define the energy of a sea state within a short-term condition, as mentioned previous. In order to realise a random sea state, parameters such as  $H_s$ ,  $T_p$ , the wave direction and the wave peakedness  $\gamma$  must be defined. Many different spectra have been developed over the years, with Pierson-Moskowitz spectrum and JONSWAP spectrum being one of the most used in the field.

### Pierson-Moskowitz Spectrum

The Pierson-Moskowitz (PM) spectrum is one of the simplest descriptions of the energy distributions and was developed in 1964 by Pierson and Moskowitz. The spectrum describes fully developed sea, i.e. the waves and wind will reach eventually reach equilibrium as a consequence of winds blowing steadily over large distances for several days (Gudmestad, 2015). According to DNV-RP-C205 Section 3.5.5.1 DNV-GL (2010b), the PM spectrum can be expressed in the following way

$$S_{PM}(\omega) = \frac{5}{16} \cdot H_s^2 \omega_p^4 \cdot \omega^{-5} \exp\left(-\frac{5}{4} \left(\frac{\omega}{\omega_p}\right)^{-4}\right) \quad (3.14)$$

where  $H_s$  is the significant wave height,  $\omega_p$  is the spectral peak frequency and  $\omega$  is the angular frequency.

### JONSWAP Spectrum

The JONSWAP spectrum can describe sea conditions under developing wave conditions and was established during a joint research project called "Joint North Sea Wave Project" (Gudmestad, 2015). The JONSWAP spectrum is similar to the PM spectrum except that waves continue to grow with distance, i.e. it describes developing sea and not a fully developed sea. The JONSWAP spectrum can be expressed by the following manner (DNV-GL, 2010b)

$$S_J(\omega) = A_\gamma S_{PM}(\omega) \gamma \exp\left(-0.5 \left(\frac{\omega - \omega_p}{\sigma_s \cdot \omega_p}\right)^2\right) \quad (3.15)$$

where  $A_\gamma$  is the normalising factor,  $\gamma$  is a parameter representing the peak shape of the spectrum. The spectral width parameter,  $\sigma_s$ , varies between  $\sigma_a$  and  $\sigma_b$  depending on the frequency  $\omega$ . Figure 5.5 below illustrates an example of the JONSWAP spectrum with different peak shape parameter (DNV-GL, 2010b)

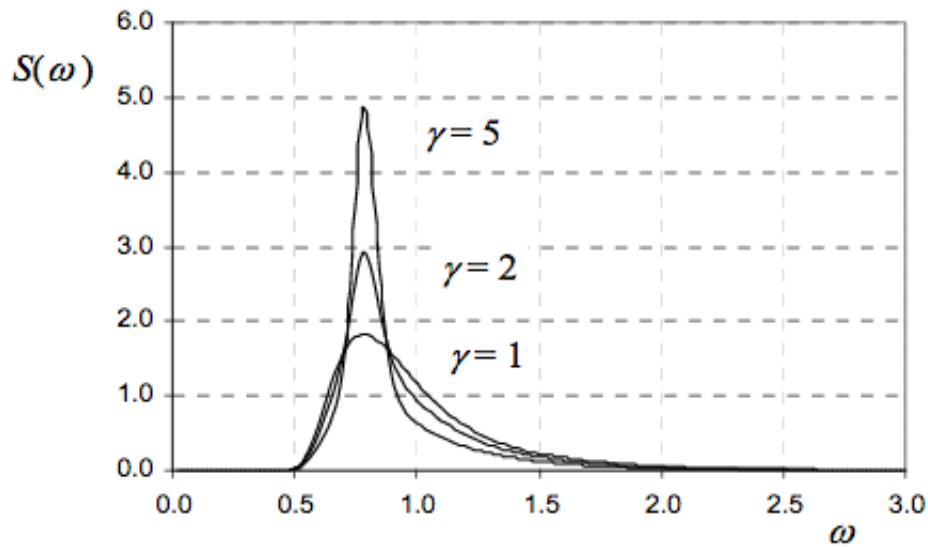


**Figure 3.4:** Effect of the peak shape parameter for JONSWAP-spectrum (DNV-GL, 2010b)

### 3.3 Hydrostatics for a Floating Cylinder

The starting point of hydrodynamic analysis is the structure weight and buoyancy force balance. It is important for the success of the hydrodynamic analysis that the hydrostatics are mentioned, even though it might be trivial.

### 3.3.1 Water Plane Stiffness and Buoyancy

According to Archimedes law, the upward buoyant force,  $F_{\nabla}$  is given by (Massie and Journée, 2001)

$$F_{\nabla} = \rho g \nabla \quad (3.16)$$

where  $\nabla$  is the volume of submerged part of the object.

The buoyancy of a cylinder floating on the sea surface is given by the distributed buoyancy, which is dependent on the level of submergence of the cylinder,  $A_{sub}$  (Thomassen, 2008)

$$B_{distr} = \rho_w g l_w A_{sub} \quad (3.17)$$

For a floating cylinder, the water plane area is the product of water plane length  $l_w$  and water plane width  $w_w$ , given by

$$A_w = l_w * w_w \quad (3.18)$$

For the water plane stiffness  $k_w$ , it is assumed that both the free surface and the cylinder are horizontal, and can be expressed by (Thomassen, 2008)

$$k_w = \rho_w g A_w \quad (3.19)$$

## 3.4 Wave Loading for a Floating Horizontal Cylinder

The feed pipe can be considered as a slender cylinder subjected to wave loads. Since the pipe is floating on the sea surface, several challenges like nonlinearities are introduced by higher waves. The following hydrodynamic theory can be considered as relevant for a floater (Thomassen, 2008):

- Wave loads and motions  $\rightarrow$  based on linear potential theory
- Wave loads on slender structures  $\rightarrow$  represented by Morison for fully submerged body

- Water impact and entry → slamming

In the case of a fixed vertical cylinder submerged in the water, the Morison equation is extensively used in the industry to find the forces that act on the cylinder. Morison equation is a well-known formula with a lot of research available. The formula is based on experiments and is originally used to calculate hydrodynamic loads on fixed vertical cylinders.

### 3.4.1 Hydrodynamic Forces

As discussed in the previous section, Morison's equation is often used to calculate wave loads on vertical circular cylindrical structural members of fixed offshore structures. The Morison equation is composed of the drag and inertia forces linearly added together, and is given by (Faltinsen, 1990)

$$dF = f_M(z, t) + f_D(z, t) = \rho_w \frac{\pi D^2}{4} C_M \dot{u} + \frac{\rho}{2} C_D D u |u| \quad (3.20)$$

where  $dF$  is the horizontal force per unit length on a vertical rigid circular cylinder,  $\rho_w$  is the water density,  $D$  is the diameter of the cylinder,  $u$  is the horizontal wave-induced water particle velocity,  $\dot{u}$  is the horizontal wave-induced water particle acceleration,  $C_D$  is the drag coefficient and  $C_M$  is the inertia coefficient. Equation 3.20 is the sum of the mass and drag force with the corresponding coefficients  $C_M$  and  $C_D$ . When the drag force is significant, i.e. when the structure is small compared to the wave length, the Morison equation can be applied. The total force acting on the entire cylinder can be expressed by

$$F(t) = \int_0^{surface} dF dx = \int_{-d}^{\xi} f_M(z, t) dz + \int_{-d}^{\xi} f_D(z, t) dz \quad (3.21)$$

Morison's equation is only applicable when the following criteria are fulfilled (Faltinsen, 1990):

- Non-breaking waves;  $H/L < 0.14$
- $D/L < 0.2$  (slender body)
- $a/D < 0.2$



### 3.4.2 Wave Forces on an Inclined Slender Cylinder

For inclined cylinders, an extension of the Morison equation is written in terms of the accelerations and the normal velocity (Chakrabarti, 1987). Figure 3.5 illustrates the force vectors which is decomposed into three components.

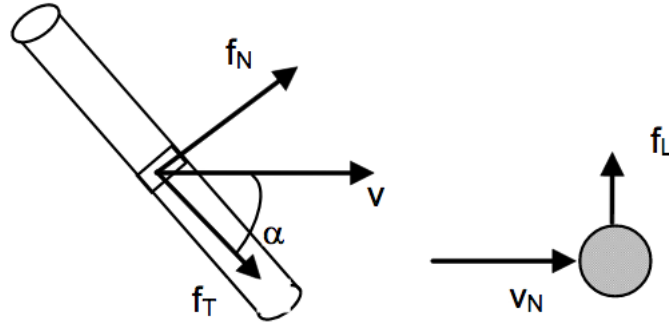


**Figure 3.5:** Normal force, tangential force and lift force on the cylinder (DNV-GL, 2010b)

According to Li et al. (2007), which analysed a straight floating pipe under wave conditions, the normal force and tangential force can be expressed in the following way

$$\text{Normal force : } f_N = \frac{1}{2} \rho C_n D v_n |v_n| \quad (3.22)$$

$$\text{Tangential force : } f_T = \frac{1}{2} \rho C_t D v_n |v_n| \quad (3.23)$$

where  $C_n$  is the drag coefficient normal to the pipe, and depends on the Reynolds number and the incident angle of the flow.  $C_t$  is the tangential drag coefficient which is mainly due to the skin friction of the element and can be treated as a constant. The tangential drag coefficient can be written as

$$C_t = C_f \cdot C_n \quad (3.24)$$

where the material dependent parameter,  $C_f$ , is equal to 0.02 for smooth circular cylinder.

### 3.4.3 Hydrodynamic Forces on Oscillating Objects

When the Morison's equation and the force coefficients has been established, the Morison's equation needs to be modified to accommodate oscillation of the cylinder. This is necessary because the pipe is not fixed, i.e. the cylinder moves with time. The fact that the pipe moves, complicates the case. It is not just the particle velocity of the waves that influences the force, but also the velocity of the body relative to the waves. There are two force components acting on the body, one related to the water particle acceleration and one related to the water particle velocity, respectively the inertia force and the drag force. For moving objects, the same principle is applied as to the original Morison's equation, except that the force components are modified to account of the movement of the body. The form is often called the extended or the modified Morison's equation and is given by the sectional force (DNV-GL, 2010b)

$$f_N(t) = \rho A a + \rho C_A A a_r + \frac{1}{2} \rho C_D D v_r |v_r| \quad (3.25)$$

where  $A$  is the cross-sectional area,  $a$  is the fluid acceleration,  $v_r$  is the relative velocity and  $a_r$  is the relative acceleration. According to DNV-GL (2010b), the use of relative velocity for the drag force is only applicable if

$$r/D > 1 \quad (3.26)$$

where  $r$  is the member displacement amplitude and  $D$  is the member diameter.

### 3.4.4 Hydrodynamic Coefficients

The Morison equation contains two hydrodynamic coefficients, which are influenced by several factors. The main factors which need to be considered when considering hydrodynamic loads can be listed as (Faltinsen, 1990):

- Reynolds number,  $R_e$
- Roughness number,  $k/d$
- Keulegan-Carpenter number,  $KC$

The Reynolds number, as shown in Equation 3.27, is the ratio between the inertial forces and the viscous forces and is given by the flow velocity, the diameter of the cylinder and the kinematic viscosity (DNV-GL, 2010b)

$$Re = \frac{uD}{\nu} \quad (3.27)$$

where  $u$  is the characteristic free stream velocity,  $D$  is the diameter of the body and  $\nu$  is the kinematic viscosity. The kinematic viscosity is highly dependent on the water temperature, so for water at 10° the value is  $\nu = 1.35 * 10^{-6}$ . For oscillating objects, the Reynolds number can be expressed by the relative velocity.

The roughness number is a non-dimensionless number given by the surface roughness  $k$  and the member diameter, i.e.  $k/D$ .

The KC-number is a measure of the distance traversed by a fluid particle during half a period relative to the diameter of the cylinder. Considering deep-water, the KC number can be written as follows (Gudmestad, 2015)

$$KC = \frac{u_0 T}{D} = \frac{\xi_0 \omega e^{kz}}{D} = \frac{\frac{2\pi}{T} \xi_0 e^{kz} T}{D} = \frac{\pi H}{D} e^{kz} \quad (3.28)$$

And at SWL ( $z=0$ ), the KC number can be written as:

$$KC = \frac{\pi H}{D} \quad (3.29)$$

where  $H$  is the wave height and  $D$  is the diameter of the cylinder.

### 3.4.5 Drag Coefficient

The drag coefficient,  $C_D$ , is a dimensionless number which is dependent on several factors, shown in the equation below (DNV-GL, 2010b)

$$C_D = \frac{f_{drag}}{\frac{1}{2} \rho D v^2} \quad (3.30)$$

where  $f_{drag}$  is the sectional drag force,  $\rho$  is the fluid density,  $D$  is the diameter of the object and  $v$  is the velocity of the flow.

Figure 3.6 below shows the drag coefficient as a function of Reynolds number. The distinct drop in drag coefficient is often referred to as the critical flow regime and is especially distinct for smooth cylinders.

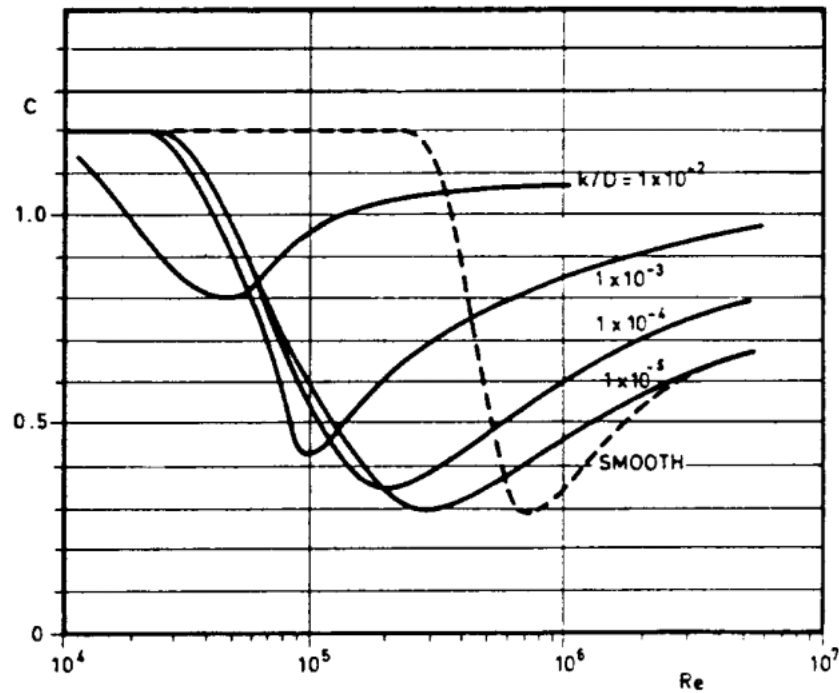


Figure 3.6: Drag coefficient (DNV-GL, 2010b)

### 3.4.6 Added Mass Coefficient

The added mass is defined by the mass of the fluid displaced by an accelerating body, where the effect reduces with distance away from the body (Gudmestad, 2015). Since the feed pipe is constantly changing in submergence, the added mass coefficient is important to identify. The added mass coefficient,  $C_A$ , likewise the drag coefficient is a dimensionless number. According to DNV-RP-C205 (DNV-GL, 2010b), the added mass coefficient can be set to 0.6 for very large KC-numbers and smooth cylinders. It can be defined by

$$C_A = \frac{m_a}{\rho A} \quad (3.31)$$

where  $m_a$  is the added mass per unit length and  $A$  is the cross-sectional area of the cylinder.

### 3.4.7 Effect of Free Surface

The feed pipes are located on the water surface, which makes the effect of free surface interesting when the forces acting on the pipe is investigated. The theory is based on slamming, and is described in DNV-RP-C205 section 8.6 (DNV-GL, 2010b). The simplified method for the slamming force  $F_S$  can be written as the force per unit length in the direction of the velocity,

$$F_S = \frac{1}{2} \rho C_S D v_s^2 \quad (3.32)$$

where  $C_S$  is the slamming coefficient and has a value of 5.15 for a smooth circular cylinder

$$C_S = \frac{2}{\rho D} \frac{dA_{33}^{\infty}}{dh} \quad (3.33)$$

and  $h$  is the submergence relative to the surface elevation, so that  $h = -r$  at the initial time instant when the cylinder impacts the water surface. The last fraction,  $\frac{dA_{33}^{\infty}}{dh}$ , is the rate of change of sectional added mass with submergence.

The variation of  $m_a$  with the depth of submergence  $h$  from the free surface to the centre of the cylinder is shown in Figure 3.7 below (DNV-GL, 2010b). In Section XX, a sensitivity study is conducted with the use of variable added mass. The values used in the study is taken from the figure below.

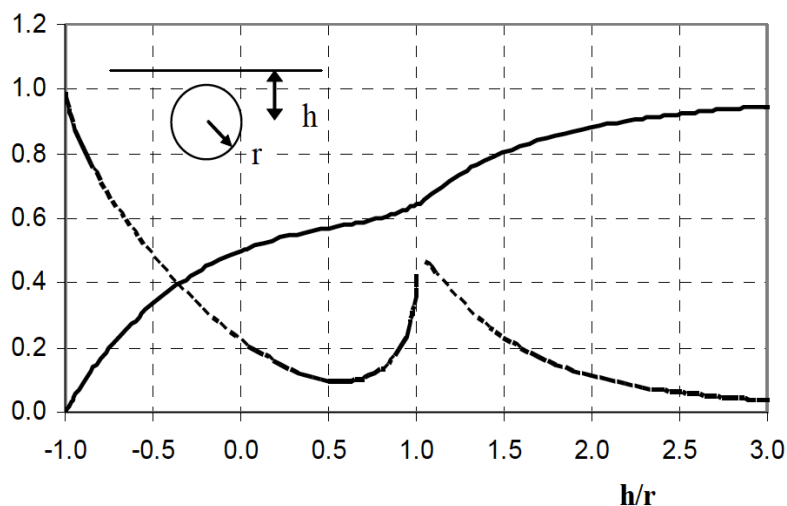


**Figure 3.7:** Variation of added mass with submergence (DNV-GL, 2010b)

Figure 3.8 below shows the pipe over the water surface (dry) and when the pipe is fully

submerged.

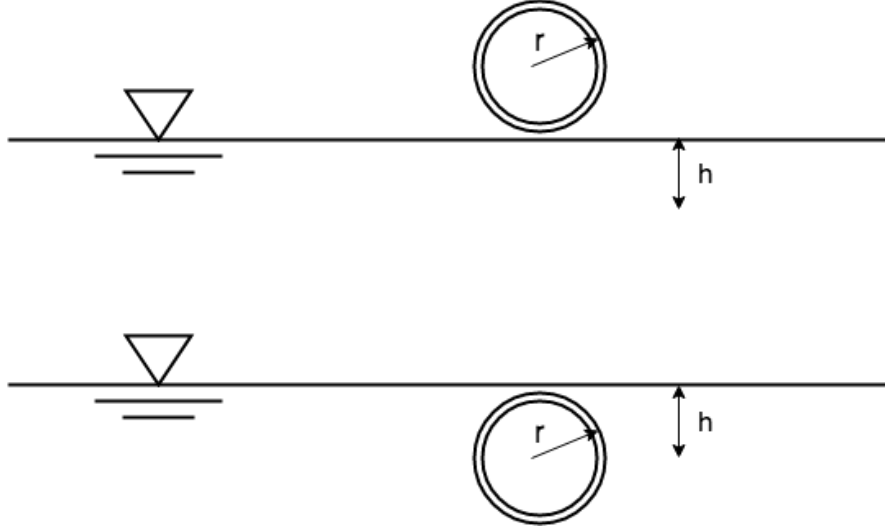


**Figure 3.8:** Dry vs. fully submerged pipe

For slamming on a slender horizontal cylinder, the expression for the vertical impact force per unit length is given by (DNV-GL, 2010b)

$$F_z(t) = \rho g A_1 + (m_{a,3} + \rho A_1) \ddot{\eta} + \frac{\partial m_{a,z}}{\partial z} \dot{\eta}^2 + \frac{\rho}{2} \dot{\eta} |\dot{\eta}| d(z/r) C_D^z \left( \frac{z}{r} \right) \quad (3.34)$$

where the first term is the buoyancy force,  $m_{a,3}$  is the vertical added mass which is a function of the degree of immersion. The spatial pressure gradient in the waves is given by the term  $\rho A_1 \dot{\eta}$ , and  $d(z/r)$  is the varying cross-section. The last term represents a drag force. As for the horizontal force, the equation can be written as

$$F_x(t) = (\rho g A_1 + m_{a,1}) \dot{u} + \frac{\partial m_{a,1}}{\partial z} \dot{\eta} u + \frac{\rho}{2} \dot{\eta} |u| h \left( \frac{z}{r} \right) C_D^z(z/r) \quad (3.35)$$

where the horizontal added mass is given by,  $m_{a,1} = \rho \pi R^2$ , and the rate of change for the horizontal added mass is  $\partial m_1 / \partial z = 4 \rho R / \pi$ .

### 3.5 The Response Amplitude Operator

The response amplitude operator (RAO) can be considered as the "fingerprints" of a vessel. The RAO describes the motion and behaviour of a vessel, and is related to the

motion amplitude of the vessel to the wave amplitude (Massie and Journée, 2001). The RAO consists of a pair of numbers that define the vessel response, for one particular degree of freedom, to one particular wave direction. A vessel has 6 degrees of freedom (DOF), so the RAO of a vessel consists of six amplitudes and phase pairs for each wave period and direction (Orcina, 2014). The phase shifts of the motion relative to the wave elevation is also an important definition of the RAO. The resulting six ship motions are given by the following equations in the ships center of gravity (Massie and Journée, 2001)

$$\begin{aligned}
\textit{Surge} : \quad x &= x_a \cos(\omega_e t + \epsilon_{x\zeta}) \\
\textit{Sway} : \quad y &= y_a \cos(\omega_e t + \epsilon_{y\zeta}) \\
\textit{Heave} : \quad z &= z_a \cos(\omega_e t + \epsilon_{z\zeta}) \\
\textit{Roll} : \quad \phi &= \phi_a \cos(\omega_e t + \epsilon_{\phi\zeta}) \\
\textit{Pitch} : \quad \theta &= \theta_a \cos(\omega_e t + \epsilon_{\theta\zeta}) \\
\textit{Yaw} : \quad \psi &= \psi_a \cos(\omega_e t + \epsilon_{\psi\zeta})
\end{aligned} \tag{3.36}$$

where  $\epsilon$  is the phase angle.

The displacement RAO is given by the following mathematical expression in a certain degree of freedom  $i$  (Massie and Journée, 2001)

$$\frac{\eta_{a,i}}{\xi_a}(\omega) \tag{3.37}$$

where  $\eta$  is the motion amplitude for a certain degree of freedom,  $\omega$  is the angular frequency and  $\xi_a$  is the wave amplitude. One can see that there is a frequency dependence in terms of the angular frequency  $\omega$ . Obtaining the RAOs in irregular waves is complicated, so it is advantageous to look at regular waves. To obtaining the RAOs in irregular waves, the frequency domains is used. According to (Massie and Journée, 2001), the cyclic expression for position in heave is given by

$$\eta_3 = \eta_{a,3} \sin \omega t + \epsilon_{3\zeta} \tag{3.38}$$

where  $\eta_{a,3}$  is the heave response amplitude and  $\epsilon_{3\zeta}$  is the phase characteristic. The velocities and accelerations can be found by taken the derivative of Equation 3.38. By inserting Equation 3.37 into the equation of motion (shown in Section 5.1.5) and the derivates, the

amplitude characteristics of the RAO can be obtained (Massie and Journée, 2001)

$$\frac{\eta_{a,i}(\omega)}{\xi_a} = e^{-kd} \sqrt{\frac{(C_{33} - A_{33}\omega^2) + (B_{33}\omega)^2}{(C_{33} - (M_{33} + A_{33})\omega^2)^2 + (B_{33}\omega)^2}} \quad (3.39)$$

where  $C_{33}$  is the hydrostatic stiffness,  $A_{33}$  is the added mass in heave,  $B_{33}$  is the damping in heave,  $M_{33}$  is the mass of the object,  $k$  is the wave number and  $d$  is the draft. The phase characteristics seen in Equation 3.37, can be expressed by the phase shift in heave motion for regular waves (Massie and Journée, 2001)

$$\epsilon_{3\xi}(\omega) = \tan^{-1} \left( -\frac{M_{33}B_{33}\omega^3}{(C_{33} - A_{33}\omega^2)(C_{33} - (M_{33} + A_{33})\omega^2) + (B_{33}\omega)^2} \right) \quad \text{for } : 0 \leq \epsilon_{3\xi} \leq 2\pi \quad (3.40)$$

Equation 3.40 also exhibits frequency dependence, which can be explained by Figure 3.9 (Massie and Journée, 2001) for a vertical cylinder

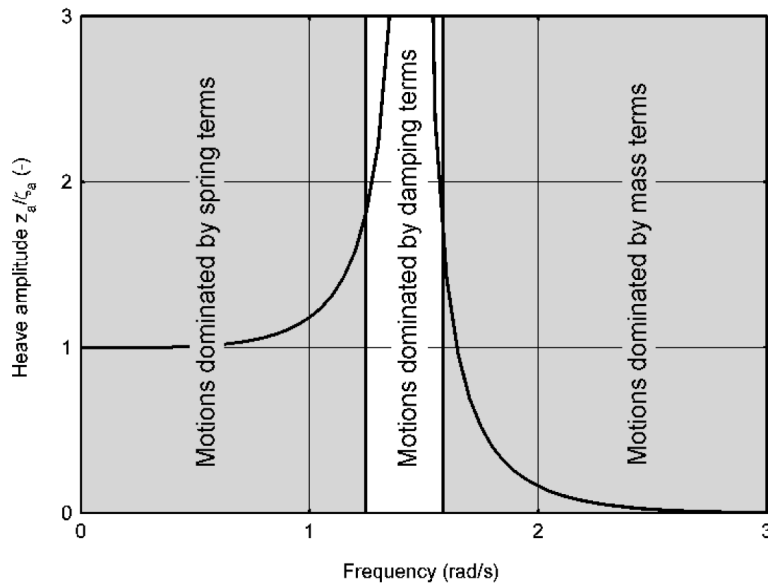


**Figure 3.9:** Description of RAO (Massie and Journée, 2001)

By looking at the low frequency area in Figure 3.9, it is shown that the RAO has a amplitude of 1, i.e. the cylinder follow the waves. For higher frequency area, the waves tends to "lose" the influence on the behaviour of the cylinder due to the wavelength being much smaller than the diameter of the cylinder (Massie and Journée, 2001). For the middle section, the vertical motions are dominated by damping term. This area is



called the natural frequency area, where high resonance is expected (Massie and Journée, 2001).

From the wave energy spectrum,  $S_\omega$ , the response spectrum can be expressed by using the RAO (transfer function) to link the two spectra (Massie and Journée, 2001)

$$S_{\eta_3}(\omega) = \left| \frac{\eta_{3,a}}{\xi_a} \omega \right|^2 \quad (3.41)$$

The wave spectra (left) and the response spectrum (right) is shown in Figure 3.10

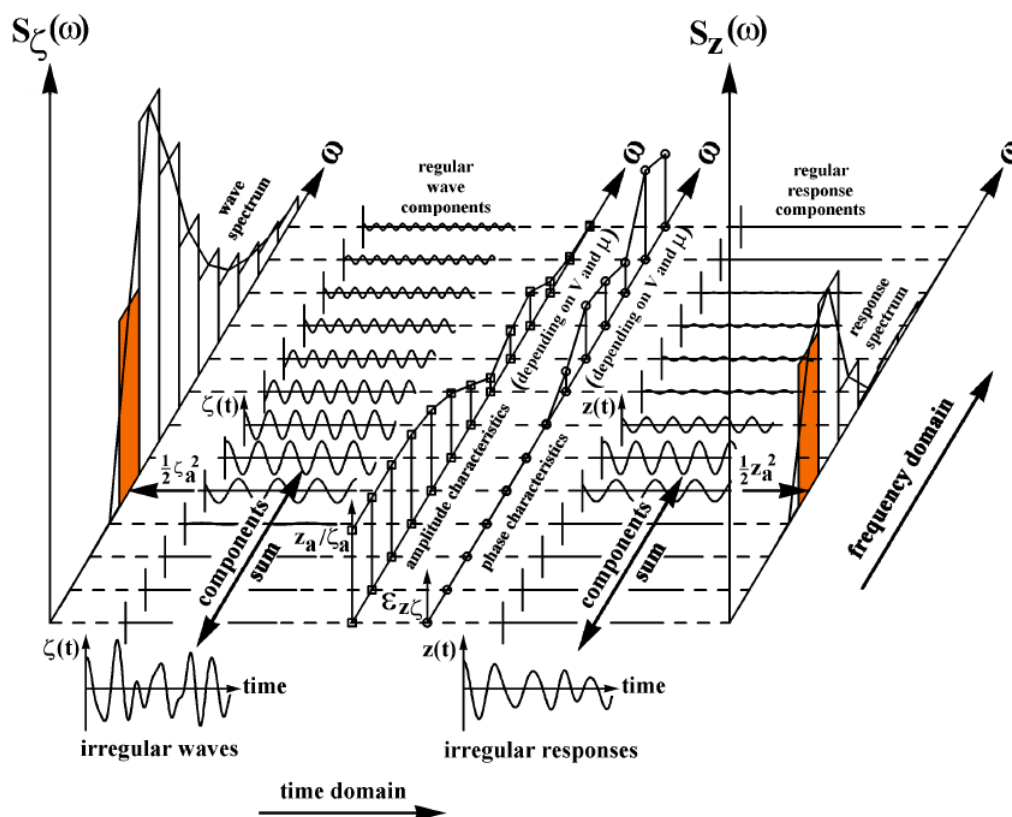


**Figure 3.10:** Principle of transfer of waves into responses (Massie and Journée, 2001)

## 3.6 Frequency Domain

The frequency domain is the linear solution to the equations of motion, which is used to study systems in irregular sea states with linear characteristics. According to DNV-RP-C205 DNV-GL (2010b) the wave induced loads in an irregular sea can be linearly

superposing loads due to regular wave components. The superposition principle is the fundamental basis for the frequency domain and is dependent on linearity, which can be seen in Figure 3.10. According to Massie and Journée (2001), the study of responses is done for several regular waves with certain frequencies and amplitudes from the wave spectra, then the use of the superposition for each regular wave is done to generate the irregular response of a vessel in an irregular sea state.

The frequency domain approach is useful to save computational time for linear analysis. Hence, approach is used in this thesis to obtain the displacement RAOs by use of the DNV GL software Wadam (Wave Analysis by Diffraction and Morison Theory) in HydroD from the SESAM programme suite (DNV-GL, 2010a).

### **3.7 Time Domain**

The time domain method involves numerical integration of the equations of motion and should be used when non-linear effects are important. Examples are slamming response and coupled dynamics, i.e. when the frequency domain approach is disregarded. In time domain analysis, deterministic waves with given periods and heights are time-stepped through the structure, which gives responses as a time history. One of the disadvantages of time domain method is that the analysis is more computer demanding than other methods (DNV-GL, 2010b). The time domain approach is implemented in this thesis by utilising OrcaFlex by Orcina LTD (Orcina, 2014).

# 4 | Hydrodynamic

## Modelling of Feed Barge

To establish an accurate and reliable analysis of the feed pipe, a hydrodynamic analysis in frequency domain is necessary to conduct. The RAOs obtained in frequency domain will eventually be implemented in OrcaFlex, for time domain analysis. To obtain the RAOs of a vessel, one has to carry out a hydrodynamic analysis using dedicated software. For this thesis, the software GeniE is used to create a panel model of the submerged part of the feed barge by utilising the finite element method (FEM). The potential solver Wadam in HydroD is used for the hydrodynamic analysis. Post-processing of the results was done in PostResp and MATLAB. The hydrodynamic modelling process consists of several stages, as shown in Figure 4.1 below. The process starts with defining the structural dimensions of the feed barge, generating a mesh in GeniE and finally performing the hydrodynamic analysis in Wadam. This chapter explains the steps involved in the design process of the feed barge, with a presentation of the RAOs in the end.

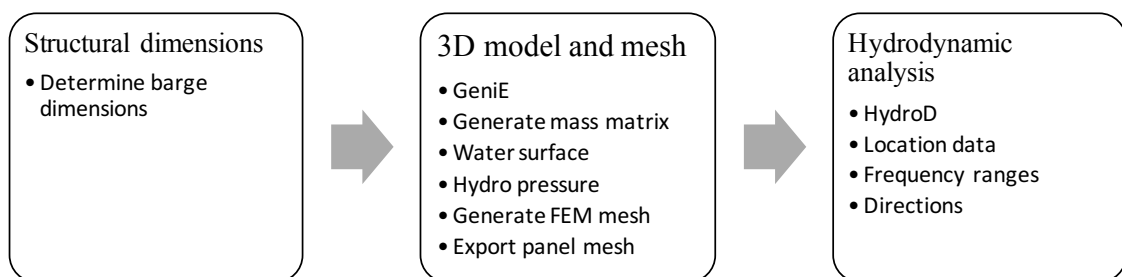


**Figure 4.1:** Hydrodynamic modelling process

# 4.1 Panel Model of Feed Barge

Sesam GeniE is a world renowned offshore structural engineering software tool for design and analysis of fixed and floating structures. GeniE v.6.7-12 is utilised to create a panel model which can be used in hydrodynamic and stability analysis in Wadam. The selected barge dimensions are based on existing feed barges used in the industry today and is designed to match some of the largest barges that are in operation. Figure 4.2 shows the process of generating a mesh in GeniE.

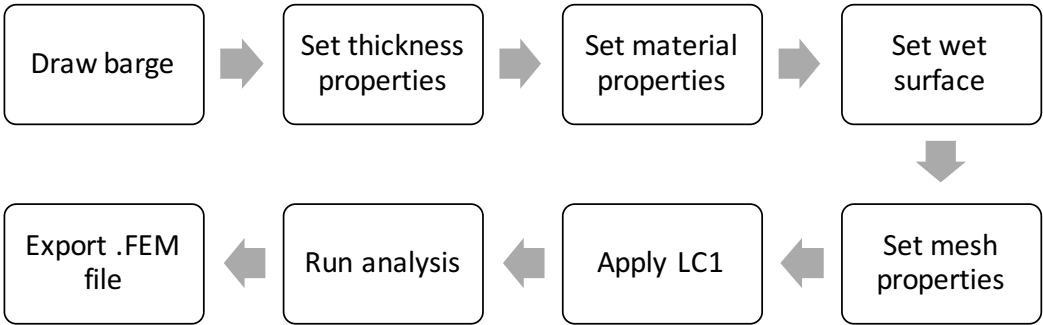
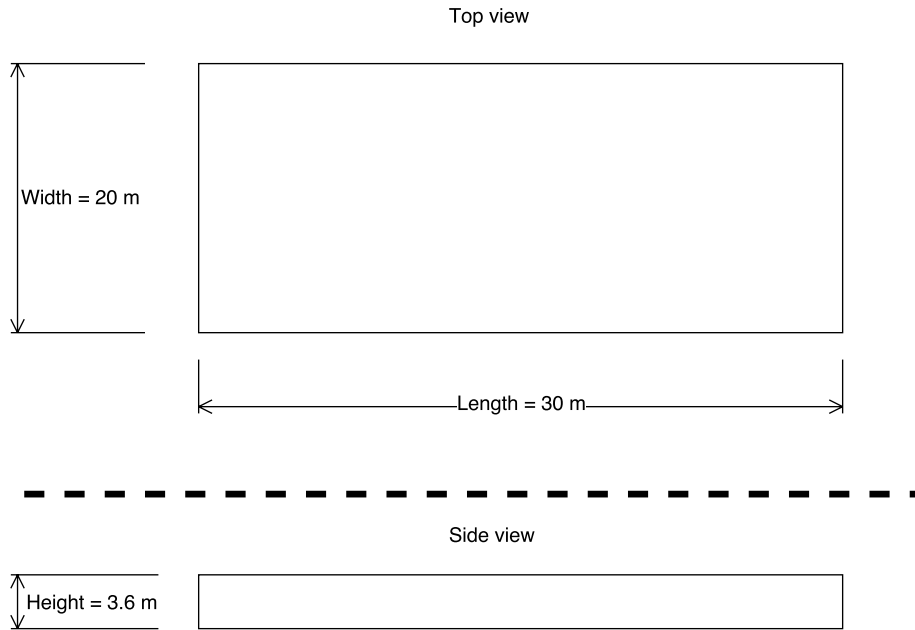


Figure 4.2: GeniE modelling process

Due to the intention of moving fish farms offshore, it was decided to select a relatively large feed barge. Figure 4.3 below shows the dimensions of the feed barge in both top view and side view, respectively. Note that the figure only shows the height of the barge hull, i.e. only the wetted area of the barge is modelled in GeniE. The overall height will be defined later in Wadam, by setting the distance between the centre of gravity (COG) and the centre of buoyancy (COB).



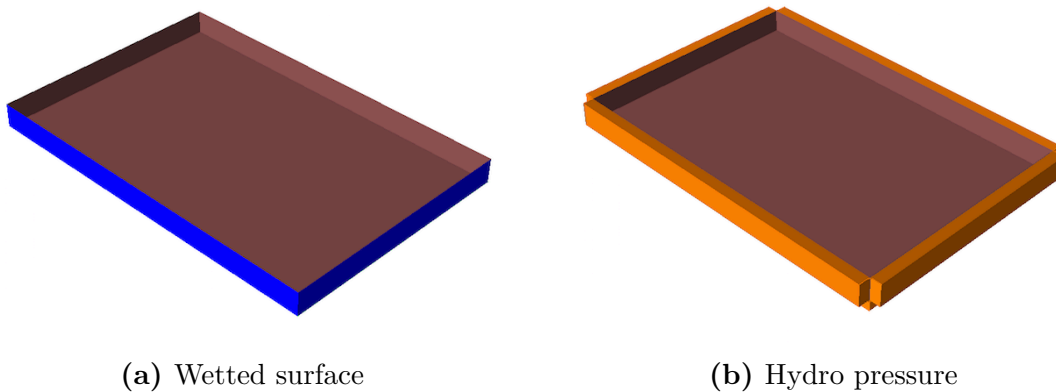
**Figure 4.3:** Barge dimensions

When the dimensions are determined, drawing of the barge in GeniE can start. This is done by setting guiding planes defined by eight points in the XY-plane. It is important to draw the barge in the correct plane, so the coordinate system in GeniE matches the one in Wadam (DNV-GL, 2010a). The barge is then constructed by drawing flat plates as the structure of the barge at the desired points. To generate the mass model, GeniE requires the material properties and the hull thickness properties of the barge. The material used for the feed barge is steel, with the given properties shown in Table 4.1 below. Since the purpose of GeniE for this case is to simply generate a mesh model, the material properties and the thickness of the barge is not of great importance for the analysis in Wadam (DNV-GL, 2010a) later. However, the software requires the input of the mentioned properties to avoid error messages. The properties are therefore arbitrary and only an assumption of the real properties used for a feed barge. If a structural analysis would be conducted, these properties would naturally have been necessary.

**Table 4.1:** Feed barge properties

Property	Value	Unit
Breadth	20	m
Length	30	m
Height of hull	3.6	m
Draft	2	m
Freeboard	1.6	m
Thickness of hull	6	mm
<b>Material properties</b>		
Yield	$4.2 \cdot 10^2$	MPa
Poisson	0.3	-
Damping	0.03	Ns/m

The finite element model (FEM) in GeniE is used for stability calculations and for calculations of the 3D wave potential in Wadam. The wetted surface setting in GeniE is therefore used to define the wet surface property load of the barge. This enables hydrodynamics loads and accelerations to be computed in Wadam(DNV-GL, 2014). A dummy hydro pressure loading condition is set, which is important for further analysis in Wadam. Figure 4.4 below shows the wetted surface of the barge and the hydro pressure on the barge, correctly set outwards from the barge.

**Figure 4.4:** Illustration of hydrodynamic properties in GeniE. (a) Wetted surface, (b) Hydro pressure

### 4.1.1 Mesh Properties

The panel method is the discretization of the mean wetted surface into flat panels. The Laplace equation is solved subsequently for the inviscid, incompressible flow for each prescribed panel (DNV-GL, 2010a). To run the analysis in Wadam it is required to create a FEM in GeniE by generating a mesh. The mesh in GeniE is created by applying the mesh density option, which is used to set the element length in meters for each surface. For this analysis, four different mesh densities will be created to confirm the validity of the model later in Wadam. The four different meshes, which is denoted m1, m2, m3 and m4 will have a different level of mesh refinement. The idea is to check and verify the results with the different meshes. The mesh refinement is dependent on the element length, which in turn gives the number of nodes and number of elements. The finer the mesh refinement is, the higher the number of nodes and elements are. Table 4.2 below shows the different meshes generated in GeniE and used in Wadam later in the process .

**Table 4.2:** Mesh properties

Mesh identity	Element length [m]	No. nodes	No. element
m1	1	851	800
m2	0.5	3301	3200
m3	0.4	5126	5000
m4	0.3	9206	9038

Figure 4.5 below illustrates panel model m2 with element length of  $0.5\text{ m}$ , generated in GeniE. It is seen that the mesh has been successfully generated with quadratic cells and is ready to be exported to Wadam.

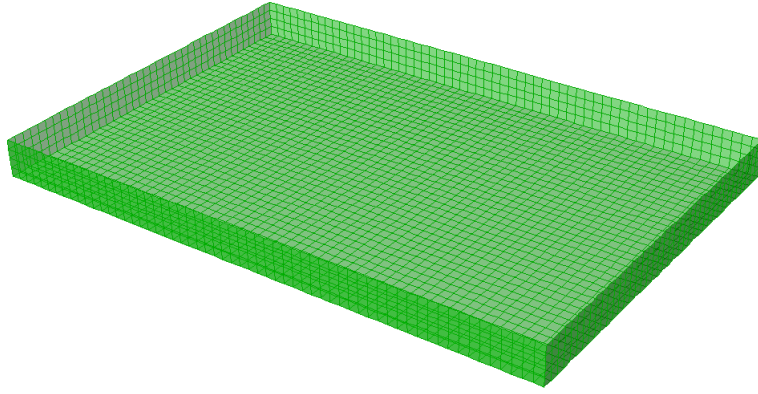


**Figure 4.5:** Visualisation of mesh identity m2, i.e. 0.5  $m$  element length

## 4.2 Frequency Domain Analysis of Hull

The potential solver Wadam in HydroD was chosen to obtain the hydrodynamic loads and responses of the feed barge from potential theory. Wadam is a general analysis program for calculation of wave-structure interaction for fixed and floating structures of arbitrary shape, e.g. ship hulls (DNV-GL, 2010a). The Wadam analysis control data is generated by the hydrodynamic analysis design tool HydroD by DNV (DNV-GL, 2010a). The overall goal of modelling the feed barge and running the hydrodynamic analysis is to obtain the displacement RAO which can be imported in OrcaFlex. The following section describes the most important input to Wadam and explains the computational choices. Figure 4.6 below illustrates the input data sequence done by utilising the Wadam Wizard in HydroD. The complete input data in Wadam can be found in Appendix A.

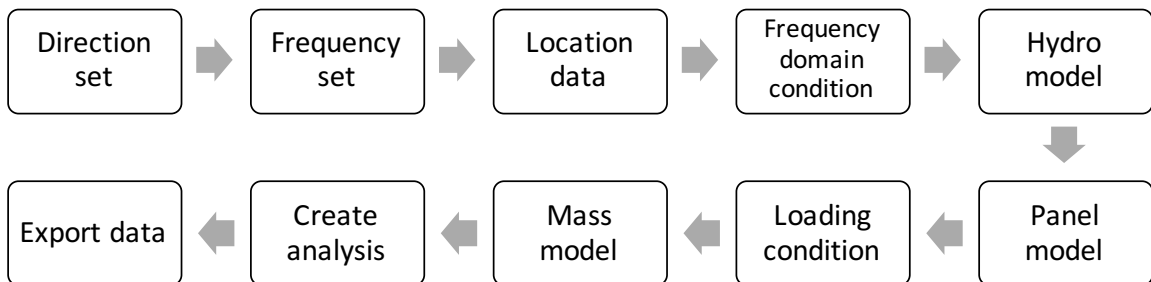


**Figure 4.6:** Wadam - Required input data to run analysis



### 4.2.1 Direction and Frequency Set

The input data required to run the hydrodynamic analysis is shown in Figure 4.6 above. The direction set is shown in Figure 4.7, where  $0^\circ - 90^\circ$  was chosen because of the symmetry of the barge, with an increment value of  $15^\circ$ . Wave direction of  $0^\circ$  represent a wave propagating along the positive x-axis, often referred to as following sea, whereas waves perpendicular to the barge is referred to as beam sea.

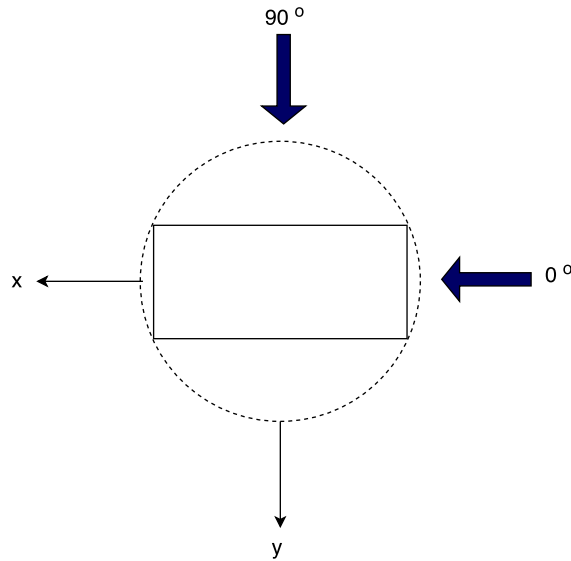


**Figure 4.7:** Direction set - increment value of  $15^\circ$  between  $0^\circ$  and  $90^\circ$

For the frequency set, an arbitrary set is chosen for the first analysis. This is to capture the initial RAO of the barge, which can be tweaked later. This frequency set has an increment of one second, which is very coarse. After locating roughly where the highest amplitude is, a finer frequency set is chosen by increasing the interval value. After the direction and frequency set is defined, input data like the hydro model, panel model and loading conditions is specified in the Wadam wizard. The panel model chosen for the preliminary analysis is the panel model with mesh identity m2. When the initial analysis is done, different meshes are studied in the convergence study.

## 4.3 Frequency Domain Results

The output of interest from Wadam is the RAO for the different motions of the barge, such as heave, pitch and roll. The postprocessor Postresp is used to extract the results from Wadam. The RAOs will ultimately be exported to OrcaFlex from Wadam. The results from the hydrodynamic analysis in Wadam are found by first conducting a sensitivity study, which is performed to locate the optimal frequency set. Finally, a convergence study will verify the accuracy of the results, before importing the hydrodynamic data into OrcaFlex.

### 4.3.1 Sensitivity Study

As mentioned, a sensitivity study is performed to locate the optimal frequency set to give the real amplitudes of the RAOs. This is done by first defining a linear frequency set, to roughly locate the peak area of the RAOs. Panel model with mesh identity m2 was used as an arbitrary panel model for the sensitivity study. Figure 4.8, 4.9 and 4.10 below illustrates the amplitudes of heave, roll and pitch with a coarse frequency set. One can see that the peaks are "cut" off, which means the true peaks and amplitudes are not shown. This will give inaccurate results, so it is necessary to increase the number of measurements in the area of interest. By studying the data, it is decided to increase the number of measurements between 4.8 seconds and 5.3 seconds.

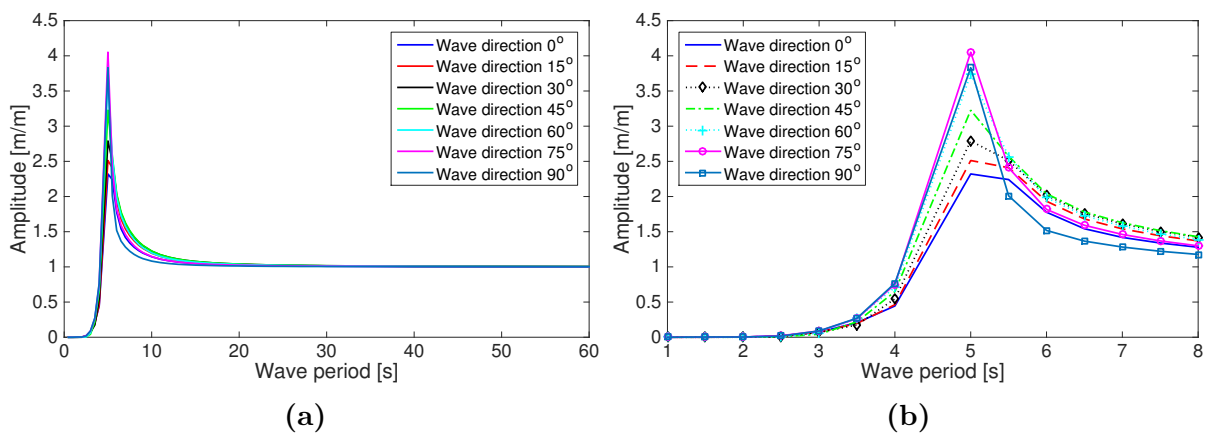


**Figure 4.8:** (a) Heave motion with coarse frequency. (b) Zoomed area

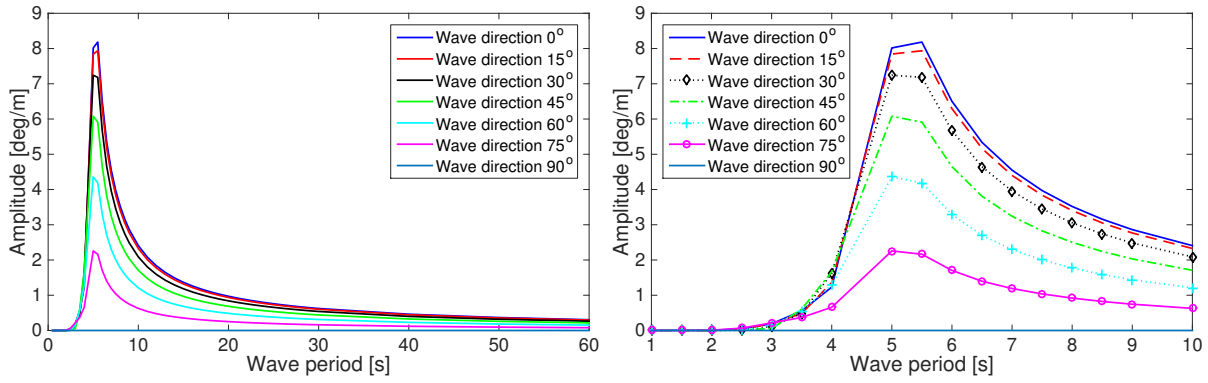


**Figure 4.9:** (a) Pitch motion with coarse frequency, (b) Zoomed area

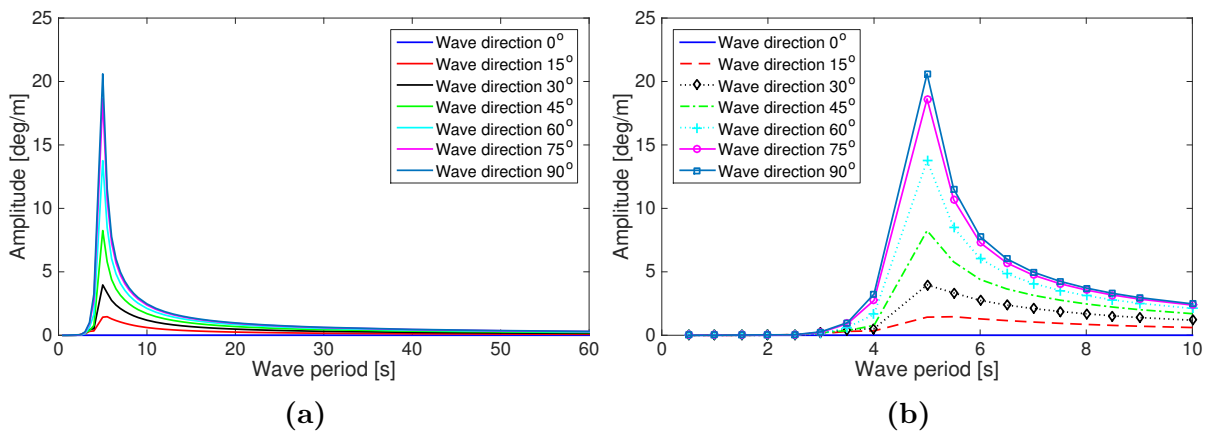


**Figure 4.10:** (a) Roll motion with coarse frequency, (b) Zoomed area

### 4.3.2 Optimal Frequency Set

The final frequency set was found by tweaking the area of interest until the highest peaks where found. By trial and error, the optimal frequency set was found and is shown in Figure 4.11, 4.12 and 4.13 below. The figures illustrate the RAO of the barge with the optimal frequency set. The importance of selecting the correct frequency set is shown by the sensitivity study; the peaks are now higher and the true vessel motion is found.

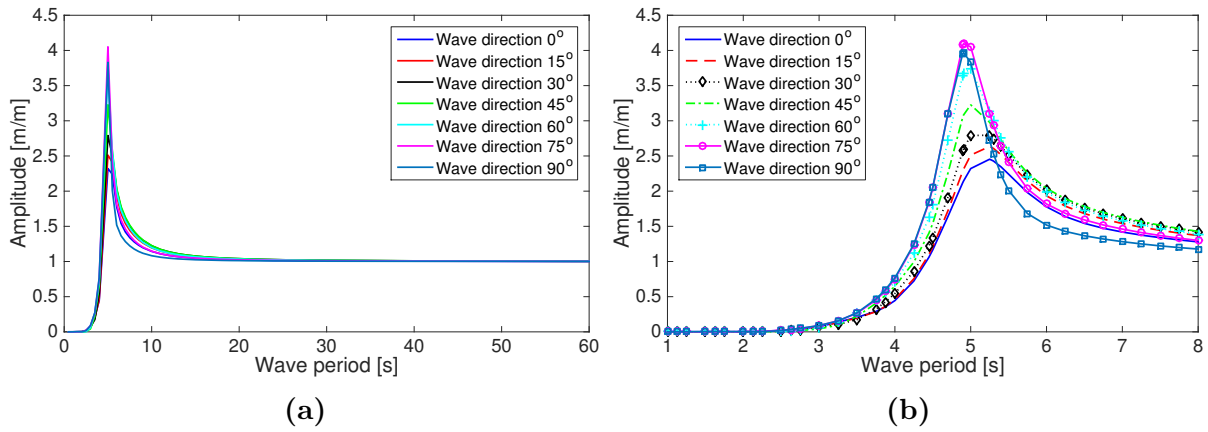


**Figure 4.11:** (a) Heave motion with refined frequency, (b) Zoomed area

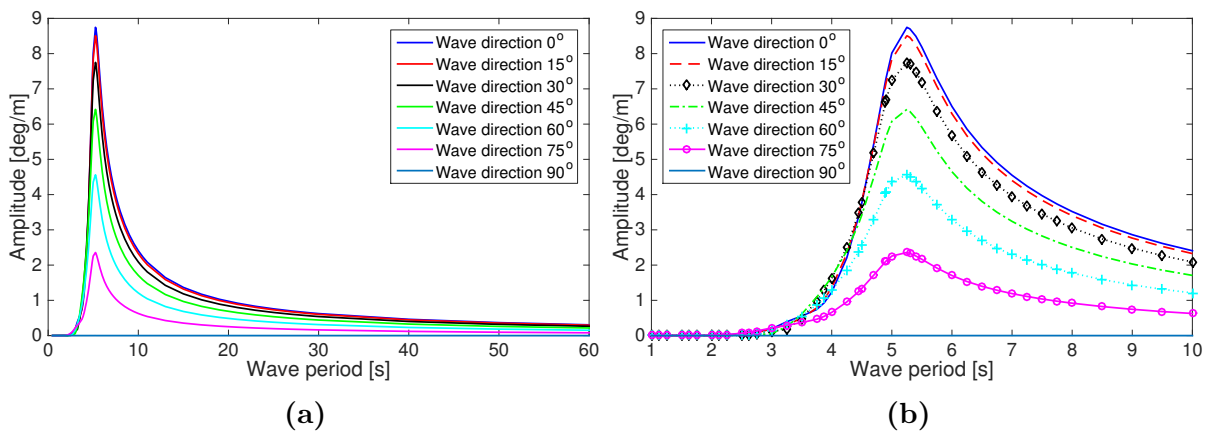


**Figure 4.12:** (a) Pitch motion with refined frequency, (b) Zoomed area

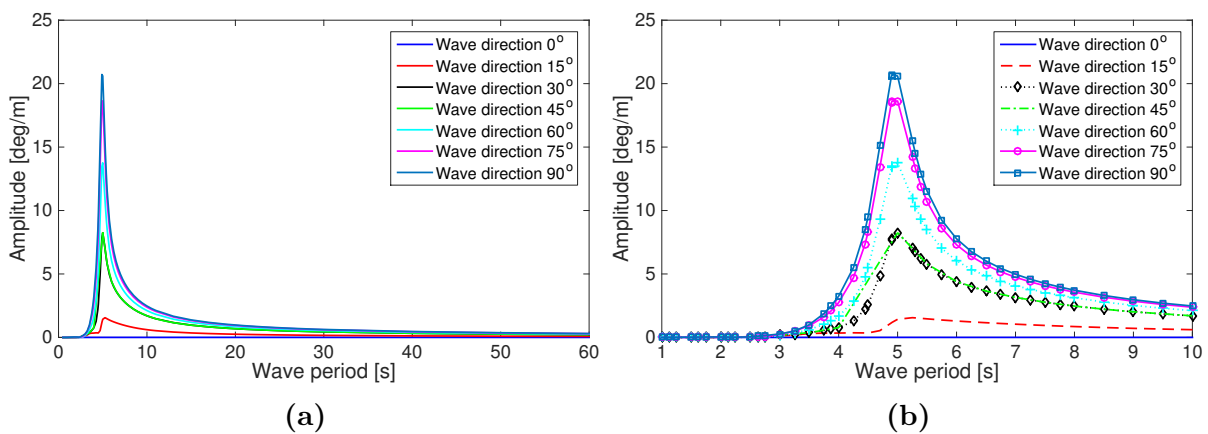


**Figure 4.13:** (a) Roll motion with refined frequency, (b) Zoomed area

By comparing the frequency set used in the sensitivity study, one can see the effect of selecting the correct frequency set. Figure 4.14 illustrates this effect clearly by showing the pitch motion for refined and coarse frequency set.

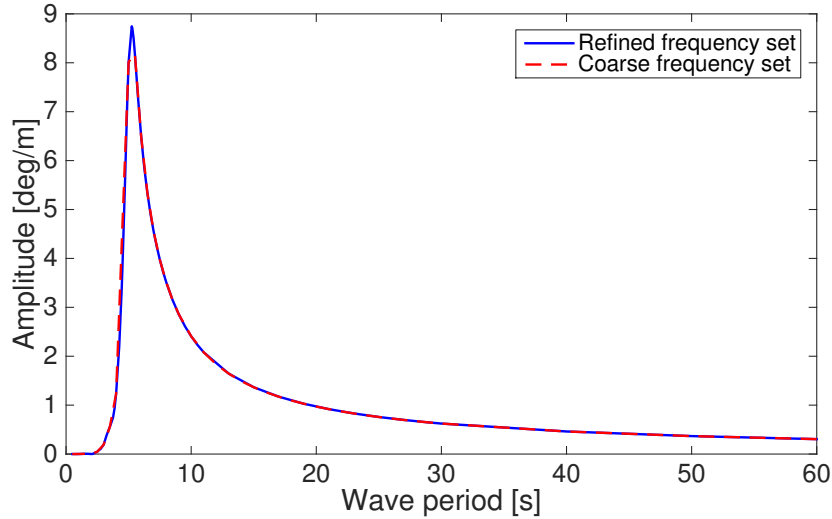


**Figure 4.14:** Comparison of frequency sets

Table 4.3 compares the maximum amplitude for heave, pitch and roll for the different frequency sets. As seen from the results, there is a slight variation between the linear frequency set and the optimal frequency set. This shows the importance of the sensitivity study to obtain the optimal frequency set and the real amplitude of the RAOs. However, due to the simple geometry of the feed barge, the results does not vary much.

**Table 4.3:** Comparison of frequency sets

RAO	Frequency set	Max. amplitude
Heave	Linear	4.05
	Optimal	4.10
Pitch	Linear	8.20
	Optimal	8.75
Roll	Linear	20.6
	Optimal	20.7

### 4.3.3 Convergence Study

In finite element modelling, a finer mesh typically results in a more accurate result. Nonetheless, by increasing the mesh density, the computational expenses increases. The

solution is to perform a convergence study, to balance the accuracy and the computing resources.

The convergence study is performed for the four different panel models modelled in GeniE. The frequency set used for the convergence study is the optimal frequency set found in the previous section.

To state convergence, the results from the different panel models should not differ greatly. Peak values, as well as graph similarity in total, should be considered when looking for convergence. A comparison between the four different panel models in heave, pitch and roll with the highest amplitudes are shown in Figures 4.15, 4.16 and 4.17 below.

By studying the graphs, the peaks and amplitudes for the different RAO's do not differ substantially. For heave, pitch and roll the highest variation is no more than 3% - 7%. It can thus be stated that convergence has successfully been achieved. Panel model with mesh identity m2 is chosen for further analysis in time domain since it deviates only by a small margin from mesh identity m4, and it has fewer elements which make the computational expenses lower.

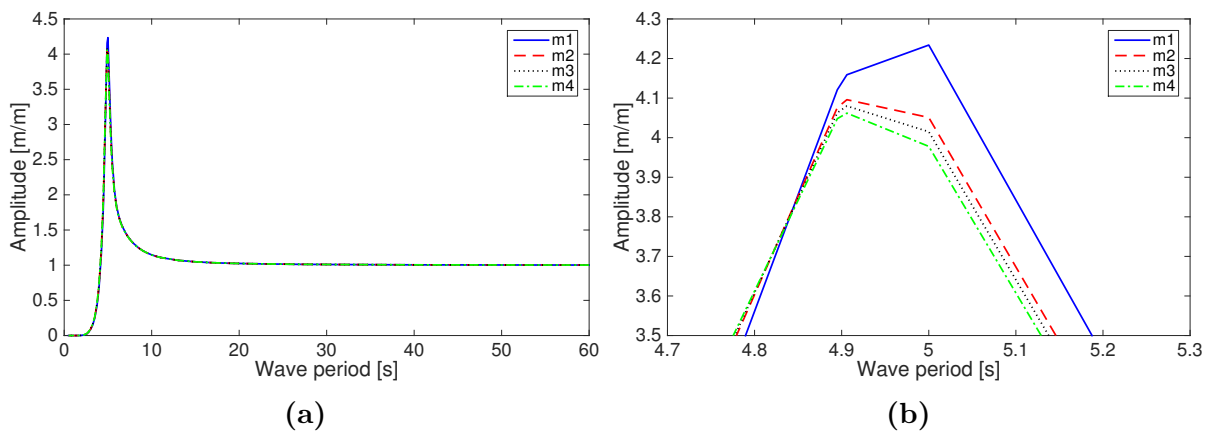


**Figure 4.15:** Convergence study in heave. (a) Heave - Wave direction 75°, (b) Area of interest

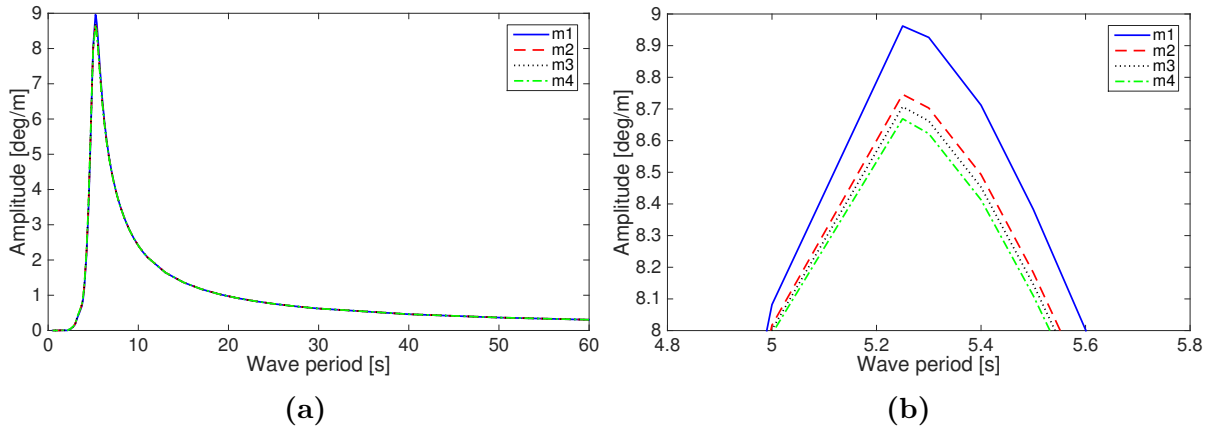


**Figure 4.16:** Convergence study in pitch. (a) Pitch - Wave direction  $0^\circ$ , (b) Area of interest

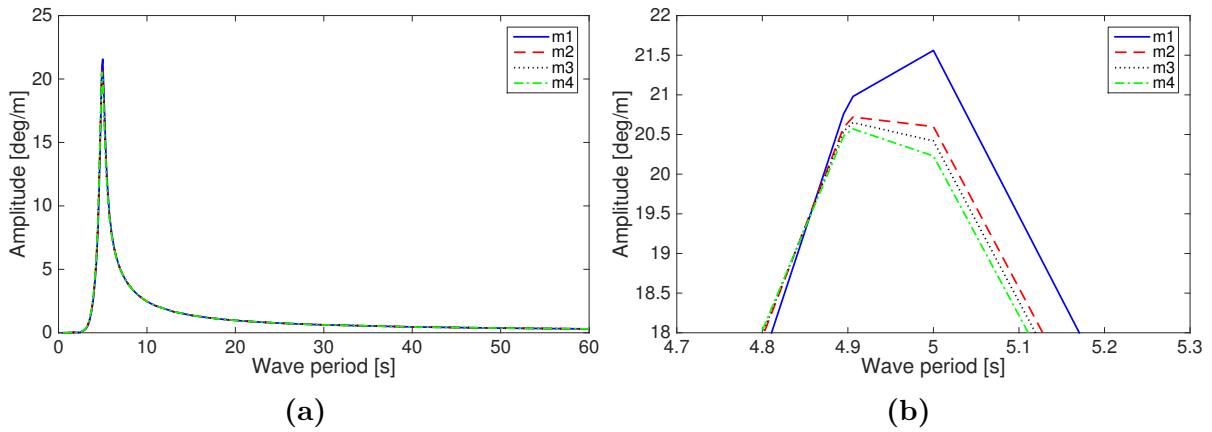


**Figure 4.17:** Convergence study in roll. (a) Roll - Wave direction  $90^\circ$ , (b) Area of interest

It is worth mentioning that only a pure panel model was considered in this analysis. This means that viscous effects have not been considered, which again gives larger amplitudes for the RAO. The results in time domain will illustrate this, by looking at the motion of the barge subjected to different environmental conditions. Since this thesis does not focus on the hydrodynamic and dynamic analysis of the feed barge, a pure panel model was chosen to simplify calculations and also lower the computational expenses in time-domain analysis.

### 4.3.4 Summary

The feed barge that will be imported in OrcaFlex was done using GeniE for the meshing of the model and Wadam for the hydrodynamic analysis. A pure panel model, without

viscous effects, was chosen due to the focus being on the responses on the feed pipe. The sensitivity study showed that it is necessary to run several simulations with different frequency sets, to locate the true amplitudes of the vessels RAO. By conducting a convergence study, the optimal mesh was found by looking at both computational efforts as well as the accuracy of the values. Panel model with mesh identity m2 is chosen to conduct further analysis in time domain.

The natural period of the barge peaks at about 5 s for heave and 6 s for both the pitch and roll. This means that the largest motions occur for these wave frequencies.

The heave motion peaks for wave direction of  $75^\circ$ , while the largest amplitude for pitch is wave direction of  $0^\circ$  as expected.

It can be seen that the roll motion is highly sensitive for both the period and the wave direction. For roll motion, wave direction of  $90^\circ$  induces the largest motion.



# 5 | OrcaFlex - Time-domain Analysis

OrcaFlex 10.1 is utilised to perform the time-domain analyses of the fish farm system. OrcaFlex is a software developed by Orcina Ltd. and is one of the world's leading software serving the offshore dynamics market (Orcina, 2014). OrcaFlex has a broad range of applications, including floating hoses. The software is a fully 3D non-linear time-domain finite element program capable of carrying everything from fields within aquaculture to defence. The following sections outline the theory and calculation methods in OrcaFlex. The theory in this section is taken from the OrcaFlex manual (Orcina, 2014). The simulation set-up and model build-up in OrcaFlex is then explained.

## 5.1 General Data

### 5.1.1 OrcaFlex Coordinate System

The coordinate system in OrcaFlex uses one global coordinate system GXYZ, where G is the global origin. In addition, there are several local coordinate systems, one for each object in the model. The last coordinate system is the Line End orientation which is denoted by Exyz. Figure 5.1 below shows the coordinate system used in OrcaFlex.

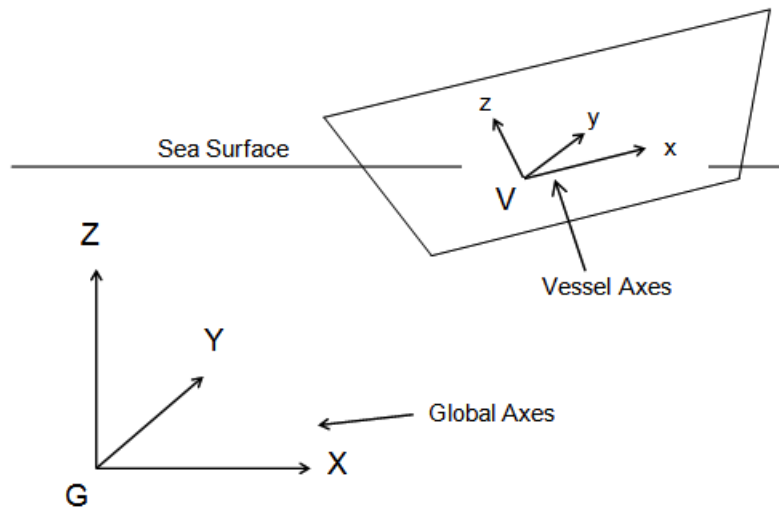


**Figure 5.1:** OrcaFlex coordinate system (Orcina, 2014)

### 5.1.2 Statics

The static analysis in OrcaFlex is done prior to the dynamic analysis. This is done to establish equilibrium of the system under weight, buoyancy, etc. and determine a starting configuration for the dynamic simulation. The static equilibrium position is determined by a series of iterative stages. The static analysis can be done in two different ways in OrcaFlex; 'Whole System Statics' and 'Separate Buoy and Line Statics'. The former was chosen due to faster and more robust performance (Orcina, 2014).

To obtain equilibrium of the system, the out-of-balance forces of the initial positions of the objects in the model are calculated. The next possible equilibrium position is then estimated by the out-of-balance forces, which is repeated until a satisfactory accuracy is achieved.

### 5.1.3 Dynamics

A dynamic analysis is a time simulation of the motions of the model over a specified period of time, starting from the mentioned position determined by the static analysis. The dynamic simulation starts with a build-up stage where the wave and vessel motions are smoothly ramped up from zero to their full size (Orcina, 2014). The length of the

build-up stage should be at least one wave period, and is thus set to -10 s in this case. The objective of the build-up stage is to avoid sudden transients when the simulation is started (Orcina, 2014)

### 5.1.4 Line Model

The lines in OrcaFlex are divided into a series of line segments which are then connected to nodes by straight massless model segments. The properties of the line are handled by the model segments and the nodes, where the model segments only model the axial and torsional properties while the nodes hold all the other properties such as mass, weight, buoyancy and drag (Orcina, 2014). As for the bending properties of the line, rotational springs and dampers between the segments and the nodes are modelled. The segmentation of the lines is shown in Figure 5.2 below.

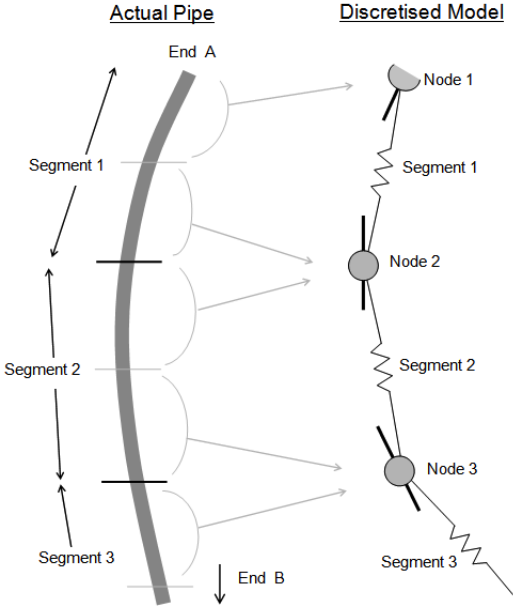


**Figure 5.2:** Segmentation of Lines (Orcina, 2014)

### Line End Orientation

When connecting a line to an object, the end orientation of the end fitting is given by its Azimuth, Declination and Gamma angles Orcina (2014). These angles fully define the orientation of the end fitting, where the frame of reference for Exyz for the end fitting are

(Orcina, 2014):

- E is at the connection point.
- Ez is the axial direction of the fitting.
- Ex and Ey are perpendicular to Ez.

Figure 6.13 illustrates the Declination angle of an end fitting. As can be seen from the figure, the declination is the angle between the vertical axis (dotted line) of the support and the line axis (blue line). The Declination angle will be investigated later in the dynamic simulations.

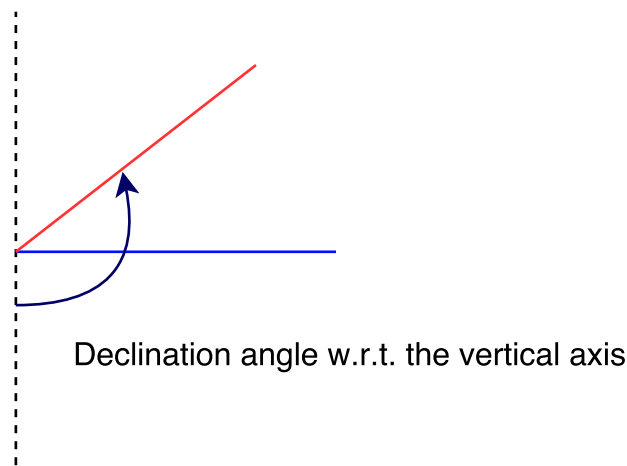


**Figure 5.3:** Declination angle (Orcina, 2014)

### Calculation Method of Lines

As described in Section 5.1.4 the line model is split into several segments which are connected by nodes. It is at the mid-nodes the forces and moments are calculated, with the following calculation stages:

Tension forces → Bend moments → Shear forces → Torsion moments → Total load

Figure 5.4 illustrates the mathematical model of an arbitrary line in OrcaFlex.

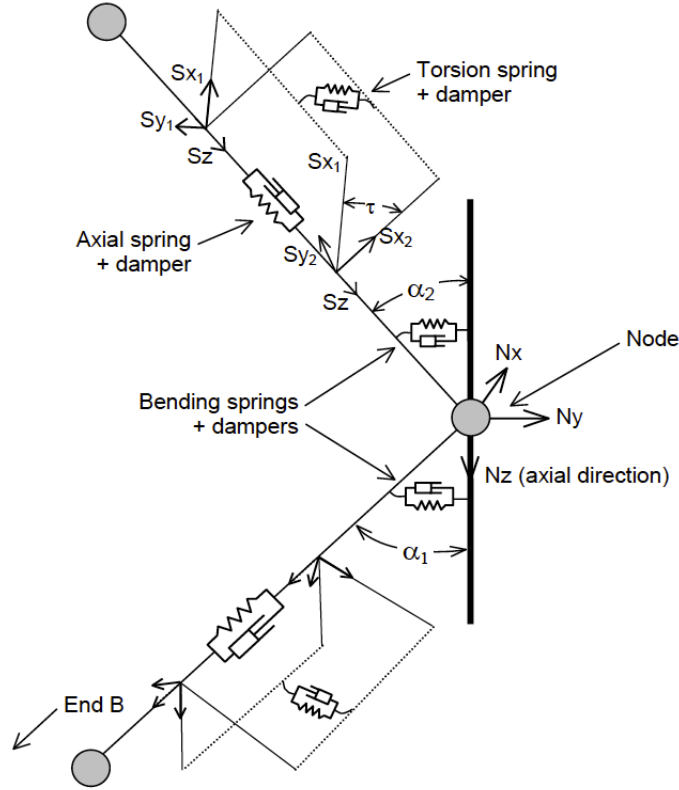


**Figure 5.4:** Detailed mathematical model of Lines (Orcina, 2014)

The effective tension is given by

$$T_e = T_w + (P_o A_o - P_i A_i) \quad (5.1)$$

where  $T_e$  is the effective tension,  $P_o$  and  $P_i$  is the inner and outer pressure respectively and  $A_o$  and  $A_i$  is the outer and inner cross sectional stress area. The wall tension,  $T_w$  is given, when implicit integration is applied, by

$$T_w = EA\epsilon - 2\nu(P_o A_o - P_i A_i) \quad (5.2)$$

where  $E$  is the Young's modulus,  $\nu$  is the Poisson ratio and  $\epsilon$  is the total mean axial strain which can be written as

$$\epsilon = \frac{L - \lambda L_O}{\lambda L_O} \quad (5.3)$$

where  $\lambda$  is the expansion factor of the segment.

The bending moment is then calculated by

$$M = EI|C| \quad (5.4)$$

where  $EI$  is the bending stiffness  $C$  is the effective curvature and is given by

$$C = \frac{\alpha}{1/2L_o} \quad (5.5)$$

where  $\alpha$  is the angle between the axial direction of the line and the segment axial axis. In Section XX (TEORI DELEN OM FORCE COEFFICIENT), the force coefficients for a cylinder are discussed. In OrcaFlex, the drag forces acting on the line is given by the equations below, which is quite similar to the previous equations discussed.

$$\begin{aligned} F_x &= P * 1/2 A_x C_{dx} V_n |V_n| \\ F_y &= P * 1/2 A_y C_{dy} V_n |V_n| \\ F_z &= P * 1/2 A_z C_{dz} V_n |V_n| \end{aligned} \quad (5.6)$$

here  $P$  is the proportion of the line that is wet or dry, often called "Proportion Wet" or "Proportion Dry" as appropriate.  $C_d$  is the drag coefficient, which may be set to vary with the Reynolds number, and is discussed in Section 5.2.3.  $A$  is the projected area and  $V$  is the fluid velocity relative to the line.

The added mass has also been mentioned in the previous section, where the added mass in Orcaflex is given by

$$F_{addedmass} = -C_a \cdot m_{fluid} \cdot a_{line} \quad (5.7)$$

where  $C_a$  is the added mass coefficient,  $C_m$  is the inertia coefficient,  $m_{fluid}$  is the mass of the fluid displaced by the line,  $a_{line}$  is the acceleration of the line and  $a_{fluid}$  is the acceleration of the fluid. The added mass coefficient can also be set as a variable data set.

### 5.1.5 Integration and Time Steps

In order to calculate the global response of the system, OrcaFlex uses either the explicit Euler integration or the implicit integration scheme. The equation of motion which

OrcaFlex solves, by either of the two schemes is

$$M(p, a) + C(p, v) + K(p) = F(p, v, t) \quad (5.8)$$

where  $M(p, a)$  is the system inertia load,  $C(p, v)$  is the system damping load,  $K(p)$  is the system stiffness load and  $F(p, v, t)$  is the external load. The parameters  $p$ ,  $v$ ,  $a$  and  $t$  are the position, velocity, acceleration and simulation time step respectively. At every time step, the system geometry is re-computed, for both integration schemes. Hence, the geometric nonlinearities are taken full account off.

In this case, the implicit integration scheme has been selected, using a variable time step and the Generalized- $\alpha$  integration scheme. This means that an iterative solution at the end of each time step is reached. The implicit integration scheme allows for faster simulation, due to the larger time steps one can choose.

The time-step for the simulation was set to a variable time-step with a maximum time-step of 0.250 s and a limitation of 20 iterations per time-step. The equilibrium positions were measured against the default tolerance of  $25 \cdot 10^{-6}$ .

## 5.2 Set-Up in OrcaFlex

This chapter describes how the different components were modelled in OrcaFlex. The system chosen to study in time-domain can be divided into three different parts; the fish cage, the feed pipe and the feed barge. The hydrodynamic data for the feed barge was imported to OrcaFlex from Wadam, while the fish cage and feed pipe were modelled directly in OrcaFlex. The water depth for the study is chosen to 40 m and the environmental conditions are shown in the NS9415 classification for fish farming in Norway. The complete set of inputs to OrcaFlex can be found in Appendix B.

### 5.2.1 Environmental condition

The environmental condition for fish farming in Norway is described by NS9415, which is shown in Section 3.1. In order to capture the different loadings acting on the feed pipe,

a set of different environmental conditions was established for the dynamic simulations. Since the thesis focuses on the responses on the feed pipe in general, a relatively small number of environmental conditions was chosen. JONSWAP-spectrum was chosen for all environmental conditions, with a peak shape factor of  $\gamma = 2.5$  for irregular sea in the North Sea. (Standard Norge, 2003). Table 5.1 below presents the environmental conditions.

**Table 5.1:** Environmental conditions used in dynamic simulation

Env. condition	$H_s$ [m]	$T_p$ [s]	Water depth [m]
EC1	2	6	40
EC2	3	7	40
EC3	4	9	40

The JONSWAP spectrum is shown in Figure 5.5 below for the three environmental conditions.

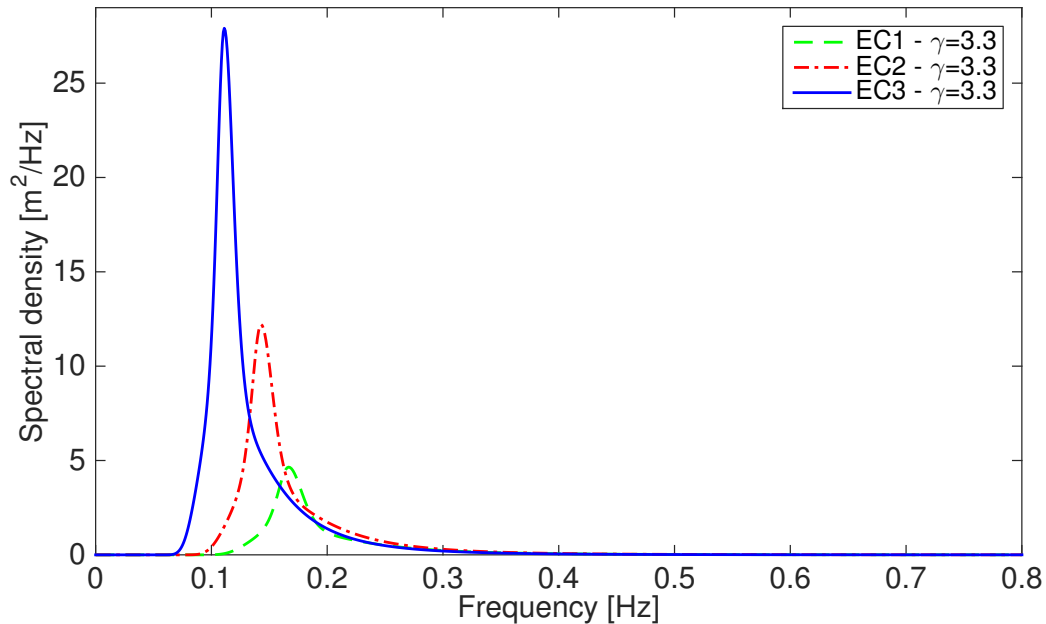


**Figure 5.5:** JONSWAP spectrum for EC1, EC2 and EC3



## 5.2.2 Modelling of Fish Cage

The fish cage used in the time-domain simulations is modelled directly in OrcaFlex, and by following the example from Orcina LTD (Orcina LTD, 2016). The fish cage can be classified as a cylindrical cage with a reverse cone base. The net model is a simplified model, i.e. the net is modelled by using lines attached by 3DOF buoys between the lines. Since bending stiffness is negligible for the net, pinned connections between the lines and the buoys are set. The net is suspended below a floating plastic ring, which is also modelled with single segment lines. Since the plastic ring of the floater naturally has bending stiffness, bending moment needs to be transferred. As a result, 6DOF buoys and built in connections are used for the floater. The value of the end connections stiffness is set to infinity, making it a rigid connection. By this modelling approach, bending moment is allowed to be transferred. Figure 2.2 below shows a schematic drawing of the fish cage with the given dimensions.

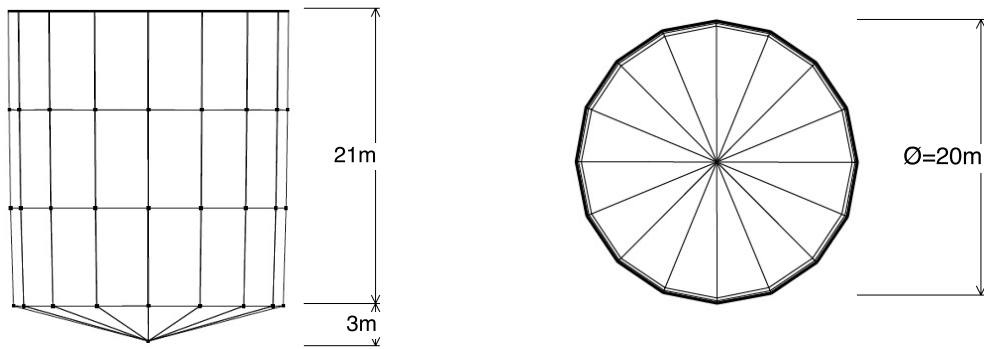


**Figure 5.6:** Side view and top view of the fish cage

A summary of the fish cage characteristics used in the analysis is shown in Table 5.2.

**Table 5.2:** Fish cage characteristics

Parameter	Magnitude	Unit
Cage Model	OrcaFlex Example	-
Material	HDPE	-
Material density	1	te/m <sup>3</sup>
Floating pipe diameter	20	m
Bottom ring diameter	20	m

### 5.2.3 Modelling of Feed Pipe

Since the material properties and dimensions vary greatly from manufacture to manufacture, a general description of HDPE material properties has been set for the feed pipe. Table 5.3 below shows the relevant dimensions of the feed pipe used in this work. The size of the pipe is chosen to represent some of the largest pipes used in the industry today.

**Table 5.3:** Feed pipe dimensions

Parameter	Value	Unit
Outer diameter	110	mm
Inner diameter	97.4	mm
Minimum thickness	6.5	mm
SDR	17.4	-
Material density	960	kg/m <sup>3</sup>

The Standard Dimension Rate (SDR) describes the geometry of the pipe and is defined as the ratio of the outside diameter and the minimum wall thickness, i.e.  $SDR = D_o/e$ . By knowing the SDR of the pipe, the minimum bending radius (MBR) is possible to find and is given by the following equation, assuming a safety factor of 1.5 (Pipelife Norge AS, 2002)

$$R_{min} = 17.4 \cdot D \quad (5.9)$$

which yields an MBR of  $R = 1.92m$ . The MBR is defined as the minimum radius one can bend a pipe without damaging or shortening its life, i.e. the MBR is a limiting value and

should not be exceeded. The mechanical properties of the feed pipe are shown in Table 5.4 below.

**Table 5.4:** Mechanical properties of HDPE

Parameter	Value	Unit
E	1100	MPa
EI	3.046	kNm <sup>2</sup>
EA	22258	kN
$\sigma_y$	25	MPa
Poisson's ratio	0.45	-
MBR	1.92	m

The bending stiffness  $EI$  is a function of the Young's modulus and the second moment area of the cross-section

$$EI = E \cdot \frac{\pi}{64}(D_o^4 - D_i^4) \quad (5.10)$$

Whereas the axial stiffness,  $EA$ , is given by

$$EA = E \cdot \frac{\pi}{4}(D_o^2 - D_i^2) \quad (5.11)$$

The maximum tension allowed of the pipe is given by the tensile stress at yield times the cross-section of the pipe

$$T_{max} = \sigma_y \cdot A_{cross-section} = 51kN \quad (5.12)$$

Figure 5.7 illustrates the pipe cross-section, with the outer diameter and inner diameter.

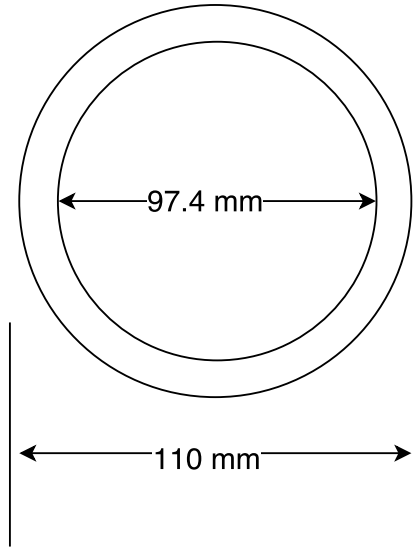


**Figure 5.7:** Feed pipe cross-section

### Force Coefficients of the Feed Pipe

Selection of the force coefficients is crucial to build a reliable and realistic computational model. To achieve an accurate assessment of the forces and the dynamic response of the system, the correct drag coefficient must be plotted in the Morison equation. This is obtained by using a variable data set which is implemented in OrcaFlex regarding the drag coefficient, which means the normal relative velocity over the element is calculated considering the effect of waves, current and speed of the line element. The relative velocity allows for the calculation of the Reynolds number which in turn computes the drag coefficient to determine the load on the element. Variable drag coefficient can be set in OrcaFlex by creating and defining a variable data set. The values used for the variable data set follows the curve given in Figure 3.6 taken from DNV-GL (2010b). This formulation of drag coefficient is given as an input of variable data set in OrcaFlex. This approach calculates the relative velocity over the elements, for each time step, considering the effect of waves, current and speed of the line element Cifuentes et al. (2014). The drag coefficient is computed by using the calculated Reynolds number. The complete variable data set is found in Appendix B.2.

## 5.2.4 Modelling of Feed Barge

The hydrodynamic data of the feed barge is imported to OrcaFlex, after the hydrodynamic modelling in Wadam is completed. This is done by saving the results from Wadam in a Wamit-formatted output file, which in turn can be imported to OrcaFlex. The feed barge characteristics is shown in Table 5.5.

**Table 5.5:** Feed barge characteristics

Parameter	Magnitude	Unit
Length	30	m
Breadth	20	m
Draught	2	m
Center of gravity	(15,10,1.6)	m
Mass	1 230 000	kg

The modelling process of the feed barge in OrcaFlex is done by creating a new vessel type and importing the hydrodynamic data found in Section 4. Since the model is limited to linear analysis only, several vessel properties are omitted. The property of interest which has been exported from Wadam in this work is the displacement RAO and the structural data. The barge is then drawn in OrcaFlex by defining the dimension of the barge. The data for the displacement RAO is too large to be shown here but can be found in Appendix XX.

## 5.2.5 Modelling of Bend Stiffener

Modelling bend stiffeners in OrcaFlex is done by using two separate lines to represent the stiffener and the line which is protects (Orcina, 2014). In this case, the feed pipe is the protected line. The protected region of the feed pipe is referred to as the protected region. This approach to modell stiffeners has the advantage of separate results for both the stiffener and the protected line Orcina (2014). There exist two different methods to model bend stiffeners in OrcaFlex, where modelling the BSR as an attachment to the line

is the simplest way. This simplified design method does not include the rigid steel mount section or friction effects between the BSR and the protected line. The design of the bend stiffener is usually left to the manufacturer, so a complete analysis regarding the design loads of the bend stiffener will not be conducted. It is assumed that the bend stiffener design already exists, so the validity of the BSR will be shown in Section 6.4.1.

The bend stiffener is modelled by specifying the outer diameter with a variable data source, so the diameter can vary with arc length (Orcina, 2014). This allows for a conical shaped stiffener. The outer diameter of the BSR is then referred in the line type data as the outer diameter of the stiffener. It is important that the segmentation of the stiffener is the same as the protected line to be able to run the simulation. The physical properties, together with the rest of line type data can be found in Appendix B.1.

**Table 5.6:** Protected region of feed pipe - Large BSR

Connection point	Protected region of feed pipe [m]
End A (fish cage)	0-3
End B (feed barge)	47-50

Figure 5.8 below illustrates the large stiffener profile graph and the small stiffener profile graph, which is used in the simulations later.

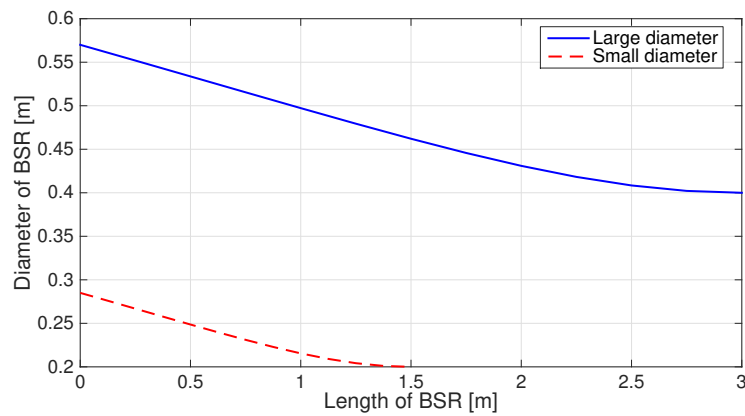


**Figure 5.8:** BSR profile graph

# 6 | Dynamic Analysis - Results & Discussion

In this chapter, the dynamic analysis of the fish farm system will be conducted. The analyses start with a simple study on the fish cage to get an understanding of how the fish cage behaves in current flow. After the brief fish cage study, several dynamic analyses examining the responses of the feed pipe is completed.

## 6.1 Deformation of Net Under Current Flow

A complete analysis of the fish cage will not be conducted, due to the lack of time and resources. Therefore, only a simple analysis will be done studying the deformation of a single fish cage under current flow.

The deformation of a net cage under current flow can drastically decrease the volume of the net. This imposes challenges concerning the well-being of the fishes inside the net, ultimately causing death due to limited space and oxygen. Research on this topic is therefore of great interest, and even more analyses of the structural integrity of the fish cage are necessary to design for safe offshore use.

The following formulae give the volume of a cylindrical cage with a reverse cone base

$$V = \pi r^2 h + \frac{1}{3}(\pi R^2 H) \quad (6.1)$$

where the first term is the volume of the cylindrical cage and the last is the reverse cone base. Here,  $r$  is the radius of the net,  $h$  is the height of the wall,  $R$  is the radius of the base net and  $H$  is the depth of the cone. For this case with the given dimensions, the volume of the cage is  $V = 6912 m^3$ . As mentioned previously, when the cage is subjected to a uniform current flow, the overall volume of the cage will decrease. The volume reduction factor  $C_V$  gives a ratio between the original volume  $V_d$  and the volume after deformation

$V_0$

$$C_V = \frac{V_d}{V_0} \quad (6.2)$$

The current subjected to the fish cage, in this case, is defined by NS 9415, see Table 3.2. Four simulations has been carried out with current velocities of  $U_c = 0.3\text{ m/s}$ ,  $U_c = 0.5\text{ m/s}$ ,  $U_c = 1\text{ m/s}$  and  $U_c = 1.5\text{ m/s}$ . Figure 6.1 below shows the deformation of the net cage during uniform current flow under various velocities.

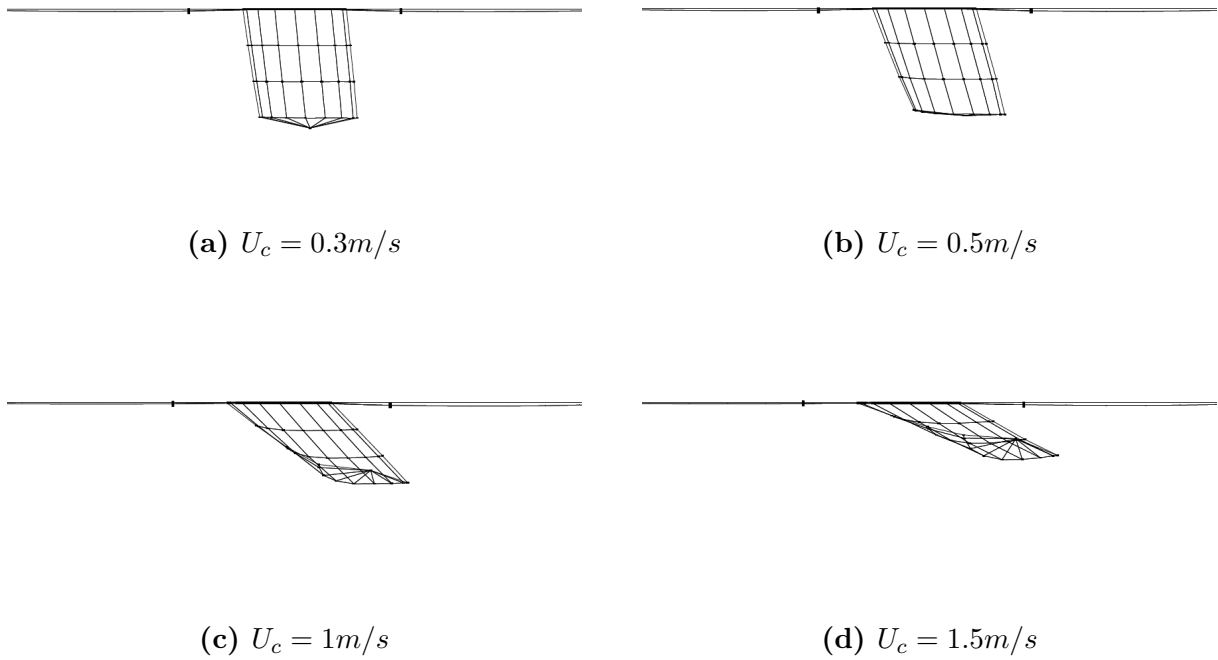


**Figure 6.1:** Fish cage deformation under various current velocities

It is shown that the volume decreases greatly, especially at current velocities of  $1 - 1.5\text{ m/s}$ . Lader and Enerhaug (2005) found that the volume of the net cage can be reduced as much as 40 % of the original volume. Since the fish cage is a simplified model, the loads and deformation of the fish cage are not accurately described in this simulation. However, one can clearly see the volume reduction of the fish cage, which corresponds well with the experiments conducted by Lader and Enerhaug.

This section does not consider a full analysis of the fish cage under various environmental conditions, due to limited time and focus on other topics. The results from the dynamic simulations act just as an indication of the forces acting on the fish cage during environmental loads, which in turn can give a better understanding of the loads subjected



on the feed pipe. The writer kindly asks the reader to look at the publications mentioned in Section 2.1.1 for complete analysis of fish cages under various environmental conditions.

## 6.2 Feed Pipe Analysis

In this section, the results from the dynamic analysis of the floating feed pipe are presented. The drag coefficient is chosen to vary with the Reynolds number, due to the variation of the relative velocity between the feed pipe and surrounding fluid. The added mass coefficient is also set as a variable data set, where the added mass varies with the submergence of the pipe. The choice of the variable data set for the drag coefficient and the added mass coefficient is validated by a sensitivity study in the following section.

The dynamic analysis is run for 3-hours to capture the highest energy in the JONSWAP-spectrum.

Range graphs are used to present the dynamic results for the pipe, showing the entire arc length of the pipe and thus showing where the maximum and minimum loads occur. The output from the dynamic simulations are as follows:

- Maximum tension
- Maximum bending moment
- Minimum bending radius
- Maximum slamming force

### 6.2.1 Sensitivity Study of Force Coefficients

One of the main challenges in modelling a floating pipe on the water surface is to estimate and determine the hydrodynamic force coefficients. The research on the topic is limited, so a sensitivity study regarding the force coefficient is necessary to perform. The sensitivity study will serve as a confirmation on whether it is necessary to include a variable data set for the drag coefficient and the added mass coefficient.

Since the feed pipe is not a fixed cylinder in the water, but rather moving relative to the waves, one cannot simply use constant drag and added mass coefficient. To determine if the variation of the hydrodynamic coefficients has a large impact on the responses of the feed pipe, a sensitivity study was conducted. The study was done in a simplified manner, where the pipe has fixed connections on both ends without any RAOs attached. The simulation time for the sensitivity study was set to 1000 seconds. Figure 6.2 below shows a sketch of the model.

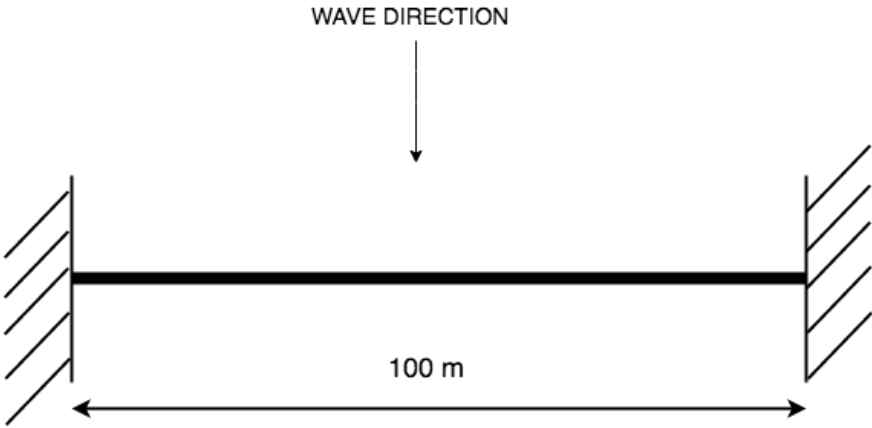


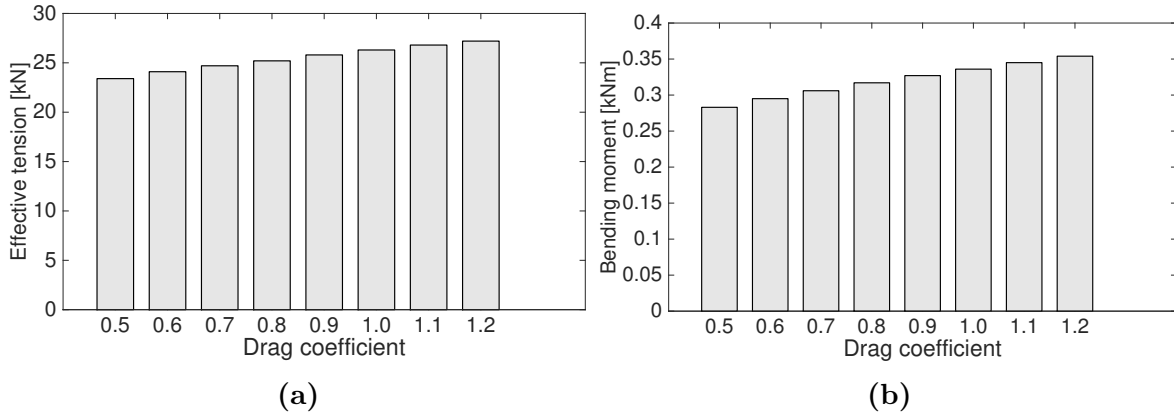
**Figure 6.2:** Sketch of model

### Drag Coefficient

Maximum tension and maximum bending moment along the pipe are output for this study. By setting the drag coefficients between 0.5 – 1.2, it is possible to look at the effect the drag coefficient has. The added mass coefficient was set to a constant value of 0.6 as a result of high KC-number. The results are shown in Table 6.1 below. By comparing the results, it can be seen that the variation in drag coefficient does not have such a large impact on the maximum tension and the maximum bending moment. As expected, the highest loads occur with the highest drag coefficient at 1.2. The variation of the responses is not large for this case but is expected to be larger when introducing the fish cage and the feed barge at both ends of the feed pipe. This will induce more motion of the feed pipe, which in turn will affect the drag coefficient even more. It is thus decided to set the drag coefficient as a variable data set. A graphical representation is shown in Figure 6.3

**Table 6.1:** Pipe responses with different drag coefficients

$C_D$	Max. effective tension [kN]	Max. bending moment [kNm]
0.5	23.4	0.283
0.6	24.1	0.295
0.7	24.7	0.306
0.8	25.2	0.317
0.9	25.8	0.327
1.0	26.3	0.336
1.1	26.8	0.345
1.2	27.2	0.354

**Figure 6.3:** Comparison between the drag coefficient and the responses on the feed pipe. (a) Effective tension, (b) Bending moment

When setting the drag coefficient as a variable data set in OrcaFlex, the Reynolds number can also be investigated together with the relative velocity of the pipe. Figure 6.5 below illustrates the Reynolds number and the relative velocity of the pipe with respect to the arc length of the pipe. By studying the figure, one can see that the drag coefficient will vary because of the variation of the Reynolds number. Since the feed pipe is long enough to follow the wave motion, the feed pipe will not have the same velocity over the pipe length. By studying the graphs, it is seen that the velocity is largest in the middle of the pipe where it will be more freely to move. As the velocity increases, the Reynolds number also increases, as shown in Equation 3.27. This is another confirmation that the variable data set that has been implemented in OrcaFlex is a reasonable choice when computing

the drag coefficient.

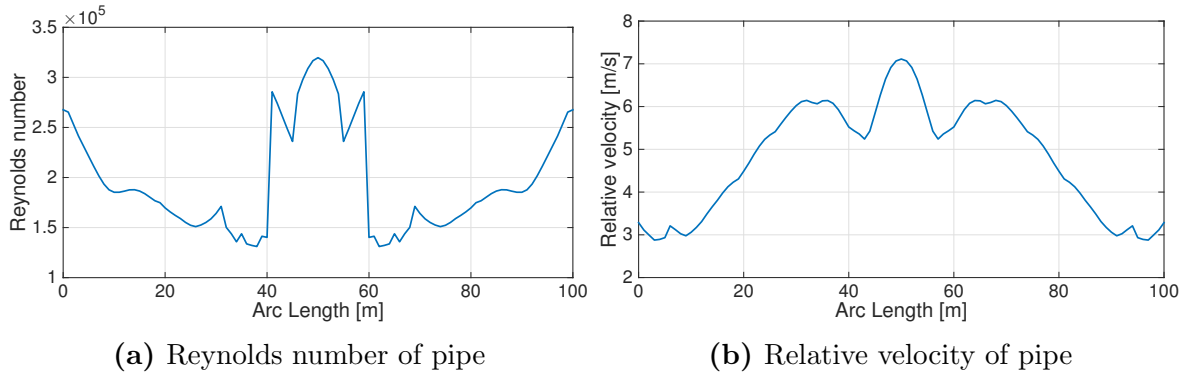


**Figure 6.4:** Illustration of Reynolds number and relative velocity of the pipe

### Added Mass Coefficient

The same has been done for the added mass coefficient as for the drag coefficient. A set of constant added mass coefficients was chosen to look at the responses of the pipe. The drag coefficient was set to 1.2 during the sensitivity study for the added mass coefficient. The results are shown in the table below for the different values of the added mass coefficient. As seen from Table 6.2, varying the added mass coefficient does not have such a large impact on the responses on the pipe. For the effective tension When a constant added mass coefficient is chosen, OrcaFlex calculates the results by fixing the added mass and varying the displacement of the pipe. This will give some uncertainties in the result when introducing the fish cage and the feed barge, as discussed above.

**Table 6.2:** Pipe responses with different added mass coefficients

Ca	Max. effective tension [kN]	Max. bending moment [kNm]
0.6	27.2	0.303
0.7	27.7	0.312
0.8	28.2	0.334
0.9	28.7	0.350
1.0	29.2	0.356

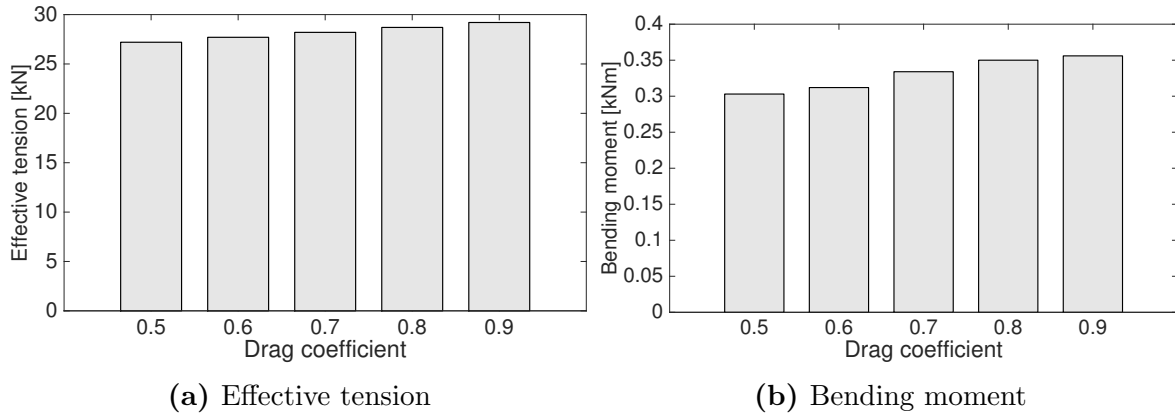


**Figure 6.5:** Comparison between the added mass coefficient and the responses on the feed pipe

### Variable Added Mass

As mentioned in section 2, the added mass coefficient changes as a function of submergence. It was thus necessary to study how this will affect the responses of the pipe as well. In OrcaFlex 10.1 it is possible to set the added mass as a variable. The complete variable data set can be found in Appendix B.2 shows the values used for the variable added mass and Table 6.3 shows the responses of the pipe.

**Table 6.3:** Pipe responses with variable added mass

Max. tension	Max. bending moment
[kN]	[kNm]
27.2	0.354

### 6.2.2 Conclusion from Sensitivity Study

For the drag coefficient, the sensitivity study have shown that for the drag coefficient, there is not a large impact on the responses of the pipe. Parameters such as the Reynolds number and the relative velocity does, however, vary along the arc length of the pipe, which results in changes in  $C_D$ . It is therefore concluded that a variable data set will be implemented in OrcaFlex to make certain the correct drag coefficient is chosen for the analysis.

For the added mass, the same can be concluded regarding the responses of the pipe. When setting the added mass to a variable, the result does not deviate from the constant added mass formulation. However, the variable added mass will be chosen when conducting the dynamic analysis of the feed pipe. This will give a more accurate and detailed result, than choosing a constant added mass coefficient. The slam force can also be shown by setting the added mass a variable data set.

### 6.3 Pipe Configuration Study

A pipe configuration study will be performed to determine the optimal configuration of the feed pipes. This can be done in several different ways, but this study will focus primarily on the total length of the feed pipes, as well as the line end orientation of the pipe at the connection points. Figure 6.6 is a representation of the coupled system in OrcaFlex, where the fish cage, feed pipe and feed barge are shown as one system.

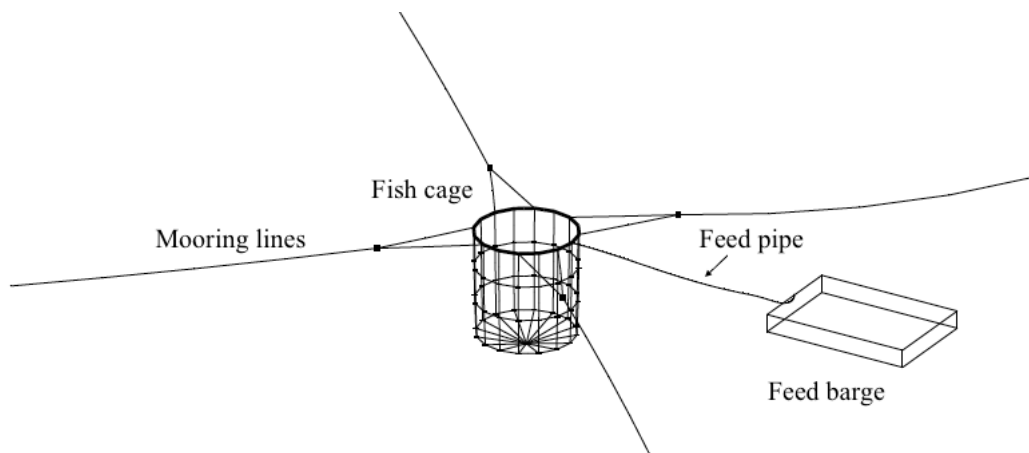


**Figure 6.6:** Coupled system in OrcaFlex

The lengths chosen to study is  $50\text{ m}$ ,  $100\text{ m}$ ,  $500\text{ m}$  and  $1400\text{ m}$ , where  $1400\text{ m}$  is the maximum pipe length provided by manufacturers. The objective of the study is to identify the optimal distance between the fish cage and feed barge, with different environmental conditions. The feed pipe is split into different segments with finer segmentation at the connection points, to get more detailed results at the critical points. Also, since

the bending of the pipe at the connection points are large, it is necessary to have finer segmentation (Orcina, 2014). The segmentation of the pipe can be found

### 6.3.1 Case 1: 50 m Pipe

The first case performed is with a 50 m long feed pipe connected to the fish cage and feed barge. Three different environmental conditions are used, as seen from Table 5.1, with wave directions of  $0^\circ$  and  $90^\circ$ .

First of all, Figure 6.7 - 6.9 shows the motion of the feed barge in heave, pitch and roll respectively for EC3. For beam sea, it is clearly shown that the roll motion is large. Since the feed barge was modelled using a pure panel model, the barge will exhibit larger motion than if viscous effects would have been modelled. The roll motion will certainly have an impact on the feed pipe, which is discussed below. The heave motion is also significant, while the pitch motion for beam sea is negligible.

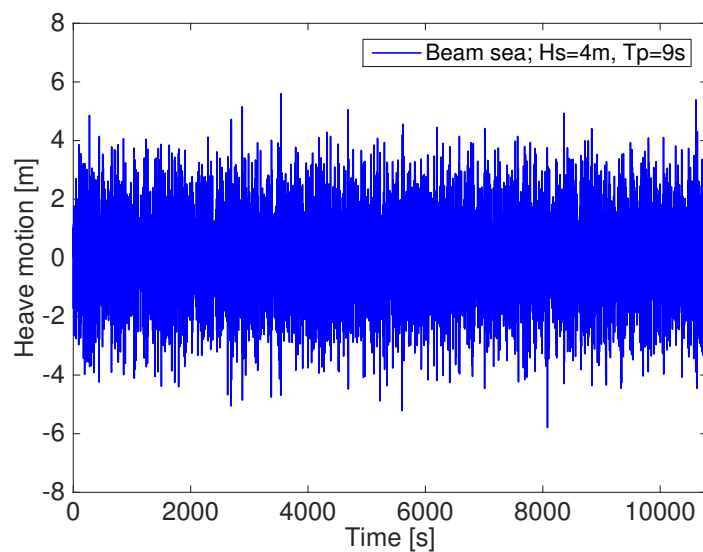


**Figure 6.7:** Heave motion of barge

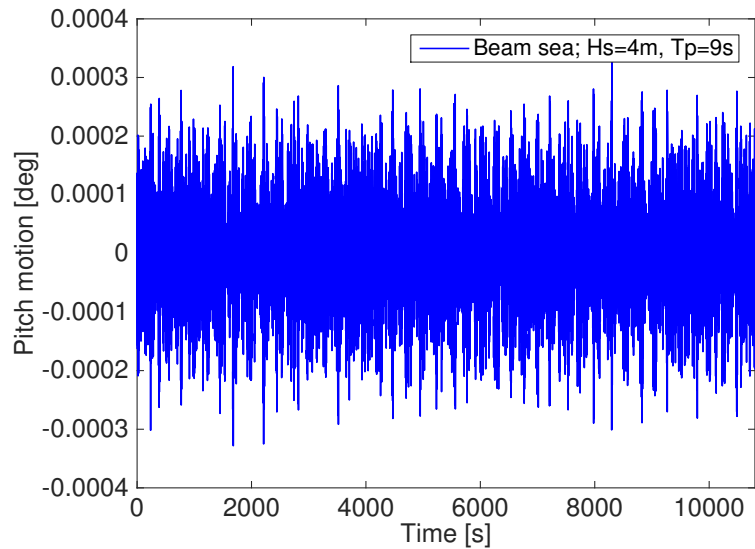


**Figure 6.8:** Pitch motion of barge

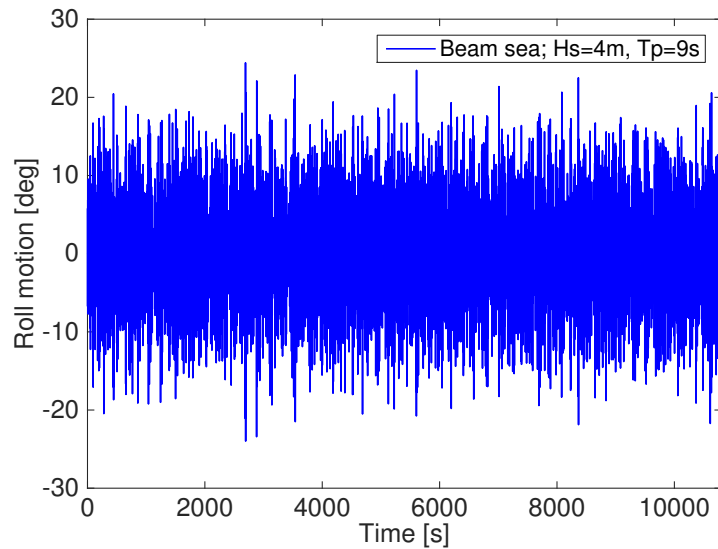


**Figure 6.9:** Roll motion of barge

Figure 6.10 below shows the range graph of the effective tension and bending moment on the pipe for EC1 with wave direction of  $90^\circ$ . Range graphs show results as a function of the arc length of the line, which is desirable in this analysis. As seen from the figure, the maximum effective tension occurs along the pipe and not at the connection points. The minimum effective tension, i.e. compression of the pipe occurs at about  $2 - 3m$  from the feed barge. This is the point where the feed pipe contacts the sea surface, and consequently the pipe will be in compression. This is also shown by the bending moment at the given point. The maximum bending moment occurs at the connection point as expected, whereas along the pipe the bending moment is insignificant, i.e. the bending radius is



larger than the limiting value of  $1.92m$ . The fact that the bending radius is sufficient along with the pipe gives an indication that the pipe has enough length to move with the waves.

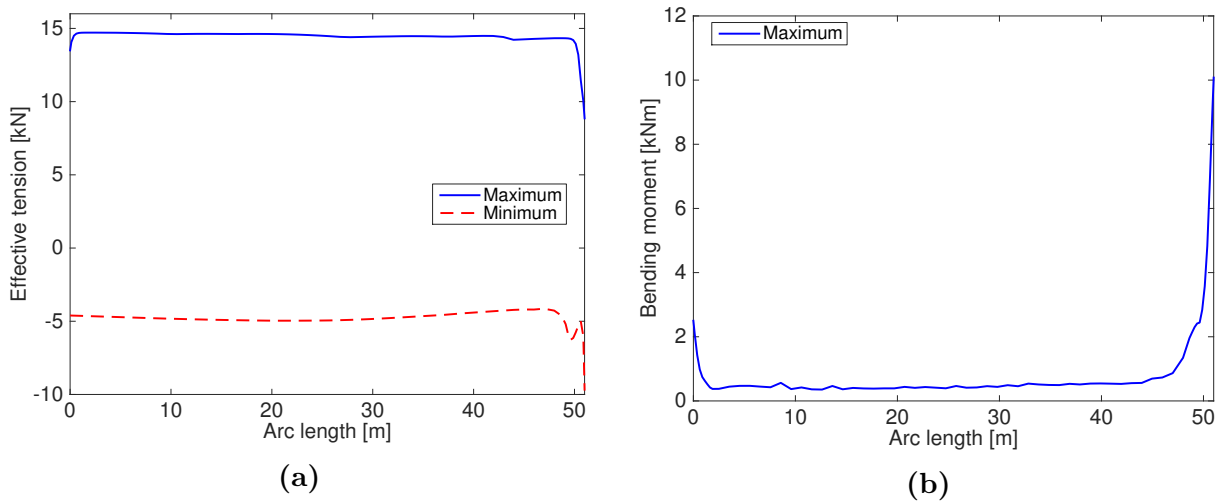


**Figure 6.10:** Range graph results. (a) Effective tension, (b) Bending moment

Table 6.4 below shows a summary of the results with a 50 m long pipe. As seen from the results, the responses on the pipe clearly increase as  $H_s$  and  $T_p$  increases for the different sea states. The forces are shown on the connection points at the fish cage and the feed barge. Overall, it is clear that the largest forces occurs at the feed barge and not at the fish cage. The effective tension is larger at the fish cage than at the feed barge. However, for the bending moment, it is shown that the largest values occur at the feed barge. This can also be observed from Figure 6.11b. This is due to the large motion of the barge under wave conditions.

**Table 6.4:** Summary of results - 50 m pipe length

Response	Connection point	EC1	EC2	EC3	Unit
<b>Wave direction - 0 °</b>					
Effective tension	Fish cage	4.86	6.82	14.2	kN
	Feed barge	1.97	4.65	5.10	
Bending moment	Fish cage	0.187	0.240	0.606	kNm
	Feed barge	7.02	7.51	10.7	
Bending radius	Fish cage	16.3	12.6	5.02	m
	Feed barge	0.434	0.406	0.285	
<b>Wave direction - 90 °</b>					
Effective tension	Fish cage	9.02	13.5	15.2	kN
	Feed barge	4.85	8.86	9.65	
Bending moment	Fish cage	2.33	2.81	3.12	kNm
	Feed barge	8.40	11.26	11.90	
Bending radius	Fish cage	1.30	1.08	0.945	m
	Feed barge	0.363	0.270	0.120	

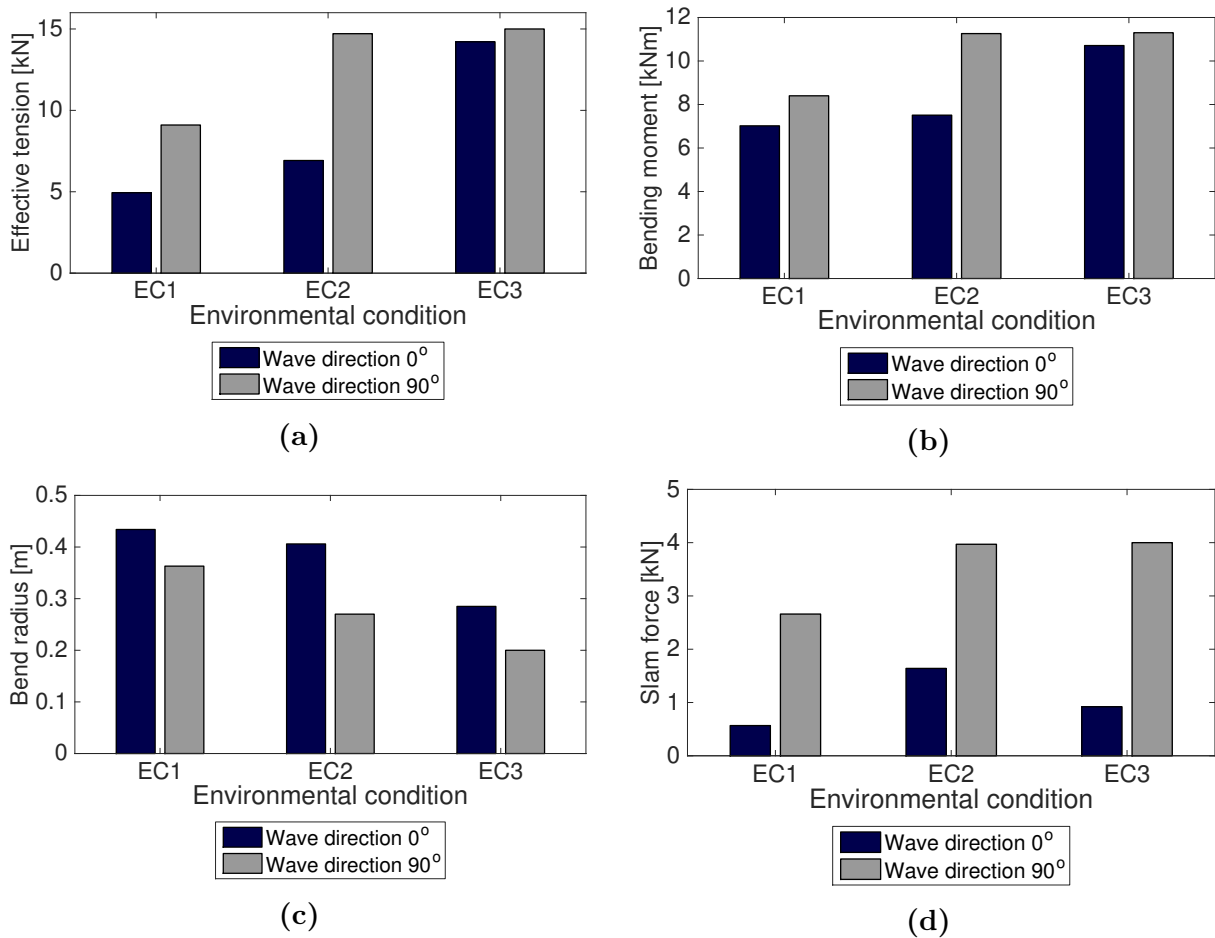
Figure 6.11a below illustrates the maximum effective tension for the different environmental conditions conducted in the simulations. The pitch motion of the barge, which peaks at about  $9 \text{ deg/m}$  for head sea, referring to Section 4.3, has a significant contribution to the effective tension on the pipe. However, for beam sea, the maximum effective tension for EC1-EC2 is around 86 – 98 % larger than for following sea. This may be because the waves push on the pipe from the side, causing overall more tension.

Figure 6.11b shows the maximum bending moment for the three sea states. The largest forces occurs as expected for sea state EC3. Beam sea yields the largest bending moment on the pipe, which may have a direct correlation with the roll motion of the barge. As seen from Section 4.3, the response in roll motion is quite large for waves hitting  $90^\circ$  on the barge, peaking at  $22 \text{ deg/m}$ . This again gives large roll motion. As a result, the feed pipe will experience larger forces when the waves hit  $90^\circ$  with respect to the pipe.

As for the MBR, Figure 6.11c shows that the MBR is below the limiting value for the given pipe. This will compromise the structural integrity of the pipe and ultimately cause failure. As a direct result, measures should be taken into account, which can secure the

pipe from not over-bending.

As shown in Section 6.2.2, the pipe was modelled with a variable data set for the added mass. This allows for results regarding the slamming force on the pipe, where the relevant theory on slamming is shown in Section 3.4.7. The slamming force is quite large, especially for wave directions of  $90^\circ$ . The fact that the pipe is suspended from the feed barge, down to the sea, gives room for slamming forces. The pipe will slam into the sea with relatively high velocity, yielding considerably high slam force.



**Figure 6.11:** 50m long pipe results for different sea states. (a) Effective tension, (b) Bend moment, (c) Bend radius, (d) Slam force

### 6.3.2 Case 2: Varying Lengths

The previous results indicate that sea state EC3 with wave direction of  $90^\circ$  relative to the pipe gives the largest forces on the feed pipe. To save time on the next simulations due

to many different cases, only sea state EC3 with wave direction of  $90^\circ$  will be performed. Table 6.5 shows a summary of the results on the connection points for the different lengths chosen. The trend is the same for all lengths, with increasing loads as  $H_s$  and  $T_p$  increases. The effective tension is highest at the fish cage, whereas the maximum bending moment occurs at the feed barge.

**Table 6.5:** Summary of results for sea state EC3 with wave direction of  $90^\circ$ - Varying lengths

Response	Connection point	Value				Unit
Pipe length	-	50	100	500	1400	m
Effective tension	Fish cage	9.02	13.10	13.57	14.11	kN
	Feed barge	4.85	7.02	5.01	9.99	
Bending moment	Fish cage	2.33	2.52	3.13	3.58	kNm
	Feed barge	8.40	9.09	9.59	11.54	
Bending radius	Fish cage	1.30	1.21	0.957	0.850	m
	Feed barge	0.363	0.335	0.318	0.264	

Figure 6.12 below compares the responses of interest with the different pipe lengths. As seen from the comparison, 50 m pipe length has the lowest effective tension. When increasing the length from 100 m to 500 m, the effective tension, bending moment and the slamming force all increases. This increase is also seen from 500 m to 1400 m. The length of the pipe may increase the overall effective tension due to the increase in weight. When the pipe is set in motion by the waves, higher forces will naturally be present.

As seen from the figure, the bending moment decreases for pipe lengths of 100 m and 500 m, relative to the 50 m pipe. The 1400 m long pipe exhibits the largest forces compared to the others, with an increase of over 90% for the effective tension. For the slamming force, pipe length of 500 m exhibits the highest forces. The largest slamming force occurs at the connection point at the feed barge.

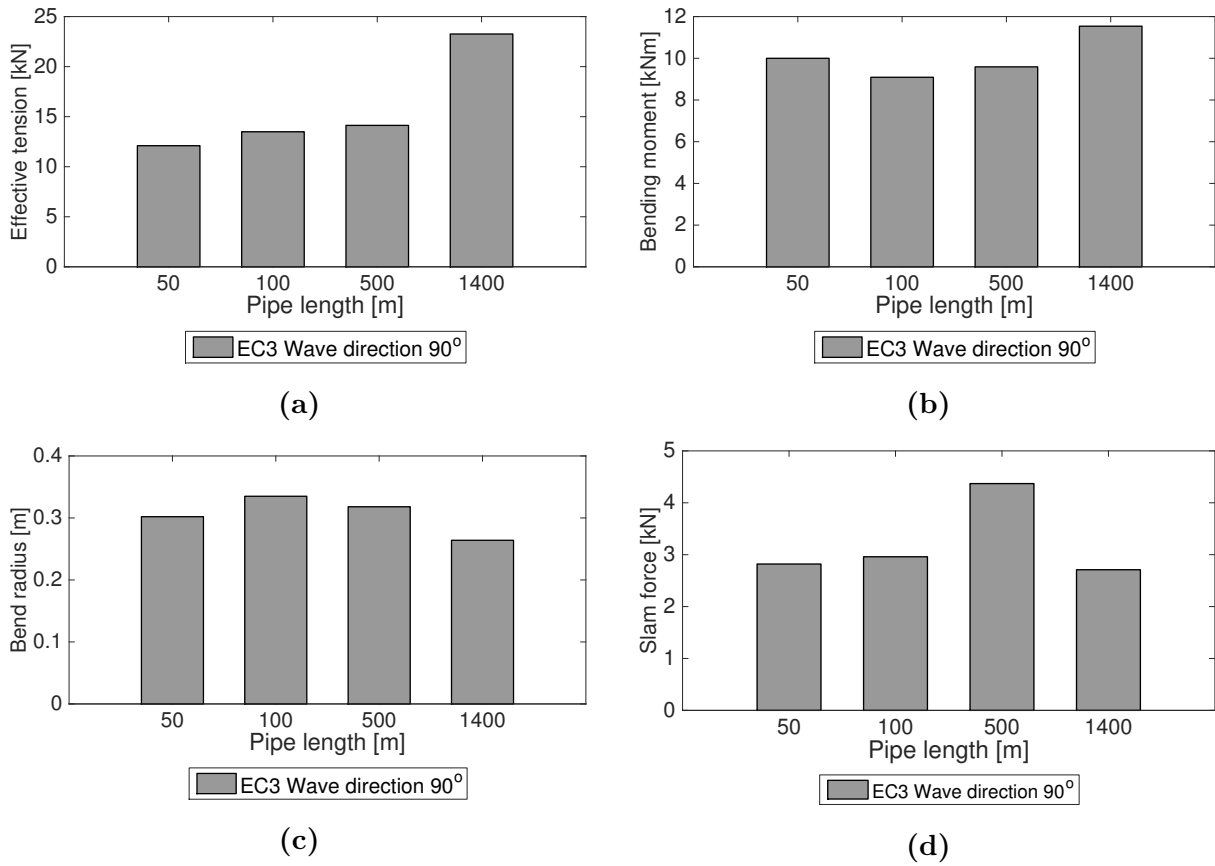


**Figure 6.12:** Comparison of pipe length. (a) Effective tension, (b) Bend moment, (c) Bend radius, (d) Slam force

### 6.3.3 Case 3: Varying Line End Orientation at End B

Another parameter which may affect the responses on the feed pipe, especially the bending moment, is the Line End Orientation of the pipe at the connection point. This is particularly true for the connection point at the feed barge because the feed pipe is connected at the feed barge above the water surface. The results will, therefore, be different for varying declination angles. The previous analyses had a declination angle of  $0^\circ$  on the connection points, so angles larger than  $0^\circ$  will be investigated in this section. Look in Section 5.1.4 for a brief explanation of the declination angle. The declination angle is set to  $90^\circ$  for the connection point at the fish cage, because the connection point is just above the sea surface. As stated by Sunde et al. (2003), there is a large focus on decreasing the feed crushed while transporting it to the fish cages. The bending of the pipe is a direct consequence of the feed crushed, so the curvature of the pipe should be controlled to avoid this particular problem.

The results shown in Figure 6.13b clearly indicates that the bending moment is much lower for increasing declination angle. A nearly 50% reduction in bending moment is achieved by increasing the declination from  $0^\circ$  to  $75^\circ$ . As a consequence, the MBR is also higher as a result of lower bending moment. By setting the declination angle to  $90^\circ$  the curvature of the pipe is much lower, i.e. it is preferred to suspend the pipe from the feed barge so that it does not face the sea directly. Figure 6.13a shows the maximum effective tension for different declination angles, which also has a declining trend with higher declination angle. This may be because of the static position of the pipe with a declination angle of  $90^\circ$ . Overall, the forces on the pipe is much smaller with a higher declination angle between the feed pipe and the feed barge. However, the slam force, as shown in Figure 6.13d, is higher with increasing declination angle. This may be as a result of the increasing height between the pipe and sea surface. With a larger distance to the sea surface, the velocity of the pipe will be higher when it hits the sea surface. This again gives larger slam force, as shown in Equation 3.34. Even though the forces has decreased significantly with higher declination angle, the MBR is still under the limiting value.

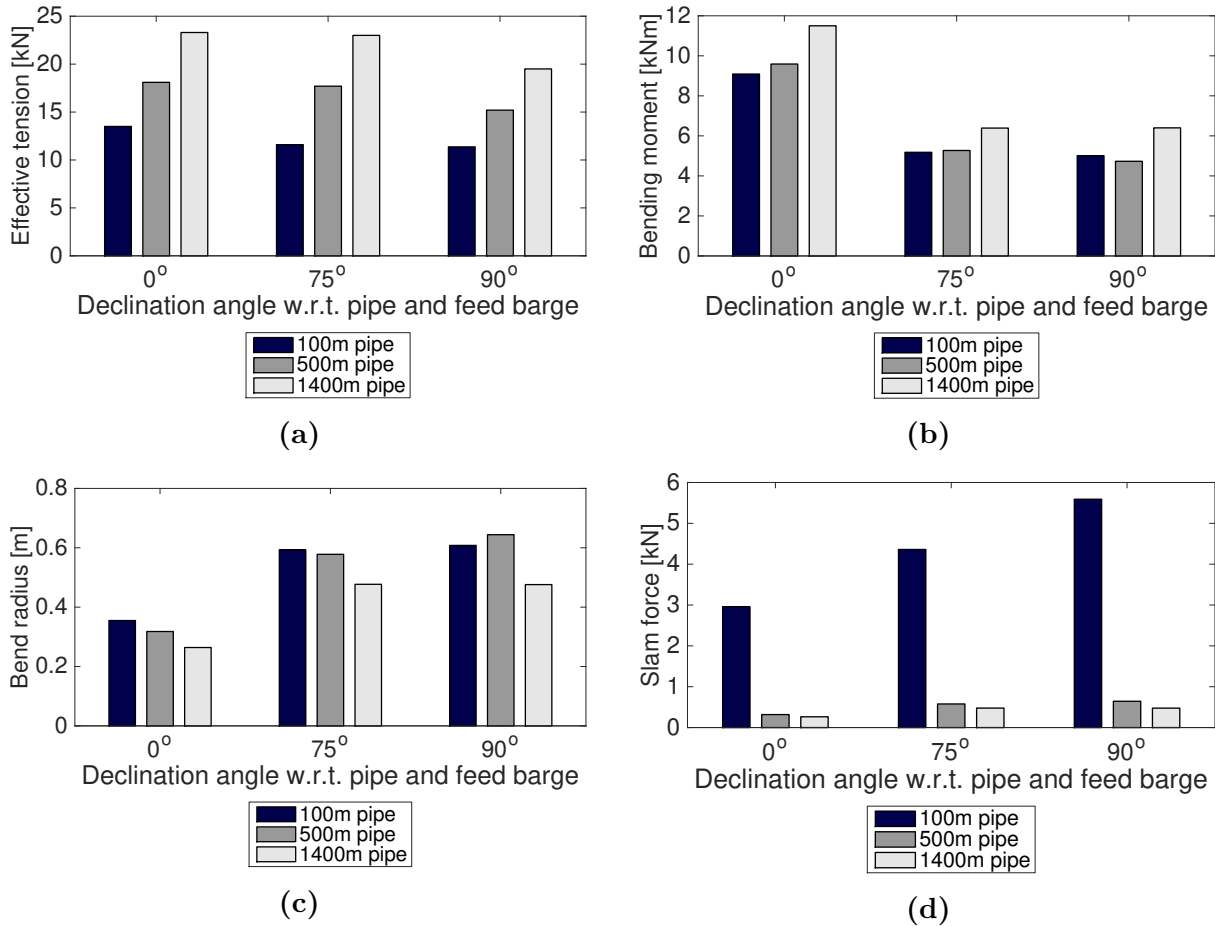


**Figure 6.13:** Comparison of different pipe length and declination angle. (a) Effective tension, (b) Bend moment, (c) Bend radius, (d) Slam force

## 6.4 Pipe Responses With Bend Stiffener

As seen from previous results, the bending moment of the pipe exceeds the allowed limit for all sea states. The curvature of the pipe is too large, so the structural integrity of the pipe is threatened. A bend restrictor device is, therefore, necessary to implement to avoid failure of the pipes. The modelling procedure of the bend stiffener is shown in Section 5.2.5. To determine the dimension of the BSR, two different sizes was used in the simulation. This is due to the lack of knowledge regarding the effect on the feed pipe when using the BSR. The main reason to use a bend restrictor device on the feed pipe is to control the large bending of the pipe at the connection points. Since HDPE material is flexible compared to other materials, the pipe will bend quite a lot when exposed to rough sea states and measures need to be taken. This has been shown in previous simulations above, where the MBR is lower than the limiting value. It was therefore decided to adopt

bend stiffeners for further analyses. Pipe length of 1400  $m$  is discarded in further analysis, because it exhibits unfavourable responses. The effective tension, as well as the bending moment, is larger than any of the lengths. The following sections show the results with the bend stiffeners attached to the feed pipe at the connection points, where the maximum bending moment occurs.

### 6.4.1 Validation of Design

Before conducting the dynamic analysis of the feed pipe with the attached BSR, a validation of the BSR design is necessary. A comparison between the feed pipe and the bend stiffener with respect to the curvature and bending moment needs to be investigated, to state if the BSR does the job. The area of interest is on the whole bend stiffener length, i.e. 3  $m$ . The top two plots in Figure 6.14 shows the curvature of the feed pipe and the bend stiffener, which exhibits great similarity. The similarity of the plots are as expected, the BSR and the feed pipe should have the same curvature. However, by looking at the bottom two plots, the bending moment experienced by the two lines are quite different. This shows that the BSR design is designed correctly, experiencing much more of the load than the feed pipe. This is the sole purpose of the BSR.



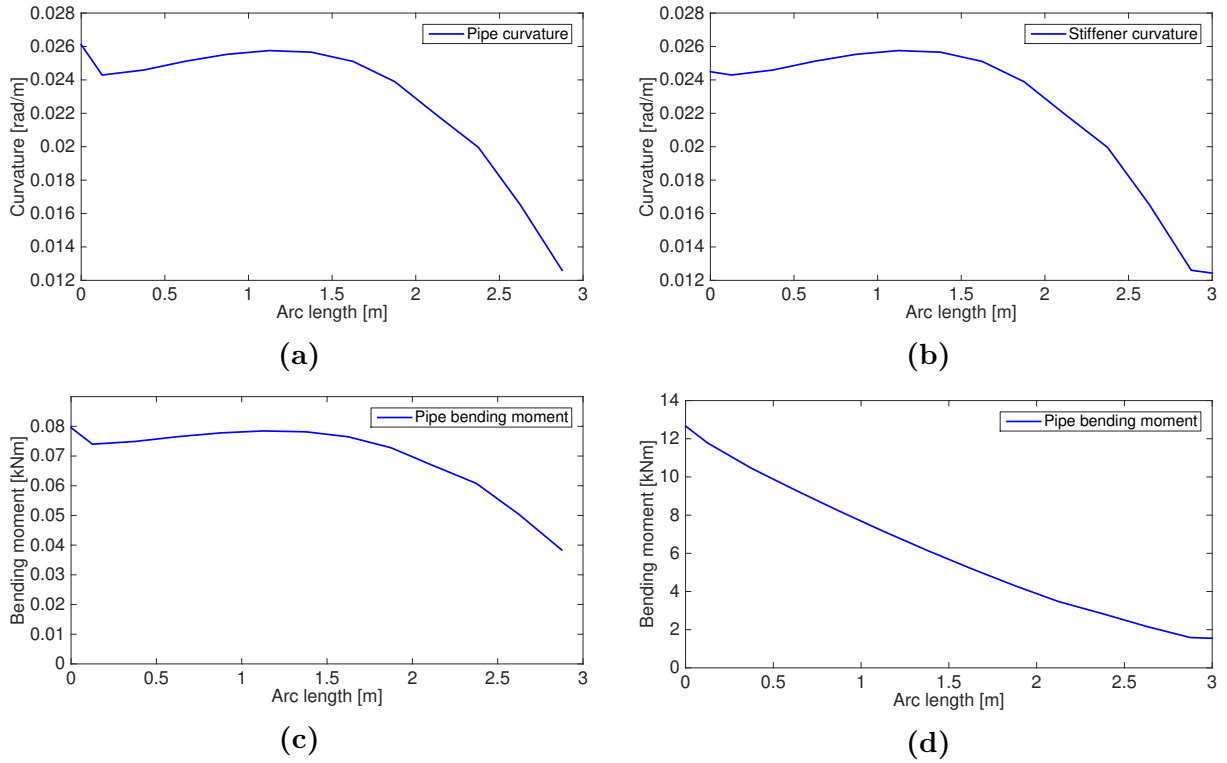


**Figure 6.14:** Curvature vs. bending moment of feed pipe and bend stiffener. (a) Feed pipe curvature, (b) BSR curvature, (c) Feed pipe bending moment (d) BSR bending moment

### 6.4.2 Case 4: Pipe Responses with BSR

After confirming the validity of the BSR design, as discussed above, dynamic analysis of the feed pipe with bend stiffeners at both connection points, can be performed. The geometry of the bend stiffeners used in this analysis is shown in Section 5.2.5.

Figure 6.16 below shows a summary of the BSR results, compared to the results without the BSR attached. As seen from the results, the MBR is much higher than previous simulations and is within the allowable limit. However, this is only true for the large BSR, which applies to all lengths of the pipe. The BSR with a smaller diameter will be discarded for further analysis because it does not satisfy the criteria to keep the pipe from over-bending.

The results show that the effective tension with BSR is larger than without the BSR attached. For 50 m pipe length without the BSR attached, the effective tension increases about 12% for the small BSR and as much as 81% for the large BSR. The same trend can also be seen in pipe lengths of 100 m and 500 m. The reason for the higher tension may

be due to the local stiffness added to the pipe, which induces higher tension forces on the pipe. Since the pipe is restricted in bending, the forces will translate to tension rather than bending moment. This effect should be investigated when considering designing the feeding system for offshore location. As for the pipe limits, it is not an issue since the tension is under the allowable tension for the pipe,  $T_e < T_{max}$ .

From the validation study in Section 6.4.1, the design of the BSR was confirmed by looking at the bending moment vs. the curvature on the feed pipe and the BSR. After running the dynamic simulation with BSR attached, one can see that the bending moment is drastically reduced. For 50 m, the reduction in bending moment with the small BSR compared to without the BSR attached is 398% and 846% for the large BSR. The bending of the pipe is controlled in a satisfying manner by reducing the bending moment to a desirable level.

As can be seen from Figure 6.16, the slam force is also reduced when incorporating the BSR. This is because the slamming force on the pipe at the connection points is not registered when attaching the BSR. The results for the slamming force are thus registered from where the BSR ends, i.e. only the pipe length 3 – 47 m experiences slamming. This is illustrated in Figure 6.15 below.

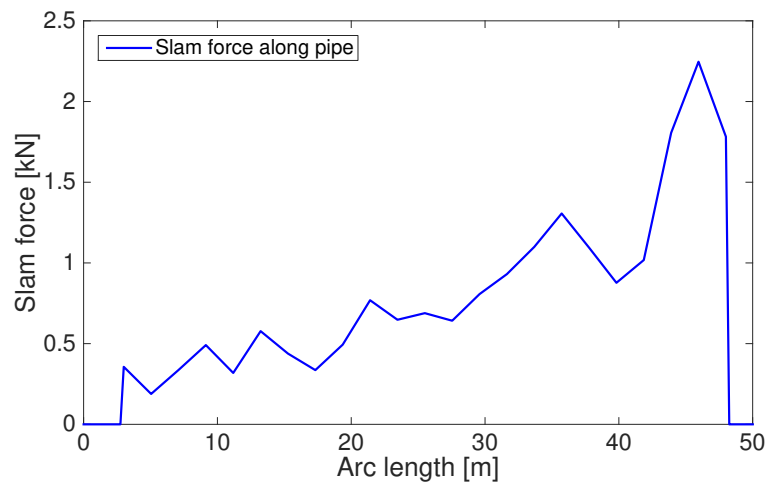
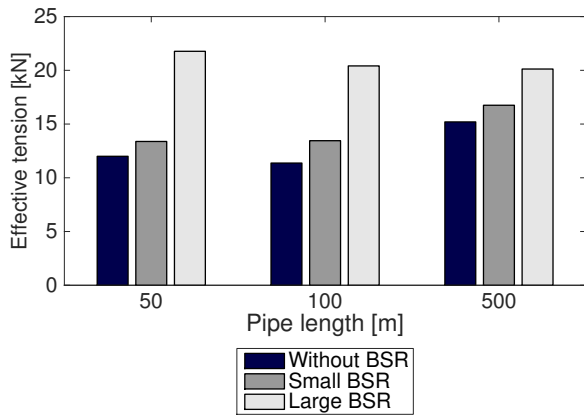
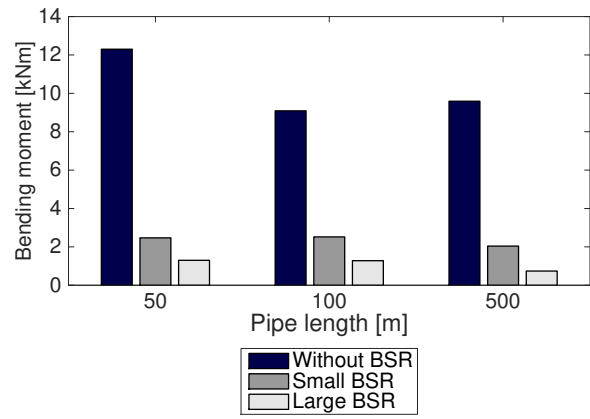


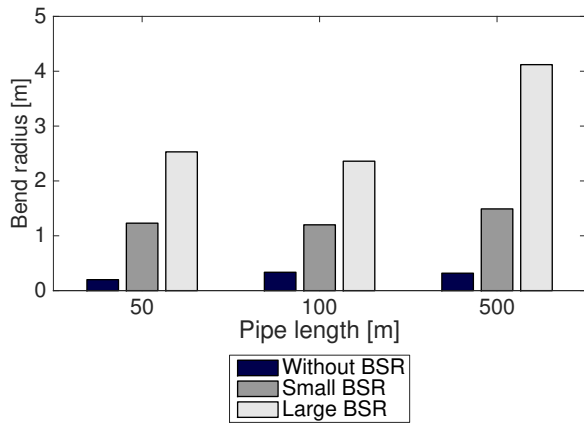
**Figure 6.15:** The slamming force on feed pipe with BSR attached



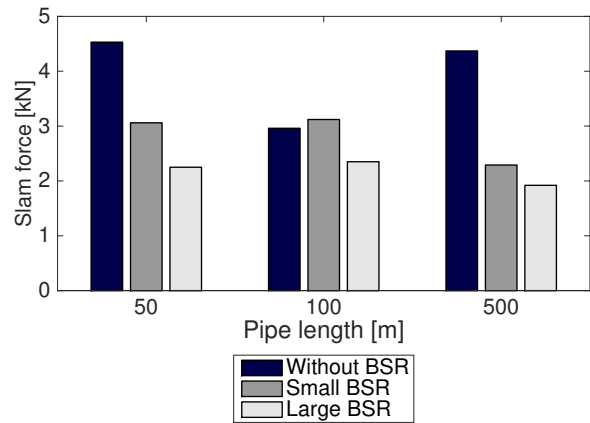
(a) Effective tension



(b) Bending moment



(c) Bend radius



(d) Slam force

**Figure 6.16:** Comparison of responses with and without BSR. (a) Effective tension, (b) Bending moment, (c) Bend radius, (d) Slam force

The main goal was to keep the MBR of the pipe over the limiting value, which has been successfully achieved by attaching BSR.

## 7 | Conclusion

The main goal of this thesis was to predict the hydrodynamic loads on feed pipes used in the aquaculture industry. The prediction of the loads is an important aspect of design and operation of the feeding system, which can support companies in the aquaculture industry with valuable knowledge.

The hydrodynamic model of the feed barge was obtained by creating a mesh in GeniE, running the potential solver Wadam in frequency domain and post-processing the results. The hydrodynamic analysis of the feed barge showed large motions in heave, pitch and roll, which in turn contributes to high loads on the feed pipes. The feed barge was modelled as a pure panel model without viscous effects, so a hydrodynamic analysis with the Morison theory applied should be performed in the future to obtain more accurate results.

A simplified fish cage was modelled directly in OrcaFlex, to obtain the complete fish farm system for the time domain analysis. A short study on how the fish cage acts under current flow was done, where the results showed significant deformation of the fish cage net.

The hydrodynamic loads on the feed pipe was the main focus of this thesis. Four different responses were of interest; the effective tension, the bending moment, the bend radius and the slamming force. A sensitivity study of the force coefficients was done to establish whether a variable data set for the added mass coefficient and the drag coefficient was necessary to set for the feed pipes. The sensitivity study showed that the variation of the effective tension was not large, while for the bending moment it was larger. The Reynolds number showed large variation for the floating pipe, so it was decided to set the drag coefficient and added mass coefficient as a variable data set for the feed pipe.

The dynamic analysis in time domain shows that for higher sea states, the loads on the feed pipe increases. Wave direction of  $90^\circ$  with respect to the feed pipe yields larger forces on the pipe than wave direction of  $0^\circ$ . The highest tension occurs along the feed pipe, while the largest bending moment occurs at the connection points of the pipe. The

motion of the feed barge is most likely a direct consequence for the high loads on the pipe.

The study of the feed pipe lengths was also done, by varying the pipe length. The results for the different lengths exhibits an increase in the effective tension. The declination angle at the connection points for the feed pipe was also considered in the study. Higher declination angle clearly showed a decrease in the bending moment of the feed pipe, especially at the feed barge.

Bend stiffener was included in the dynamic simulations, due to the large bending of the feed pipe for all sea states. A validation study of the BSR was done to confirm the design of the BSR. The effective tension of the feed pipe increased 53% for 50 *m* pipe length, 50% for 100 *m* pipe length and 23% for 500 *m* with the large BSR attached to the pipe. The reason for the increase in tension may be because of the restriction in bending with the BSR attached, which translates the forces to tension. The reduction in bending moment, with as much as 846 % with the large BSR attached, shows that the bending of the pipe is controlled in a satisfying manner.

The hydrodynamic loads on the feed pipe may be considered as too high for rough sea states. The industry has expressed a demand for knowledge regarding the feed pipes, which is a high motivating factor for this thesis. Unfortunately, there exist no work on hydrodynamic loads on feed pipe to this date, which makes it hard to compare it with other work. However, the findings of the analysis conducted throughout this thesis exhibit some interesting findings. The main conclusion of the analyses is that the bending of the pipe is an issue for harsh environments, so bend stiffeners at the connection points is necessary to install. Longer feed pipes than 500 *m* should possibly be avoided due to the present of high loads, but also because of the disadvantageous of feed crushing for longer pipes. As a concluding remark, more research and study is necessary on the given topic.

## 8 | Further Work

This thesis work lays the basis for further investigation on the hydrodynamic loads on feed pipes for fish farming in general. For the time being, the research on the topic is limited and should be expanded to further strengthen the knowledge on the feeding system in its entirety. The future work, with improvements can be considered as:

- The feed barge modelling should be improved in frequency domain by including viscous effects, i.e. the Morison theory. This would give a more accurate description of the hydrodynamic loads on the feed barge.
- The fish cage should be improved by including the solidity ratio of the net and bottom weights. A complete mooring analysis of the fish cage should also be modelled.
- The numerical model in OrcaFlex can be improved regarding the force coefficients of the feed pipe. Even more research is needed, so comparison of results can be made. Several environmental conditions may be considered in the dynamic analysis, in which more cases with different configurations of the feed pipe can be done. Also, a complete bending stiffener analysis should be done to design the optimal stiffener design.
- A fatigue analysis using SN-curves and rainflow counting should be performed for the feed pipe. The fatigue aspect of the feed pipes are believed to be significant, so a study on this should be carried out.
- Finally, concept evaluation on new developments can be considered in the future. New technology such as underwater feed lines could be interesting to look at for harsh environments.



# Bibliography

- AKVA Group ASA (2015a). Ac650 panorama feed barge. [Image] Available from: <http://www.akvagroup.com/news/image-gallery> [Accessed 27.02.17].
- AKVA Group ASA (2015b). Akvasmart. [Online] Available from: <http://www.akvagroup.com/news/image-gallery> [Accessed 27.02.17].
- Bakketeig, I., Hauge, M., Kvamme, C., Sunnset, B., and Toft, K. (2016). Havforskningsrapporten. Fisken og havet, 1-2016.
- Betten Maskinstasjon (2016). Forautomat t1a. [Online] Available from: <http://www.betten-m.no/> [Accessed 30.02.17].
- Cardia, F. and Lovatelli, A. (2015). Aquaculture operations in floating hdpe cages: A field handbook. *FAO Fisheries and Aquaculture Technical Paper*, (593):152.
- Chakrabarti, S. K. (1987). *Hydrodynamics of offshore structures*. WIT press, Southampton.
- Cifuentes, C., Kim, M., Sims, N. A., Key, G., et al. (2014). Coupled analysis of a spm buoy-feeder-cage system for offshore aquaculture. In *The Twenty-fourth International Ocean and Polar Engineering Conference*. International Society of Offshore and Polar Engineers.
- DNV-GL (2010a). *Sesam User Manual - Wadam (Wave Analysis by Diffraction and Morison Theory)*. Det Norske Veritas Software, Høvik.
- DNV-GL (2010b). *Environmental conditions and environmental loads*. Recommended practice DNV-RP-C205.
- DNV-GL (2014). *Sesam User Manual - GeniE Vol.1*. Det Norske Veritas Software, Høvik.
- Faltinsen, O. (1990). *Sea loads on ships and offshore structures*. Cambridge University Press, Cambridge.



- Gudmestad, O. T. (2015). *Marine technology and operations*. WIT Press, Southampton.
- Lader, P. F. and Enerhaug, B. (2005). Experimental investigation of forces and geometry of a net cage in uniform flow. *IEEE Journal of Oceanic Engineering*, 30(1):79–84.
- Lee, C. W., Lee, J., and Park, S. (2015). Dynamic behavior and deformation analysis of the fish cage system using mass-spring model. *China Ocean Engineering*, 29(3):311–324.
- Lekang, O.-I. (2013). *Aquaculture Engineering*. Blackwell Publishing Ltd, Singapore, 2nd ed. edition.
- Li, Y., Gui, F., and Teng, B. (2007). Hydrodynamic behavior of a straight floating pipe under wave conditions. *Ocean Engineering*, 34(3–4):552–559.
- Lillevik, O. (2014). Statisk elektrisitet i førslanger. SINTEF.
- Massie, W. and Journée, J. (2001). Offshore hydromechanics. *Delft University of Technology: Delft, The Netherlands*.
- Orcina (2014). *OrcaFlex Manual*. Version 9.8a.
- Pipelife Norge AS (2002). Technical catalogue for submarine installations of polyethylene pipes. [PDF] Available from: [http://www.pipelife.com/media/generic/pdfs/Technical\\_Catalogue\\_for\\_Submarine\\_Installations\\_of\\_Polyethylene\\_Pipes.pdf](http://www.pipelife.com/media/generic/pdfs/Technical_Catalogue_for_Submarine_Installations_of_Polyethylene_Pipes.pdf) [Accessed 03.02.17].
- Sarpkaya, T. (2010). *Wave forces on offshore structures*. Cambridge University Press, Cambridge.
- Standard Norge (2003). *Marine fish farms - requirements for design, dimensioning, production, installation and operation*. Norsk Standard NS 9415.
- Sunde, L., Heide, M., Hagen, N., Fredheim, A., Forås, E., and Prestvik, Ø. (2003). *Teknologistatus i havbruk*. SINTEF Fiskeri og havbruk. Report number: STF80 A034002.
- Thomassen, P. E. (2008). *Methods for Dynamic Response Analysis and Fatigue Life Estimation of Floating Fish Cages*. Phd thesis, NTNU.

Trelleborg (2016). Bend stiffener. [Online] Available from: <http://www.trelleborg.com/en/offshore/products/bend--control--solutions/subsea--bend--stiffeners> [Accessed 15.04.17].

# A | Wadam Input

Wadam input - Physical data

<b>ENVIRONMENT</b>	
<b>Gravity</b>	9.80665 m/s <sup>2</sup>
<b>Water density</b>	1025 kg/m <sup>3</sup>
<b>Water kinematic viscosity</b>	1.350E-6 m <sup>2</sup> /s
<b>Water depth</b>	40 m
<b>Frequency Set</b>	Various frequency in 0-60s range
<b>Direction Set</b>	0 °– 90 °, interval of 15 °
<b>HYDRO STRUCTURE</b>	
<b>Panel model</b>	T1.05m.FEM
<b>Translation of model</b>	None
<b>Symmetry planes of panel model</b>	None
<b>Number of panels</b>	3200
<b>MASS MODEL</b>	
<b>Coordinate system</b>	COG Centered System
<b>Buoyancy</b>	Calculated from panel model
<b>Total mass</b>	123 00 00 kg
<b>Center of gravity</b>	15m, 10m, 1.6m
<b>Radii of gyration</b>	rx=5.8, ry=8.7, rz=10.4

Wadam input - Execution directives

<b>EXECUTION DIRECTIVES</b>	
<b>Tolerance waterline</b>	5 %
<b>Tolerance center of gravity</b>	5 %
<b>Characteristic length</b>	100m
<b>Drift forces</b>	Pressure integration (6DOF)
<b>Roll damping</b>	None
<b>Equation solver</b>	Direct matrix solver
<b>Result files</b>	<ul style="list-style-type: none"> <li>- SIF formatted</li> <li>- Calculate eigenvalues</li> <li>- Use global origin as reference point</li> </ul>
<b>Logarithm singularity</b>	Analytical
<b>Numerical integration</b>	One node gauss
<b>Panel dimension</b>	Maximum diagonal
<b>Other</b>	<ul style="list-style-type: none"> <li>- Save temp. Wamit files</li> <li>- Calculate mass matrix in HydroD</li> </ul>

# B | OrcaFlex Input

## B.1 General data

OrcaFlex input - General data

<b>STATICS</b>	
<b>Statics method</b>	Whole System Statics
<b>Buoy degrees of freedom included in Static Analysis</b>	Individually specified
<b>Starting velocity</b>	None
<b>Statics convergence parameters:</b>	
- Max iterations	400
- Tolerance	1E-6 (Default value)
- Min Dampin	1 (Default value)
- Max damping	10 (Default value)
<b>DYNAMICS</b>	
<b>Duration build-up</b>	10 s
<b>Duration stage 1</b>	10800 s
Logging:	
- Precision	Single
- Target sample interval	0.1s
<b>INTEGRATION AND TIME STEPS</b>	
<b>Integration method</b>	Implicit
<b>Time step</b>	Variable
<b>Maximum time step</b>	0.250 s
<b>Maximum number of iterations</b>	20
<b>Tolerance</b>	25E-6
<b>RESULTS</b>	
<b>Spectral density fundamental frequency</b>	0.01 Hz

OrcaFlex input - Sea and seabed

<b>SEA</b>	
<b>Surface Z</b>	0 m
<b>Kinematic viscosity</b>	1.350E-6 m <sup>2</sup> /s
<b>Temperature</b>	10 °Celsius
<b>Reynolds number calculation</b>	Flow direction
<b>SEA DENSITY</b>	
<b>Density variation</b>	None
<b>Water density</b>	1.025 ton/m <sup>3</sup>
<b>SEA BED</b>	
<b>Type</b>	Flat
<b>Seabed origin</b>	(0m,0m,-40m)
<b>Direction</b>	0 deg
<b>Slope</b>	0 deg
<b>Seabed model</b>	Elastic
<b>Normal stiffness</b>	100 kN/m/m <sup>2</sup>
<b>Shear stiffness</b>	-
<b>Damping</b>	0

OrcaFlex input - Waves and current

<b>WAVES</b>	
<b>Simulation time origin</b>	0 s
<b>Kinematic stretching model</b>	Vertical stretching
<b>User specified seeds</b>	-
<b>Spectrum discretisation method</b>	Equal energy
<b>Significant waveheight, Hs</b>	2m, 3m, 4m
<b>Zero crossing period</b>	4.66s, 5.44s, 7s
<b>Wave origin</b>	(0m,0m)
<b>Wave time origin</b>	0 s
<b>Wave type</b>	JONSWAP
$\gamma$	1
<b>Peak frequency, fm</b>	0.1667 Hz, 0.1429 Hz, 0.111 Hz
<b>Peak period, Tp</b>	6s, 7s, 9s
<b>Wave directions</b>	0 deg and 90 deg
<b>Number of wave components per direction</b>	100 (default)
<b>Relative frequency range</b>	
- r_min	0.5 (default)
- r_max	10 (default)
<b>Maximum component frequency range</b>	0.05 Hz
<b>CURRENT</b>	
<b>Ramp during build-up</b>	No
<b>Horizontal current variation</b>	No
<b>Vertical current variation</b>	No
- Method	Interpolated
- Speed surface	0.25 m/s, 0.5 m/s
- Exponent	30
- Direction	0 deg and 90 deg

**Table B.1:** Lines types

<b>Name</b>	<b>Feed pipe</b>	<b>Bending stiffener</b>
<b>Category</b>	Homogeneous pipe	Homogenous pipe
<b>Outer diameter</b>	0.110 m	Variable data set
<b>Inner diameter</b>	0.0974 m	0.120m
<b>CG Offset</b>	Not applied	Not applied
<b>Bulk modulus</b>	Infinity	Infinity
<b>Material density</b>	0.960 ton/m <sup>3</sup>	1.00 ton/m <sup>3</sup>
<b>Compression limit</b>	No	No
<b>Allowable tension</b>	25 kN	-
<b>Bending stiffness</b>	3.046 kNm <sup>2</sup>	-
<b>Axial stiffness</b>	2257.7 kN	
<b>Poisson ratio</b>	0.450	0.500
<b>Torsional stiffness</b>	2.101	-
<b>Drag coefficient</b>	Variable data	1.00
<b>Added mass coefficient</b>	Ca Rate Close to Surface	1.00
<b>Added mass coefficient</b>	Ca Close to Surface	1



## B.2 Force Coefficients

Variable data set - Drag coefficient

<b>Reynolds number</b>	<b>Drag coefficient</b>
10E3	1.2
50E3	1.2
240E3	1.2
255E3	1.19
300E3	1.16
340E3	1.05
380E3	0.8
425E3	0.42
510E3	0.4
600E3	0.42
675E3	0.48
850E3	0.57
1.3E6	0.68
1.7E6	0.7
8.5E6	0.7
25E6	0.7

Variable data set - Added mass coefficient

<b>Ca Rate Close to Surface</b>	
<b>Norm. submergence</b>	<b>Rate of change of Ca</b>
-1	0
-0.5	0.5
0	0.23
0.5	0.1
1	0.43
1.5	0.23
2	0.13
2.5	0.07
3	0

Variable data set - Added mass coefficient

<b>Ca Close to Surface</b>	
<b>Norm. submergence</b>	<b>Ca</b>
-1	0
-0,5	0,35
0	0,5
0,5	0,58
1	0,65
1,5	0,8
2	0,9
2,5	0,94
3	0,95